ZEUS– –
24. October 2002

The Transverse Polarimeter (TPOL) Test Beam at CERN in July-August 2001

T. Behnke, C. Collins-Tooth, V. Gharibyan, R.Hamatsu,
M. Inuzuka, K. Long, K.Matsuzawa, F. Metlica, S. Schmitt

k.long@ic.ac.uk, metlica@mail.desy.de, c.collins-tooth@ic.ac.uk: IC-London, ZEUS

hamatsu@comp.metro-u.ac.jp, inuzuka@mail.desy.de, kmatsu@mail.desy.de: Tokyo Metro-Univ, ZEUS

behnke@mail.desy.de, vaagn@hermes.desy.de: FLC-DESY

sschmitt@mail.desy.de: FH1-DESY

Abstract

The HERA ring has been upgraded, during the 2000-2001 shutdown, to increase its luminosity and provide longitudinal lepton beam polarization to the HERA experiments. The transverse polarimeter TPOL, which measures the transverse HERA lepton beam polarization, has been also upgraded to improve the transverse polarization precision measurement from $\sim$5% to $\sim$1%. The TPOL upgrade consists in a fast DAQ and silicon position sensitive detector. At first the TPOL was tested at the beginning of 2001 in a DESY test beam, instrumented with a prototype silicon and fiber detector; then during July-August 2001, the TPOL instrumented with the final setup silicon position sensitive detector (silicon and fiber detectors), was tested at higher energies at a CERN test beam. The CERN test beam results are presented in this note.

Contents

1 Introduction

This ZEUS note is written to report on the TPOL test beam results obtained at the CERN test beam in summer 2001 (23/07/01-3/08/01). The aim of the CERN test beam was to study the TPOL polarimeter in its final setup, before its installation in the HERA tunnel near HERA-B (HERA WEST RIGHT), which took place during the HERA 3 day access 19-21/11/2001. A previous ZEUS note (ZEUS-01-019) [1] was written for the test beam conducted at DESY at begining of 2001 (29/01/01-12/02/01), with the TPOL in a prototype setup. In this previous note the physics motivations for the TPOL upgrade project are delineated [2], [3], [4], [5], [6]. The Transverse Polarimeter (TPOL) consists of 3 subdetectors: a position sensitive silicon detector, a scintillation fiber detector and the spare TPOL calorimeter. In both test beams the spare TPOL calorimeter was used. At the DESY test beam a small prototype silicon detector (1 cm * 1 cm active silicon) was tested; at the CERN test beam the full size silicon detector (6.3 cm * 6.3 cm active silicon) instrumented the TPOL. Regarding the single scintillating fiber detector, at the DESY test beam the fiber's position was changed manually by height bushes (height spacers), at CERN a computer controlled stepping motor was used to position the fiber vertically in front of the silicon. In the time lapse between the two test beams the TPOL DAQ was also improved and upgraded. The next sections contain information on the TPOL CERN test beam setup and results.

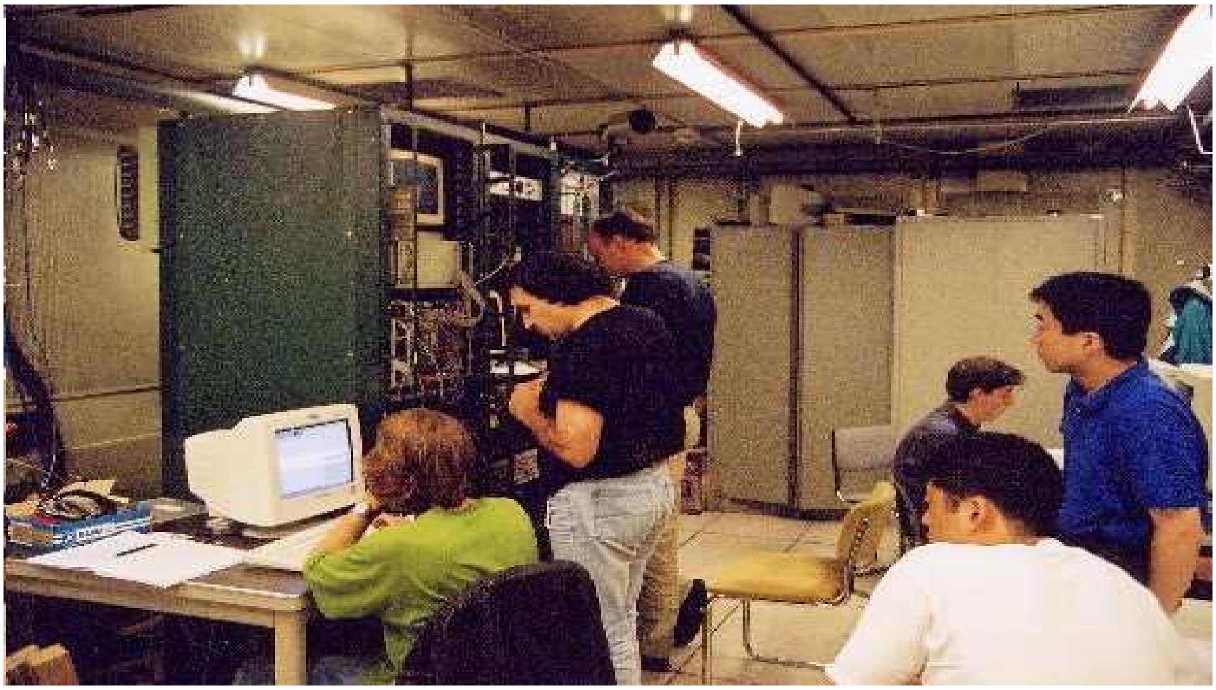

Figure 1: *Photo of the TPOL CERN test beam DAQ room, with some TPOL participants.*

2 The Test Beam Setup

The CERN test beam took place in summer 2001, from 23/07/01 to 3/08/01. The test beam area was located in the CERN-Prevessin site. The test beam called H6, consisted of a secondary particle beam that provided hadrons, electrons, positrons and muons of energies ranging between 5 and 205 Gev. The H6 beam was part of the SPS North Area, located in EHN1(bldg. 887) at Prevessin. For the TPOL tests positron/electron beams with energies ranging between 6-50 GeV were chosen; being the region of interest for the TPOL detector. The diagram below fig.2 shows the TPOL test beam setup.

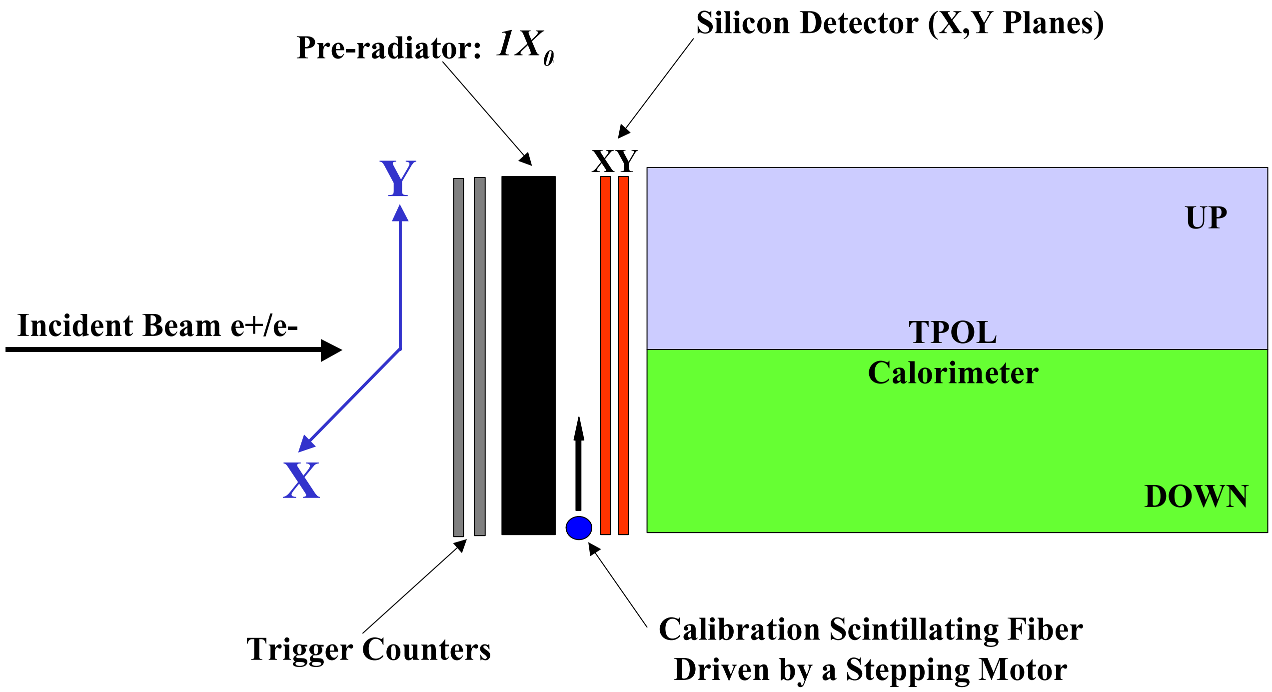

Figure 2: *Diagram showing the TPOL polarimeter detector setup for the CERN test beam, consisting of three sub-detectors: calorimeter, silicon, and fiber detector. The trigger was given by the coincidence of the two trigger counters placed upstream of the TPOL. In the HERA tunnel setup, Compton photons are the particles incident on the TPOL. The pre-radiator is necessary for Compton photon conversion. A pre-radiator material consisting of 1 radiation length thick ($1X_0$) lead, was also included to simulate the HERA tunnel setup. The horizontal and vertical directions are indicated by the X-Y axis arrows. The X-Plane silicon detector was a dummy.*

Only the Y-plane silicon detector was present. The X-plane was still in preparation at IC-London, so a dummy detector was used in its place to simulate the X-plane material thickness in front of the calorimeter, see fig.2. A faulty ZEUS MVD silicon detector was used as a dummy. In the HERA tunnel setup, Compton photons are the particles incident on the TPOL. A pre-radiator is necessary for Compton photon conversion. The pre-radiator, consisting of lead one radiation length thick ($1X_0$), was included to study and simulate its presence. The three TPOL sub-detectors (silicon, fiber and calorimeter detectors) where contained in an aluminum box support structure (107 cm long, 69 cm wide, 47 cm high). The box base plate was 2 cm thick aluminum, and the cover consisted of 2 mm aluminum sheets. The trigger counters were positioned outside and upstream of the box. The TPOL box and trigger counters were positioned on a remote controllable test beam movable table; which was located in the closed test beam area see figs. 3, 4, 5. The trigger signal was given by the coincidence of the two trigger counters. Each trigger counter consisted of a photomultiplier (Hamamatsu H3167) connected to a light guide and scintillator plate (6 cm * 6 cm). The two trigger counters where fixed on a support such that the two scintillator plates totally overlap and cover the silicon detector active region. The silicon electronics were placed on a rack about 2 m from the TPOL detector box. Instead the TPOL DAQ was located in the test beam hut DAQ room $\sim$15 m distant. The necessary calorimeter and fiber signals were transported to the test beam hut by coaxial cables. The same calorimeter was also used in the previous DESY test beam; a detailed description of it is found in [1]. The calorimeter, silicon and fiber detectors are the final setup detectors and a description will be given in the next sub-sections.

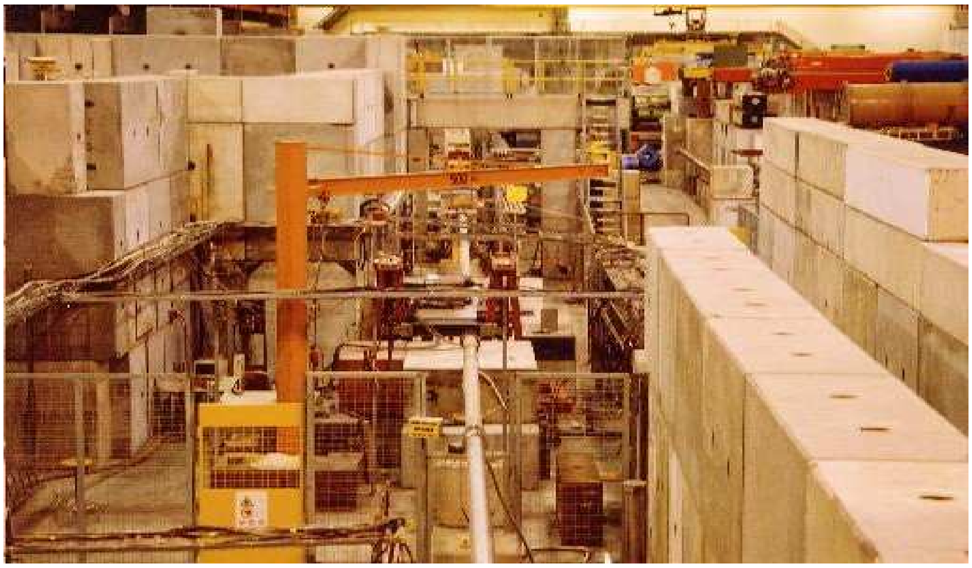

Figure 3: *View of the CERN test beam area. The TPOL is positioned on the movable table in the middle of the photo, just under the crane. The beam direction is out of the page.*

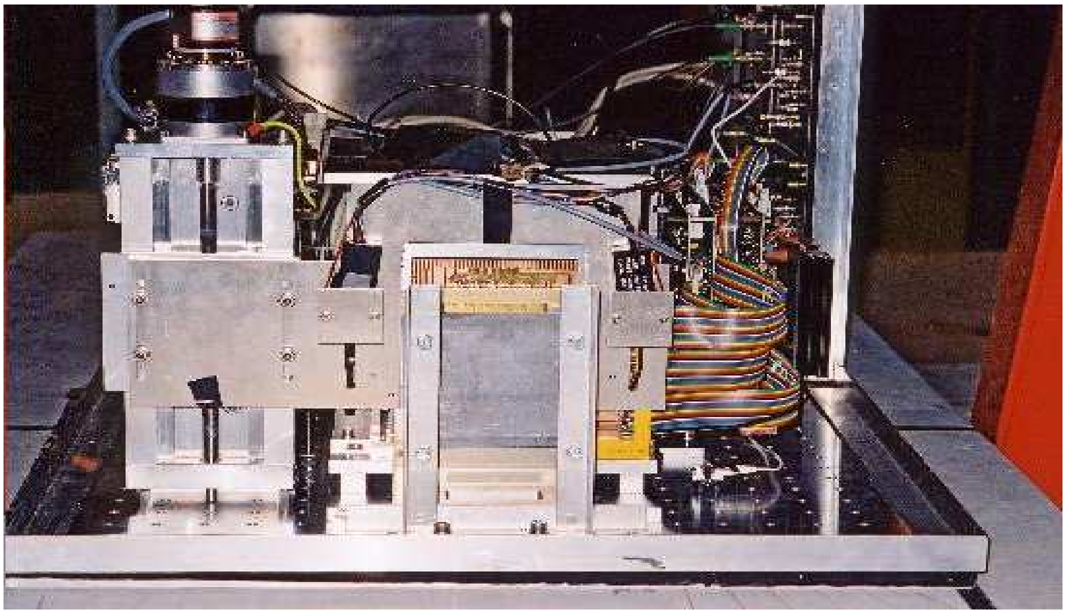

Figure 4: *Front view of the TPOL in the CERN test beam setup. In the picture, on the left hand side the stepping motor can be seen, in the center the silicon and fiber detectors are position behind the lead pre-radiator. The calorimeter is behind the silicon and fiber detectors, not to be seen because covered by the quadratic aluminum support structure.*

Figure 5: *Closeup view of the TPOL enclosed by the aluminum box, positioned on the test beam movable table. The trigger counters can be seen right in front of the beam-pipe exit window. In this photo the TPOL is not in its data taking setup; it still needs to be finely positioned.*

3 The Trigger and DAQ

The CERN test beam trigger and DAQ system were very similar to the readout system used for the TPOL in its present HERA setup. The main difference was the source of the triggers. For the CERN test beam, a pair of scintillator trigger counters were used to trigger on the incident beam particles. At HERA the trigger is derived from the calorimeter signal.

The three sub-detector components (calorimeter, silicon, fiber) were readout in two VME crates, each equipped with a RIO2 processor board running under LynxOS. A Linux PC with several disks and a tape drive was used to store the raw data files, to merge events collected by the VME crates, and for online analysis and control plots. The event data was read out by the VME processors and written directly to the PC disk, which was accessible from the VME processors by NFS. After a run was completed, the PC merged the two raw data files and produced a Ntuple file containing for each event the data from all sub-detectors.

3.1 The silicon VME crate

The silicon VME crate is described in detail in section 5. For the trigger and readout the following components are most relevant:

RIO2,FED: the RIO2 processor ran the silicon data-acquisition program. The FED was physically located on the PMC (PCI Mezzanine Card) bus of the RIO2 board. The FED digitized the analog signals received from the APV25 chips. Only after the digitization was finished, the event data could be read out on the PMC bus.

IO register: the **DELAYED TRIGGER** input channel of the IO-register was configured such that it generated an VME interrupt. It was used to initiate the readout process as soon as a trigger had arrived and the data had been digitized by the FED. The **CLEAR BUSY** output channel of the IO-register was used to reset the trigger logic. It indicated that the readout of the current event was finished.

SEQSI: in addition to the dead-time caused by the VME readout, the DAQ was blind while digitizing the APV data. The SEQSI generated the **INHIBIT** signal to indicate these conditions. In order to simplify the trigger logic, this signal was active if a trigger was allowed to pass through the silicon trigger logic (silicon DAQ waiting for a trigger) and it was not active if triggers needed to be inhibited (APV25s being readout and digitized) . A signal on the SEQSI **TRIGGER** input initiated the readout of the APV25s.

3.2 The calorimeter VME crate

The calorimeter VME crate housed the following components.

RIO2 processor: the RIO2 processor ran the calorimeter/fiber readout program and other programs for slow control tasks (to position the fiber detector stepping motor, to control the high voltage, etc.).

H1 lumi ADC: the ADC was digitizing the analog signals from the calorimeter and the fiber detector. It was a 12-bit sampling ADC with eight inputs. The sampling frequency was 40 MHz.

The samples were stored in a pipeline, 1024 samples long. The pipeline was controlled by a TTL signal, which could be read out by VME access. The TTL signal to enable the pipeline was accessible by the H1 lumi bus only. This bus was available for some slots of the VME crate on the P2 connector. For the CERN test-beam only the pipeline enable signal was generated on that bus, using a home-made trigger module (see below).

For each trigger only 16 out of the 1024 samples were read out, starting from a fixed position relative to the pipeline counter. This reduced significantly the amount of data to be stored for each event, but still leaved enough room for a detailed analysis of the pulses (a typical pulse was not longer than 3 samples), including online pedestal subtraction.

Trigger module: because the service module for controlling the H1 lumi bus was not ready for the CERN test-beam, a home-made trigger module was used. It generated a 10MHz signal, serving as clock for the ADC. In addition it contained a flip-flop controlling the ADC pipeline. The flip flop had two inputs, **START PIPELINE** and **STOP PIPELINE** and one output **PIPELINE ENABLED**.

IO register: the IO-register was used to control the trigger logic and the ADC pipeline. In addition it stored information about special trigger condition (pedestal events, small finger trigger). The following functions were assigned to its inputs and outputs:

VME TRIGGER: this input indicated a trigger condition. The IO register was configured to initiate a VME interrupt. The DAQ software started the readout after the interrupt was received.

ARTIFICIAL TRIGGER: this latched input got active if the last trigger was a pedestal trigger.

FINGER TRIGGER: this latched input got active if a particle passed through the finger trigger.

ENABLE PIPELINE: this output restarted the pipeline after the readout had finished.

TDC: a VME based TDC was used to measure the time difference between the falling edge of the 10MHz clock and the arrival of the trigger. The calorimeter and fiber pulses were sampled at random positions because there was no beam clock at the CERN test beam. Using the TDC information corrections to the observed ADC charge were made.

CAN bus controller: the high-voltage settings of the calorimeter and the fiber detector photo-tubes were monitored and adjusted using ADC and DAC modules connected by a CAN bus. The CAN bus controller interfaced those modules to the VME bus.

RS232 interface: the stepping motor of the fiber detector was controlled by an RS232 line. The RS232 line was interfaced to the VME bus using this module.

SCALER: a scaler was used to monitor trigger rates.

PULSE GENERATOR: a pulse generator was used to produce artificial triggers at a low a rate during normal data taking. These events were used to calibrate the silicon detector. For special runs the test pulser was connected to an LED, producing output signals on the calorimeter photo tubes. These runs were useful to calibrate the relative timing of the four calorimeter channels.

3.3 The trigger logic

The trigger logic for the calorimeter and fiber readout is shown in figure 6. In conjunction with the silicon trigger logic, depicted in figure 13, the same triggers are guaranteed to be recorded in both subsystems, thereby respecting any cause of dead-time that may arise. The actual trigger scheme implemented for the CERN test-beam was slightly more evolved than is shown here, including special synchronization signals at the start of a run and signal monitoring by the scaler.

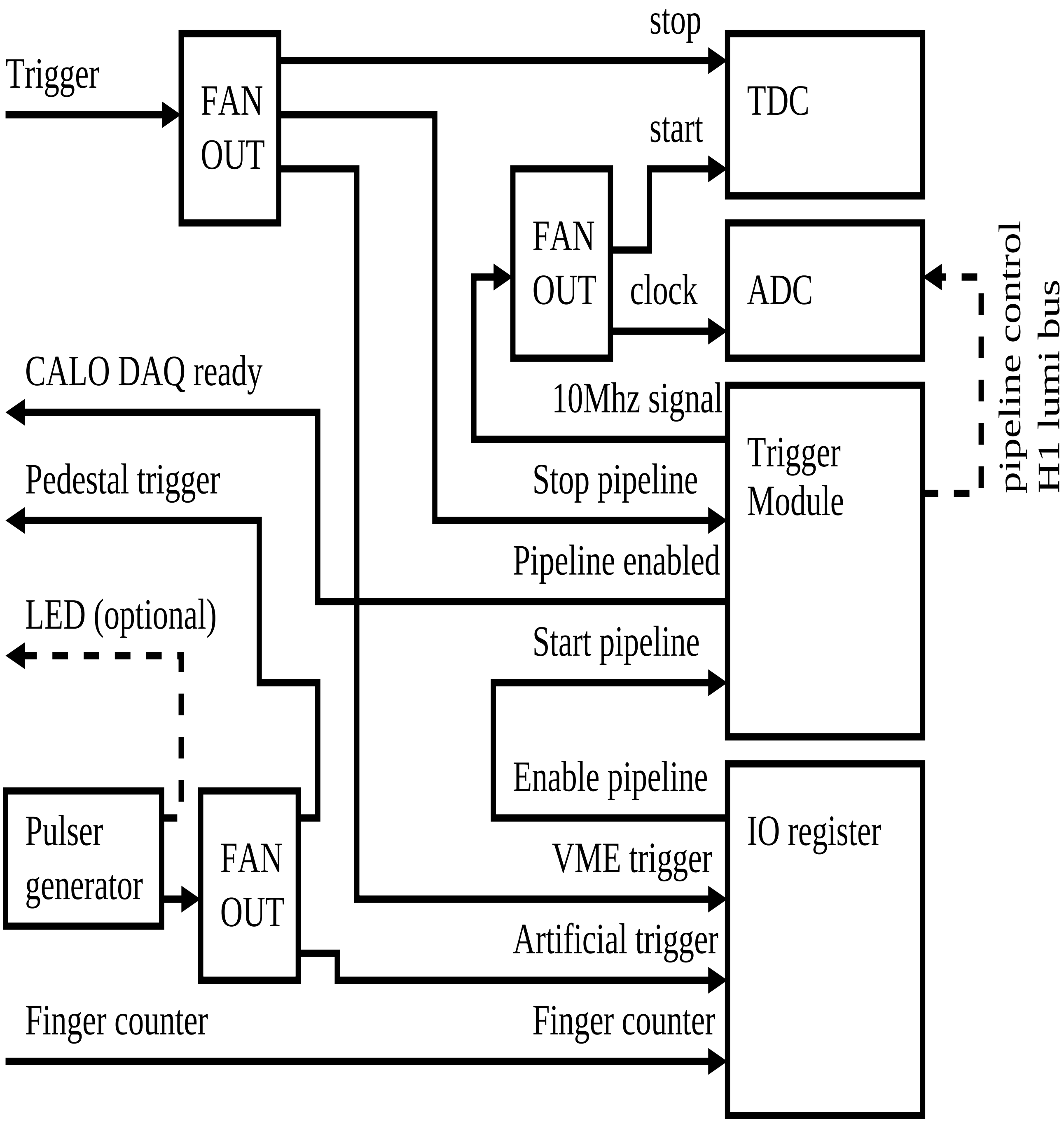

Figure 6: *Trigger logic for the calorimeter and fiber detector readout.*

3.4 The calorimeter and fiber detector analog signal chain

Positioned near the calorimeter a driver board provided several amplifiers with gain-factor 10. The calorimeter and fiber channels were transported to the electronics hut by long cables after amplification only. The four calorimeter channels (up, down, left, right) were each amplified by a factor of 10. The two fiber channels were each amplified by a factor 100, using a chain of two amplifiers for each channel.

In the electronics hut the signals arriving from the test-beam area were connected to a shaper, compensating distortions of the pulse shape caused by the cables. In addition the noise picked up in the cables was subtracted from the analog signals in the shaper unit. This noise subtraction was achieved by running another cable of the same type as the signal cables from the driver board to the shaper board. At the driver side this dummy line was connected to an amplifier, however the input of that amplifier was grounded. Any coherent noise picked up by the cables was removed after the subtraction. Figure 7 illustrates the effect of that noise subtraction. The output of the shaper was a differential

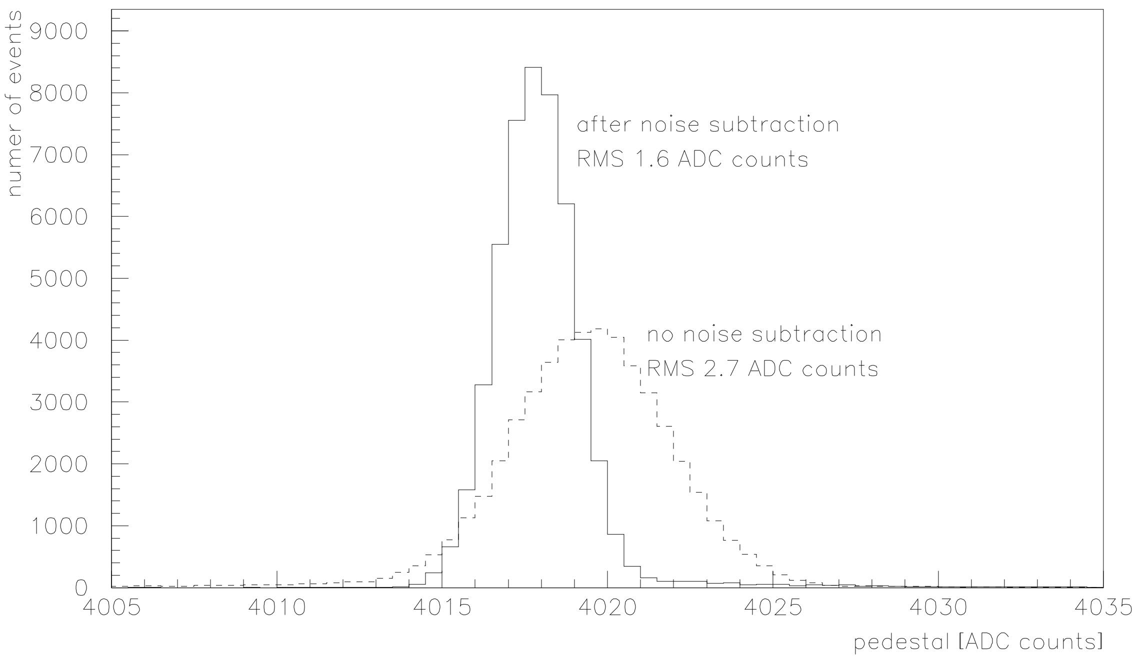

Figure 7: *Calorimeter pedestal with and without noise subtraction*

signal, in order to match the dynamic range of the ADC. The ADC had differential inputs with a dynamic range of $\pm 2\,\mathrm{V}$. In order to make use of the full dynamic range of the ADC for the (negative) signal pulses, a DC offset $\Delta \approx 2\,\mathrm{V}$ was added to the non-inverted shaper output. That DC offset was adjusted such that any baseline-fluctuation was still well contained in the dynamic range of the ADC.

4 The Calorimeter

The calorimeter ([5], [6], [7]) consists of 12 layers of tungsten and scintillator as shown in figure 8 . Each layer consists of a single absorber plate (DENSIMET17, $60 \times 55 \times 6.2$ mm^3, $1.6X_0$) set in a lead frame of $120 \times 100 \times 6.2$ mm^3 and two optically decoupled scintillator plates (SCSN-38, $120 \times 100 \times 2.6$ mm^3). Conceptually the calorimeter can be considered to consist of two calorimeters, one on top of the other; i.e. an UP and a DOWN calorimeter module.

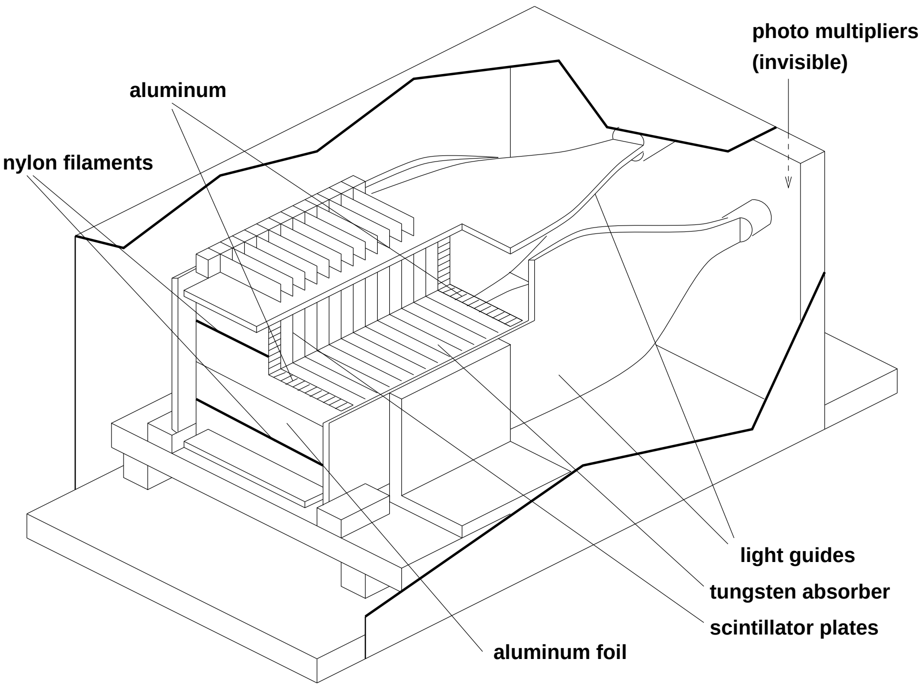

Figure 8: *A cut away, perspective view of the tungsten scintillator calorimeter. The calorimeter has an upper and a lower half which are optically decoupled. The scintillating light is collected by wavelength shifters on all four sides. The asymmetry of the shower development in the upper and lower half is used to measure the vertical projection of the impact point of the Compton photon.*

The scintillation light from each half is collected with wavelength shifters (WLS) along the top and the bottom of the detector (channels U and D). The WLS is made of an acrylic plate doped with a fluorescent material commercially called Y-7. The energy of an incoming photon is derived from the sum of the energies in the two halves:

$$E_\gamma = (E_U + E_D) \, , \tag{1}$$

and the vertical position is measured using the asymmetry of the energies:

$$\eta_V(y) = \frac{E_U - E_D}{E_U + E_D}. \tag{2}$$

For calibration purposes there are also WLSs on the right and the left sides which read the upper and lower halves together (channels R and L). Photo multiplier tubes (Hamamatsu R580) transform the light from the WLSs into an electrical signal. The voltages of the individual electrodes of the PMTs are generated by Cockroft–Walton bases which deliver constant cathode and anode voltages up to anode currents of 40 μA [8].

The calibration of the calorimeter is made by adjusting the voltages of the four PMTs with the detector centered in the electron beam. The relative calibration of channels L and R is done by measuring the distribution of the horizontal energy asymmetry η_H:

$$\eta_H(x) = \frac{E_L - E_R}{E_L + E_R}. \tag{3}$$

The distribution is Gaussian and the width is determined by light attenuation and photo-electron statistics. When the two channels are properly calibrated the mean of $\eta_H(x)$ is zero.

The vertical channels are calibrated utilizing the calibrated horizontal channels through the energy ratio

$$R(\eta_V) = \frac{E_V}{E_H} = \frac{E_U + E_D}{E_L + E_R}\,. \tag{4}$$

As the horizontal and vertical readout channels view the same scintillators, this ratio, apart from minor effects due to light attenuation in the scintillator, is independent of the position and energy if the relative calibration of U and D is properly set. The relative calibration of the horizontal and vertical channels is set with the requirement that at the center ($\eta_V = 0$) $R = 1$.

The fractional energy resolution defined as $\sigma(E)/E$ is dominated by sampling fluctuations and photo-electron statistics leading to $\sigma(E)/E$ scaling with $1/\sqrt{E}$. At high energies deviations from $1/\sqrt{E}$ can occur because of noise, pedestal fluctuations, non-uniformities and incomplete shower containment. Such effects are usually included by adding a constant term to $\sigma(E)/E$. In our case the additive constant term arises mainly from the momentum resolution of the DESY test beam and may be neglected by properly including the resolution into data errors.

The vertical position y_0 of an incoming high energy electron or photon is measured using the energy asymmetry η_V deposited in the upper (UP) and lower (DOWN) halves of the detector:

$$\eta_V(y_0) = \frac{E_U - E_D}{E_U + E_D}. \tag{5}$$

Using the sum of two exponentials as a parametrisation of the electro-magnetic transverse shower shape dE/dy [5], [9] :

$$f(y - y_0) \equiv \frac{dE}{dy} = P_1 e^{-P_2|y-y_0|} + P_4 e^{-P_3|y-y_0|} \; , \tag{6}$$

the vertical impact point y_0 can be calculated from the energies E_U and E_D

$$E_D = E_V \int\limits_{-\infty}^{0} f(y - y_0) dy \tag{7}$$

$$E_U = E_V \int\limits_{0}^{\infty} f(y - y_0) dy \; , \tag{8}$$

with $E_V = E_U + E_D$. The normalization

$$\int\limits_{-\infty}^{\infty} f(y, y_0) dy = 1 \tag{9}$$

reduces the number of free parameters

$$\frac{P_1}{P_2} + \frac{P_4}{P_3} = \frac{1}{2} \; , \tag{10}$$

so that the following expression for the energy asymmetry η_V as a function of the vertical position y_0 of the electron is obtained:

$$\eta_V(y_0) = \frac{|y_0|}{y_0} \left[1 - e^{-P_3|y_0|} + \frac{2P_1}{P_2} (e^{-P_3|y_0|} - e^{-P_2|y_0|}) \right] \; . \tag{11}$$

The vertical position resolution σ_y is expected to scale as $1/\sqrt{E}$ and is approximately a linear function of the vertical position with respect to the split between the upper and lower halves.

5 The Silicon Detector

The silicon detector is a position sensitive detector, consisting of two silicon sub-detectors which measure the horizontal X and vertical Y positions of the incoming beam particles (see fig.2, fig.9). The silicon detector Y position measurement is vital for the TPOL polarimeter calibration i.e. in situ and real time eta-Y transformation measurement ([1], [7]), while the purpose of the X position measurement is to gain the complete information of the cluster positions on the calorimeter face. The silicon detector for the CERN test beam setup consisted of a Y-silicon detector and a dummy X-silicon detector. The Y-silicon detector was a Hamamatsu ATLAS prototype: 64 mm * 63.6 mm *pn* detector, 80 μm pitch, 768 strips, $\sim$ 300 μm thick, operation bias voltage 80 V. The X-silicon detector was not ready, so a dummy detetcor was used in its place to simulate the material thickness of the real X-detector. The dummy was a faulty MVD ZEUS silicon detector which was of the same type as the real X-detector being built at Imperial College of London. The Y-detector (fig.10) was readout by 6 APV25 amplifier/multiplexer chips. In the experimental setup the Y detector was positioned always downstream with respect to the X detector, because the Y detector needed to be as close as possible to the calorimeter face in order to obtain a good eta-Y calibration by measuring as precisely as possible the vertical Y shower impact position on the calorimeter's face.

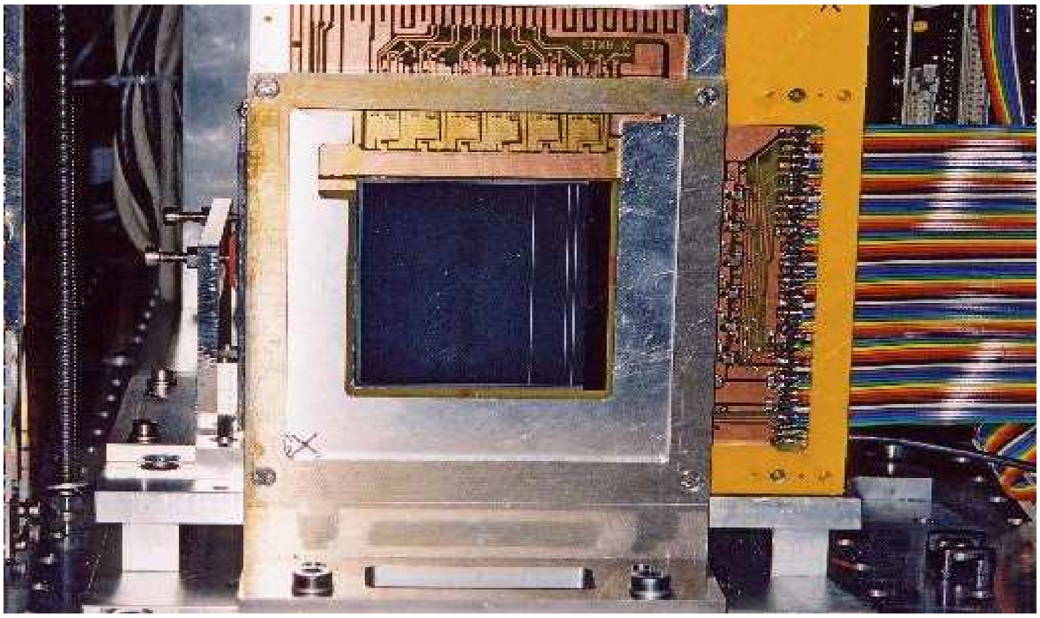

Figure 9: *Front view of the silicon detector in the CERN test beam setup. The X-dummy detector is seen here, the Y-detector is directly behind and not visible.*

5.1 The Silicon Detector Components

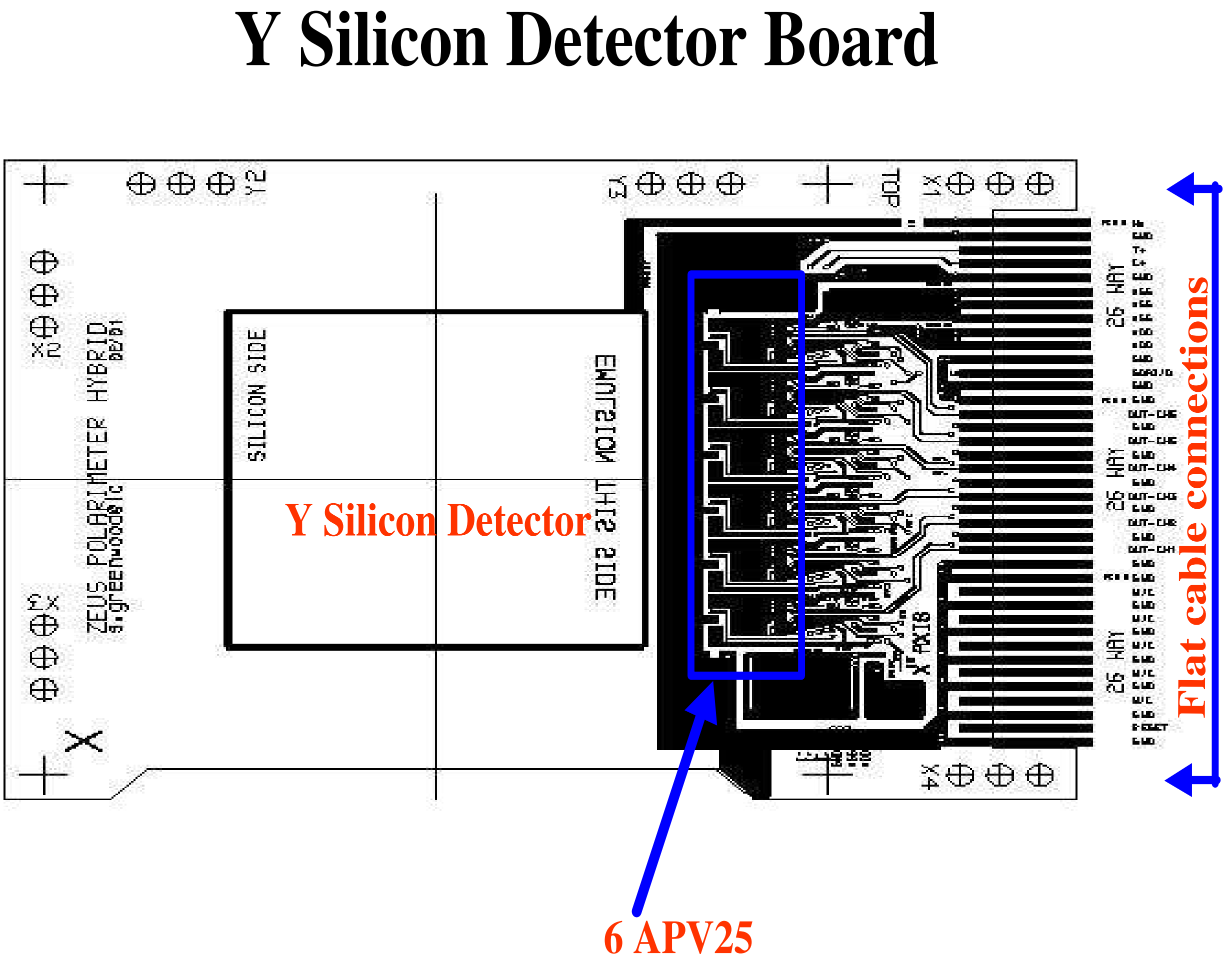

Figure 10: *The Y silicon detector board schematic. The active silicon area (64 mm * 63.6 mm), and the 6 APV25s are visible.*

The various silicon detector components that where used in the CERN test beam setup for the silicon detector operation are listed below. The silicon detector setup was designed, built and tested at Imperial College of London during the first half of 2001. The silicon electronics were in two crates (VME and NIM) placed in a rack nearby (~2 m) the test team movable table and TPOL detector box.

- The **Y silicon detector board**: (see fig.10) which consisted of the Y silicon detector that was a Hamamatsu ATLAS prototype [10], 64 mm * 63.6 mm pn detector, 80 μm pitch, 768 strips, $\sim$ 300 μm thick, operation bias voltage 80 V; and 6 APV25 Amplifier/Multiplexer Readout chips, developed for CMS, $\sim$ 1*1 cm^2, 128 channel analogue pipeline (192 deep) chip, 40 MHz sampling rate, 20 MHz data readout rate [11].

- The **X dummy board** (see fig.9) which simulated the material thickness of the not yet ready X silicon detector board; a faulty ZEUS MVD silicon detector was used.
- The **Y Interface board**: interface board between the Y Silicon detector board and the VME modules.
- The **Y Reset board**: for sending a hardware reset signal to all 6 APV25s on the Y silicon detector board, and also provided the APV25 OUTE signal (APV25 output enable signal). The OUTE signal was mainly used for test purposes. It was used for oscilloscope triggering when visually inspecting the APV25 OUT+/- analogue differential current output signals.
- The **Y Driver board**: provided the the APV25 OUT+/- signals (analogue differential current APV25 output signal) for digitization.
- **NIM crate**: housed the silicon trigger NIM electronics, see fig.11 and fig.13.
- **VME crate** which housed all the silicon detector controls, see fig.11 and fig.12; below the VME modules are listed.
  1. **RIO2** 8062 PowerPC based RISC I/O Board processor from CES (Creative Electronic Systems S.A.), running LynxOS operating system [12] .
  2. Front End Digitizer **FED-PMC**: for digitization of the APV25 analogue signals [13]; 8 ADC channel PCI Mezzanine Card (PMC), 9 bits, at 40 MHz.
  3. **SEQSI**: a sequencer which provided the control signals for driving the APV25s [14].
  4. **I2C** module: served as a control interface using the I2C standard to set and check the APV25 configuration [15].
  5. **HV** module (ISEG VHQ 202M) : remotely and precisely controlled the silicon bias high voltage [16].
  6. **Input/Output Register** (CAEN V513): for sending hardware reset signals to the APV25s; switch on/off power supply to the silicon detector board; and for synchronization with the TPOL DAQ [17].
  7. **Power Board**: built at IC to supply the necessary power to the four above mentioned silicon detector boards (detector, interface, reset, and driver boards).
  8. **Trigger and Clock Board**: built at IC to distribute the trigger and clock signals from the SEQSI to the silicon board and FED.

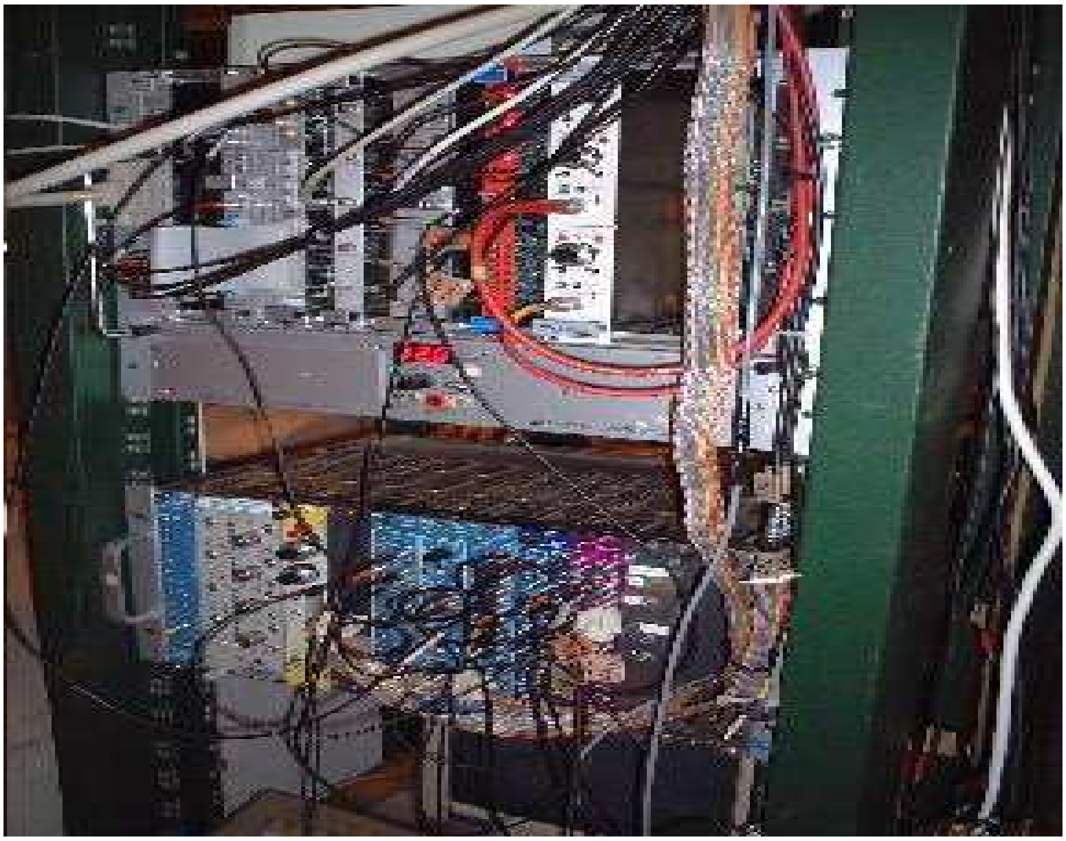

Figure 11: *Two crates were needed for the silicon detector operation. One NIM crate which housed the NIM electronics for the silicon trigger logic (bottom crate) and the VME crate (top crate) which housed all the silicon detector operation and control modules. These two crates were fixed to a rack nearby (∼2 m) the TPOL detector box.*

5.2 The Silicon Detector Operation

Fig.12 shows the schematic diagram for the silicon detector operation; only the Y-silicon board was ready for the CERN test beam. The Y-silicon detector board contained both the Y-silicon detector and the 6 APV25s amplifier/multiplexer readout chips. In the schematic, the box labeled "*Y Silicon Detector*", represents the four Y-silicon detector boards: the Y silicon detector board, the Y Interface board, the Y Reset board, and the Y Driver board.

All the silicon detector operation and control modules were housed in the VME crate. The RIO2 processor which ran the LynxOS operating system, controlled all the VME modules and ran the silicon DAQ.

The silicon bias HV was set to 80 V for the whole test beam running time by the HV module, via the Y Interface board.

The I2C module was used to set and check the APV25 parameters; it served as a control interface using the I2C standard (via the Y Interface board).

The Input/Output Register (IO Register) was used to send a hard reset signal to the APV25s whenever the APV25 parameters had to be reseted (via the Y Reset board). The Power Module was controlled by the IO Register; it supplied power to the 4 Y-silicon boards. During the whole test beam running time power to the Y-silicon boards was left on. The IO Register also generated two signals necessary for the TPOL trigger (Clear Busy and Delayed Trigger see fig.13), see next section about the Silicon Trigger i.e. section 5.3.

The SEQSI module is a pulse generator (40 MHz clock) which provided control signals for driving the APV25s. The SEQSI controls signals were: a Reset signal -reset the 6 APV25s; a Trigger signal -sent to readout the APV25s, and a Clock signal -the 40 MHz clock required for the APV25s operation. The SEQSI is designed to respond to random external triggers. For the CERN test beam the following sequence was used, which was very similar to the one used for the prototype silicon detector test beam at DESY [1].

The SEQSI generated a sequence, which looped back to the start of the sequence *loopstart* each time the end of the sequence *loopend* was reached i.e. a continuous looping sequence. The sequence was incremented by one sequence unit for each clock cycle. Near the beginning of the sequence a Reset signal was sent to the 6 APV25s, then the SEQSI waited for a random external trigger to arrive (labeled *TPOL Trigger* in the schematic fig.12), if not it looped back at the beginning of the sequence *loopstart*, this happened when the sequence end *loopend* was reached. If an external trigger (*TPOL Trigger*) arrived, generated by the TPOL trigger electronics, then the SEQSI sequence jumped to a point beyond the end of the looping sequence $loopend + jump$, in this case the sequence continued until *seqendexttrig* was reached. In this extended part of the sequence, between $loopend + jump$ and *seqendexttrig*, a trigger signal was sent to the 6 APV25s for readout and then sufficient time was given for the APV25s to be readout and for the analogue data to be digitized by FED (Front End Digitizer at 40MHz). When *seqendexttrig* was reached the SEQSI looped back to the beginning of the sequence *loopstart*, starting the SEQSI sequence loop all over again.

The random external trigger signal was sent to the SEQSI from the TPOL trigger electronics (*TPOL trigger*). In the silicon NIM crate (see fig.13) a coincidence between the *Raw Trigger* signal and the *SEQSI Inhibit* signal was made. The *Raw Trigger* was allowed to reach the SEQSI whenever the *SEQSI Inhibit* was off. The *SEQSI Inhibit* was on when the SEQSI was resetting the APV25s (beginning part of the sequence) and when the APV25s were triggered for readout (between $loopend + jump$ and *seqendexttrig*).

The SEQSI ran with a $40MHz$ clock which corresponds to a 25 ns clock cycle, necessary for the APV25s operation. When the external random trigger signal was inputted into the SEQSI, it had to synchronized with the SEQSI system clock, which can be done only within one clock cycle. This created a 25 ns jitter, in the SEQSI trigger signal sent to the APV25s for readout, between different events. The APV25s processed pulse shapes corresponding to the silicon detector hits, which were continuously sampled every 25 ns, and were wide enough to limit the effect of this jitter. The digitized signal value can vary between 5% - 10%, due to this jitter effect [11].

The trigger signal sent by the SEQSI to the APV25s for readout must have the correct clock sequence timing to match the latency of the silicon detector system. The trigger signal was sent by the SEQSI to the APV25s at a specified clock number value in the SEQSI sequence, between $loopend + jump$ and $seqendexttrig$, to readout the APV25 pipeline column containing the Y-silicon signals generated by a hit in the silicon. The correct SEQSI sequence clock number value was obtained by doing a latency scan. The approximate silicon latency (approximate sequence clock number) was calculated beforehand from the total cable lengths and delays in the silicon detector system. The APV25 OUT+/- analogue outputs were checked with an oscilloscope for visible silicon signals at this approximate sequence clock number using a radiation source at DESY before sending the TPOL to CERN. At CERN, several data runs (see section 9.2) with different sequence clock number values around this approximate sequence clock number were then collected and normalized to have the same number of signal events. All signals in each given run were summed up (ADC counts summing). The run with the highest total sum signal value was the one with the correct clock sequence number i.e. the SEQSI clock latency for the silicon detector was thus found. This clock sequence number was used in the SEQSI sequence, to send correctly timed trigger signals to the APV25s for readout, for all test-beam runs.

The SEQSI trigger and clock signals were supplied to the *Trigger and Clock Board* which functioned as a signal distribution board. It distributed the trigger and clock signals to the Y Interface board and to the FED.

The APV25 readout was at $20MHz$, its analogue output signal was sent to the FED for digitizing. The analogue output signal was a differential current output consisting of two signals equal but opposite OUT+,OUT-. The FED operated in Header Finding Mode, that is, the APV25 data capture was automatically triggered on the recognition of a valid APV25 frame header on the FED ADC channel 0 only. The APV25 raw data was digitized for the whole length of the APV25 frame plus some extra clock cycles to get the APV25 baseline value, see section 9.1, [13]. The FED's clock was external ($40MHz$) generated by the SEQSI and inputted in the FED via the *Trigger and Clock Board*. This clock was delayed internally by the FED to synchronize the clock's phase relative to the incoming

APV25 analogue data stream. The APV25 readout was at $20MHz$, so that FED was set to sample every second clock i.e. the FED worked in *downsampling mode*. The FED was physically placed on the RIO2 board. The cable lengths for the trigger/clock signals sent to the 6 APV25s and the 6 APV25s OUT+/- analogue signals, had to be the same to within 1nsec, to insure that all 6 APV25s OUT+/- signals arrive synchronously at the FED.

The APV25 digitized data were sent to the TPOL DAQ where they were combined offline for each event with the fiber and calorimeter data. Only after that the FED had sent all the digitized data for a given event to the TPOL DAQ, could the TPOL trigger send another trigger to the Silicon detector, see section 3.

At the beginning of each test beam run the HV setting was checked, the APV25s were reseted and the SEQSI sequence restarted.

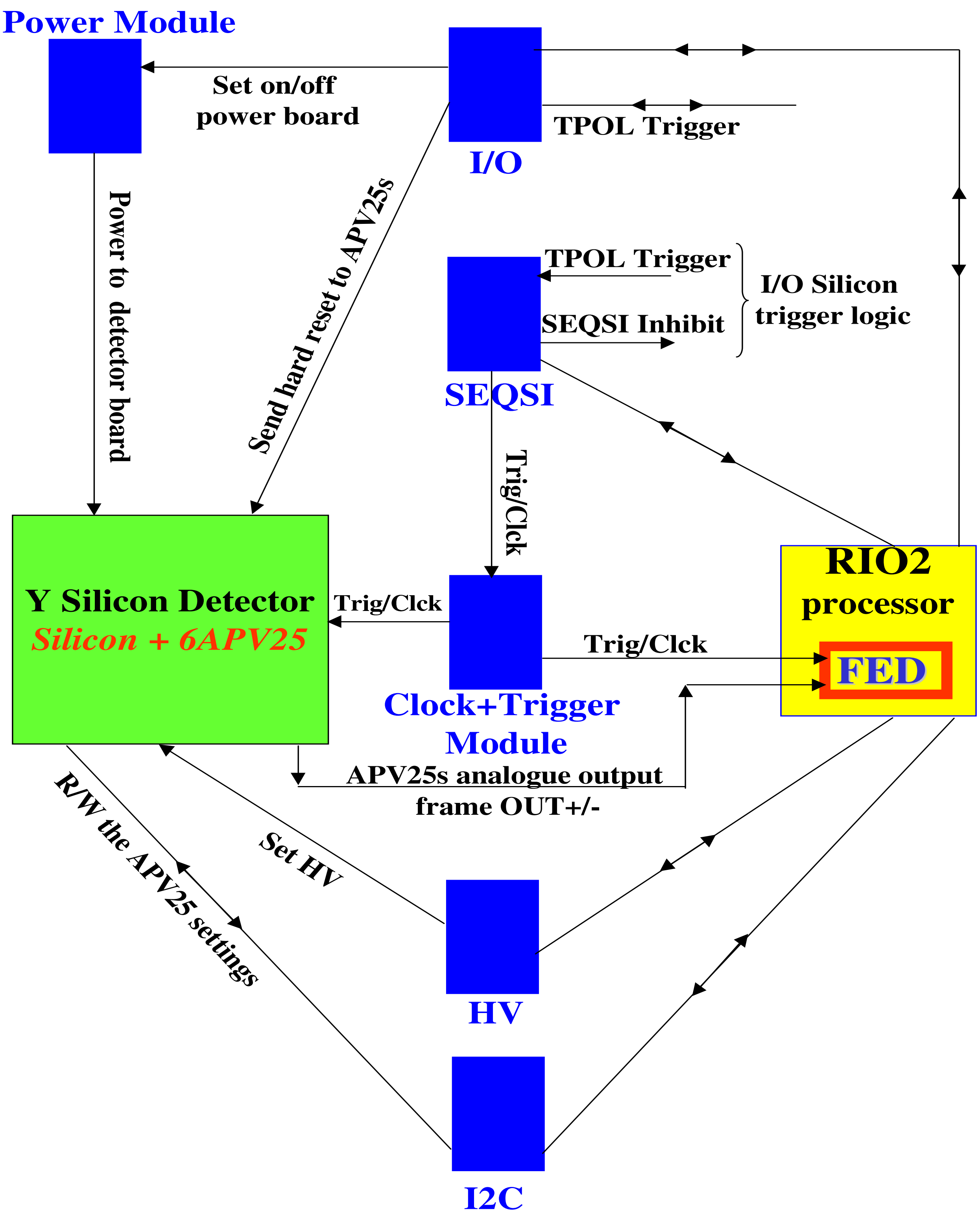

Figure 12: *Schematic for the silicon detector operation and DAQ setup in the CERN test-beam. All the shown modules are housed in the VME crate.*

5.3 The Silicon Detector Trigger Setup

Fig.13 displays the setup for the silicon trigger setup, which is based on NIM logic. The physics trigger was generated by the crossing of an incident test beam particle through the two scintillator trigger counters (see section 2). The analogue signals of these two trigger counters were fed into two NIM discriminators to generate NIM signals, so that the NIM logic could be used.

A coincidence (*AND* unit) was then made. One of the outputs was sent to a TPOL DAQ scaler for monitoring the raw trigger coincidence rate; another output was fed into an *OR* unit. The *OR* unit had as an input the raw physics trigger and the TPOL pedestal trigger.

There were two types of triggers for the silicon detector. A physics trigger, derived from the raw physics trigger, that was used to collect physics data; and a pedestal trigger (called also artificial trigger) generated from the TPOL DAQ, which sent a trigger to the silicon trigger logic randomly, whenever there was no physics trigger. The pedestal trigger (TPOL pedestal trigger) was used to collect pedestal events. So in a given data run there were both physics events and pedestal events.

The output of the *OR* unit was inputted into an *AND* unit together with the *SEQSI INHIBIT* signal. The *SEQSI INHIBIT* signal was used to inhibit trigger signals whenever the SEQSI was not ready to receive triggers: i.e. when resetting the APV25s and when the APV25s were triggered for readout and digitization by the FED, see section 5.2. Then the output was again *ANDed* with the *CALO INHIBIT* signal: i.e. the TPOL DAQ would send a NIM signal only when the calorimeter DAQ was ready for a new event.

The output of this *AND* was then fed into the *SET* input of a *LATCH* unit, which would then start a *latch* NIM signal. This *latch* NIM signal was closed only when the I/O Register supplied a *CLEAR BUSY* signal fed to the *RESET* input of the *LATCH* unit. The *CLEAR BUSY* signal was first passed through NIM discriminator unit to make sure that a proper NIM signal is produced. The *CLEAR BUSY* was generated by the TPOL DAQ only when the TPOL DAQ was ready to acquire another event i.e. it reset the silicon trigger logic. No other trigger could get through the silicon trigger logic at this point of the schematic until the *CLEAR BUSY* signal was generated.

The output of the *LATCH* unit was then fed into a NIM discriminator unit to provide the proper trigger signal to the SEQSI. The SEQSI required a NIM signal about 35 nsec long. Another output from the NIM discriminator unit was sent to the TPOL DAQ (the TPOL VME crate), for monitoring the actual number of triggers seen by the SEQSI and thus seen by the silicon DAQ. This was necessary for event synchronization and unification of the two data streams (silicon and fiber+calorimeter) offline.

Another output from the *LATCH* unit was fed into a *GATE* generator unit, which generated a 10 μsec delayed short NIM signal called *DELAYED TRIGGER*. The *DELAYED TRIGGER* signal was inputted into the I/O Register to generate a VME interrupt. This interrupt was used to initiate the TPOL silicon data readout process as soon as a trigger had arrived, and the data was readout from the APV25s and digitized. The delay was taken to be 10 μsec to give enough time for the APV25 output frame to be readout by the FED, which is about 7.5 μsec long and have some extra time available for other processes.

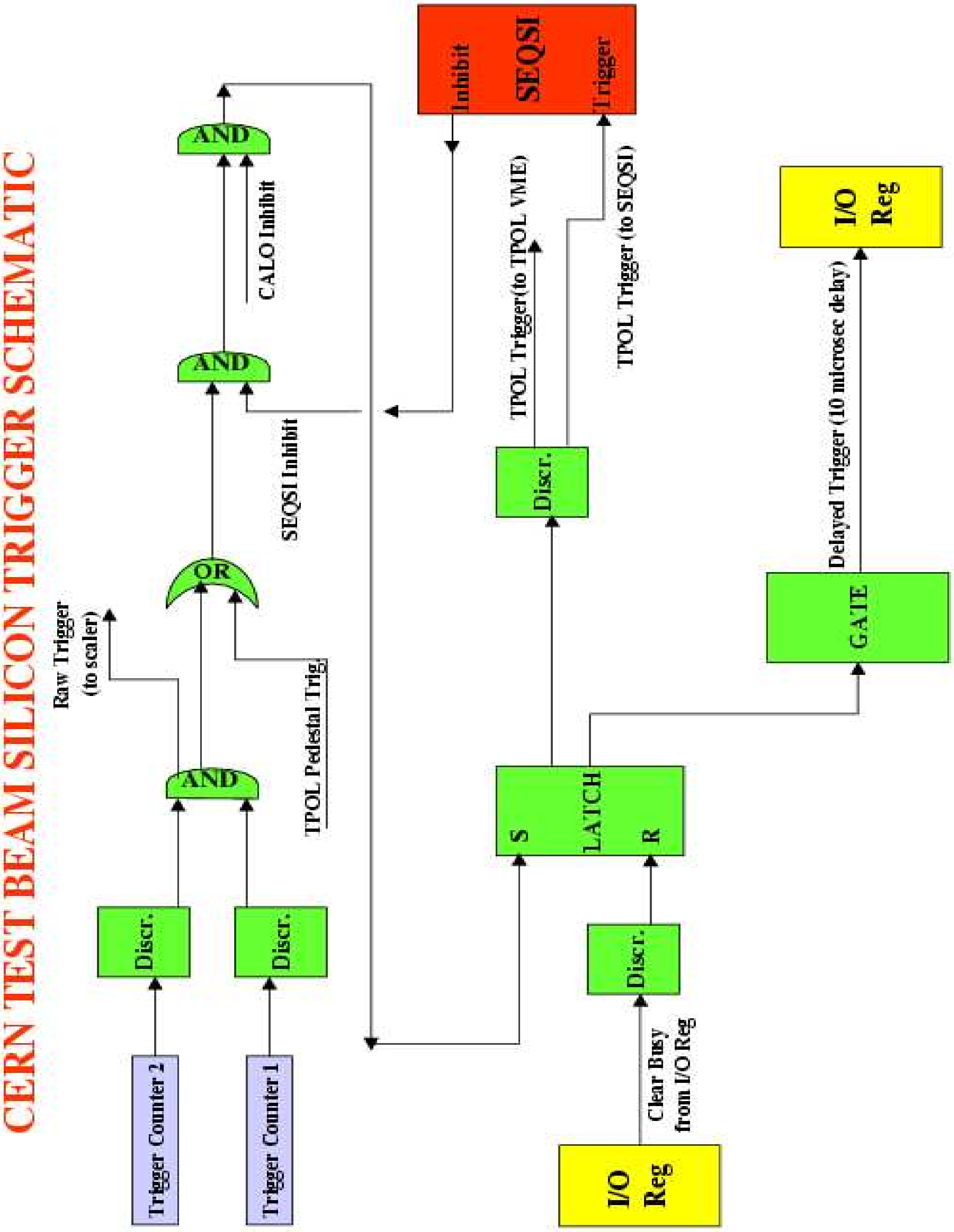

Figure 13: *Schematic for the silicon trigger setup. NIM logics is used.*

6 The Fiber Detector

Before the long shutdown of HERA in 2000, the rate of the back-scattered Compton photons and the bremsstrahlung photons was found to be about 100 kHz in total at the TPOL calorimeter. From a Monte Carlo simulation study, the radiation dose at the silicon detector is estimated to be 1.9 Mrad/year [18]. This may damage the silicon detector after a long period operation. As shown in fig. 2, the fiber detector was installed about 1 cm in front of the silicon detector to calibrate the linearity of the response of the silicon detector [1].

6.1 Overview of the Detector

Fig. 14 is a photograph of the fiber detector, which was mounted on the baseplate and in front of the silicon detector. The scintillating fiber and photosensor modules were supported on an aluminum plate.

Figure 14: *A photograph of the fiber detector, installed on the TPOL support structure.*

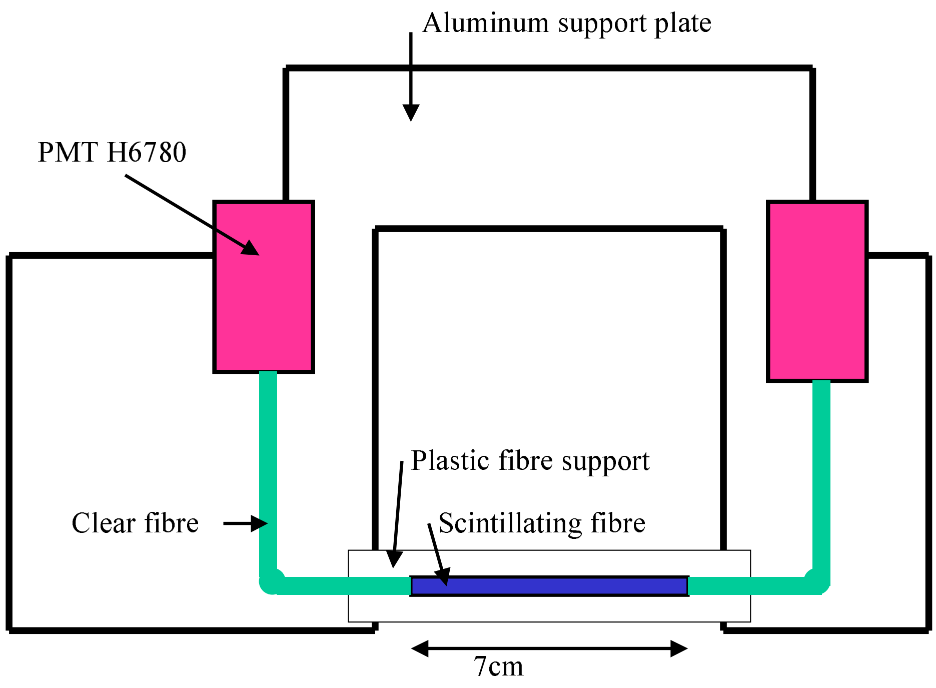

Figure 15: *A front view drawing of the fiber detector.*

The mechanical design of the fiber detector is shown in fig. 15 in more detail.

The detector components are described below:

- A double claded scintillating fiber (KURARAY, SCSF-81M) was put horizontally into a groove on a plastic support stick and fixed with tape. The length and diameter of the fiber were 70 mm and 1 mm, respectively.
- Signals from both ends of the scintillating fiber were transported via double claded clear fibers (Edmund Scientific Japan Co., Ltd.), which were bent upwards to the photosensor modules.
- The photosensor module (HAMAMATSU, H6780) included a compact photomultiplier (PMT) and a power supply. These PMTs feature low voltage operation (varying from +11.5 V to 15.5 V). The gains of PMTs were adjusted by a control voltage (from 0 V to 1.0 V). The control voltages were set to 0.87 V during the test beam.
- As seen in fig. 14, the above components were supported by an aluminum plate.
- The aluminum plate was fixed to a stepping motor, which is seen left of the plate in fig. 14. The vertical position of the scintillating fiber was controlled by the stepping motor with the precision in the order of 1 μm.

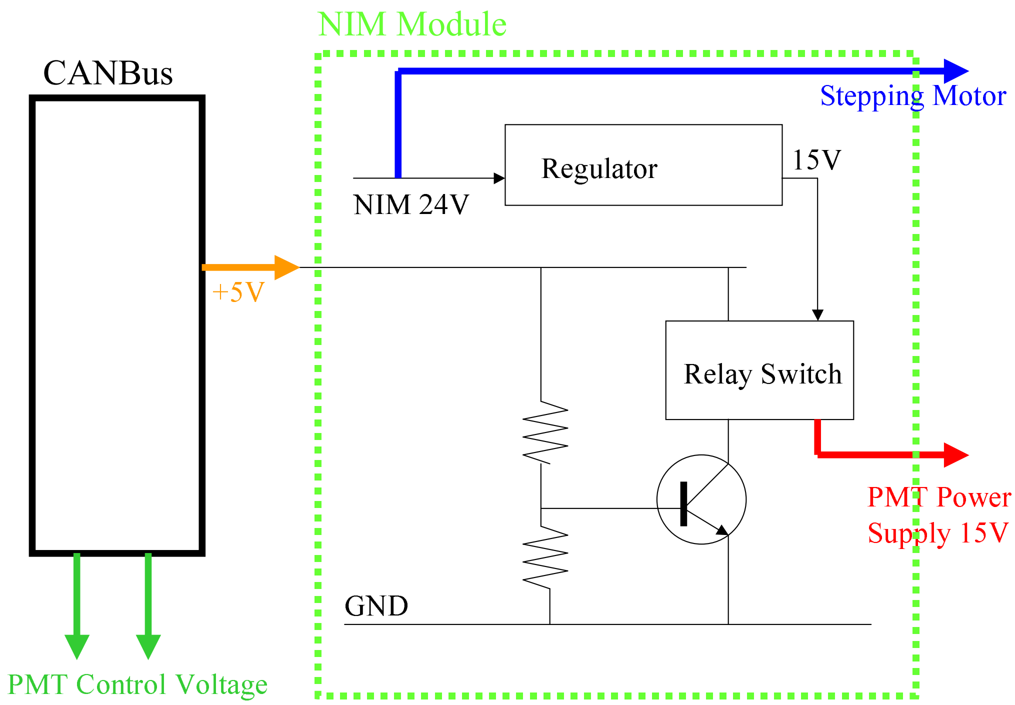

Figure 16: *A power supply system for the fiber PMTs.*

6.2 High Voltage Supply System

Fig. 16 is a schematic diagram of the power supply system for the PMTs. As mentioned above, in order to operate the high voltage power supply in the photosensor H6780, it is necessary to supply a low voltage (from +11.5 to 15.5 V) and a control voltage (from 0 to 1.0 V) by which the gain of PMT is adjusted. As shown in fig. 16, the power system was operated with a CANBus module and a NIM module, which were positioned nearby the TPOL detector.

The CANBus module sends a TTL signal with +5 V, which turns on the relay switch in the NIM module. When the switch is turned on, +15 V is applied to PMT high voltage supply. The regulator transforms +24 V given by the NIM crate into +15 V as shown in fig. 16.[1]

The DAC in the CANBus module provides the control voltages as shown in fig. 16. During the testbeam, the control voltages were set to 0.87 V for both PMTs.

[1] In the final setup in the HERA tunnel, the +24 V is also applied to the stepping motor driver as shown in fig. 16. However, it was not done during the CERN testbeam.

6.3 Stepping Motor

As shown in fig. 14, the aluminum support plate was fixed to a movable stage of the stepping motor with screws. The vertical position of the scintillating fiber was controlled by the motor with a precision of the order of 1 μm. An optical datum switch was attached on top end of the motor. The fiber position should always be measured relative to the datum position. The optical datum switch is the reference position for the stepping motor. Fig. 17 is a schematic diagram of the stepping motor control system. The motor drive, PDFX controls the motion of the motor, monitors the current position and so on, by exchanging RS232C serial data with a VME module, VMIVME-6015. Both VMIVME-6015 and PDFX drive were put close to the TPOL detector in the beam area.

As shown in fig. 17, three cables were connected between the stepping motor and the drive. The cable A is mainly to energize the stepping motor. The cable B is to get the position information from the encoder. The cable C is for user I/O pins, which were mainly used for the datum switch. In order to operate these switches, it is necessary to supply +24 V to the connector C on the PDFX drive (Pin 1). This was provided by the NIM crate as shown in fig. 16.

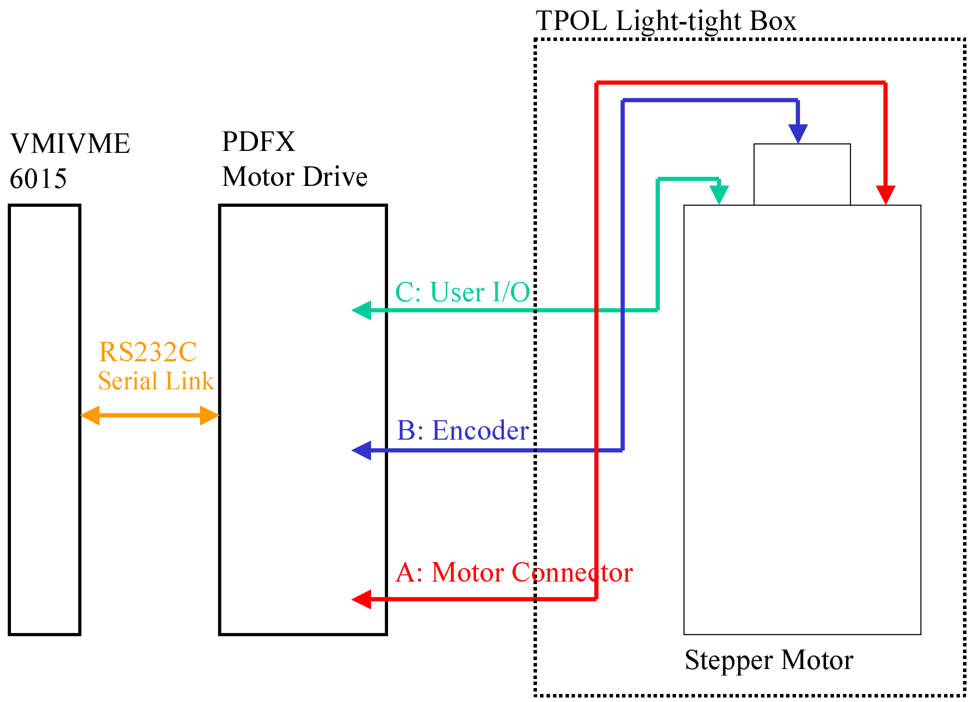

Figure 17: *The stepping motor control system.*

7 The CERN Test Beam Data Set

During the test beam, data was accumulated for positron/electron test beams with energies ranging between 6 GeV and 50 GeV; this being the region of interest for the TPOL detector. Some data was also collected for the LPOL calorimeter in same energy range and particle type. The LPOL (Longitudinal Polarimeter) was brought to CERN for calibration, in the spare test beam time. In this note only the TPOL data analysis will be discussed. The data was collected with the TPOL in its final hardware setup, that is, the same detector setup that was installed in the HERA tunnel later on in the year, in November 2001. The pre-radiator in front of the silicon was always present. Data was taken for several fiber scans, where the fiber was positioned by the stepping motor at a given set of positions in front of the silicon, at a fixed test beam energy; and table scans, where the movable test beam table support positioned the whole TPOL detector at several vertical and horizonatl positions with respect to the incident test beam, at a fixed test beam energy. An energy scan was also made. The main aims of the CERN test beam are listed below. These aims have been fullfilled, as will be seen in the next sections.

- **Calorimeter:** energy linearity and resolution and spatial uniformity;
- **Silicon:** eta-Y measurement with fiber and table scans and general testing of the silicon detector;
- **Fiber:** resolution of the fiber linearity calibration and general testing of the fiber with the stepping motor setup;
- **TPOL:** integrate the 3 TPOL subdetectors and operate the TPOL as one detector.

The data collected basically consists of the following data sets.

- **Table scans** at 10 GeV, 15 GeV, 20 GeV with electrons; number of events in a run typically 20000 or 30000.
- **Fiber scans** at 10 GeV, 15 GeV, 20 GeV with electrons; number of events in a run typically 20000 or 30000.
- **Fine Fiber scan** at 10 GeV with positrons; number of events in a run typically 20000.
- **Energy Scan** with energy varying between 6 GeV and 50 GeV (6 GeV, 8 GeV, 10 GeV, 12.5 GeV, 15 GeV, 17.5 GeV, 20 GeV, 22.5 GeV, 25 GeV, 27.5 GeV, 30 GeV, 35 GeV, 40 GeV, 50 GeV) with positrons; number of events in a run typically between 10000 and 50000.

8 The Calorimeter Data Analysis and Results

The TPOL calorimeter specific test beam results are presented here. The analysis techniques applied here are the same as used in the DESY test beam [1].

In this test, data were taken with 6, 8, 10, 12.5, 15, 17.5, 20, 22.5, 25, 27.5, 30, 35, 40 GeV energy of positron and 10, 15, 20, 25, 40 GeV energy of electron.

The calorimeter vertical table scan performed with 30 GeV electrons, shows a good vertical spatial uniformity. This can be seen by plotting the calorimeter ADC channel value versus the impact point position. Fig. 18 displays the scatter plot of the calorimeter ADC channel signals Up and Down, versus the vertical impact point Y measured by the silicon detector. A negative Y value (impact position) corresponds to a hit in the lower part of the calorimeter (Down part). To compare the behavior of the Up+Down, Up and Down channels, one should look to the top plot of fig. 19, which has the same structure for the channels. The two plots in fig. 19 display the mean ADC channel values for all combinations (Up+Down, Up, Down, Left+Right, Left, Right) versus Y.

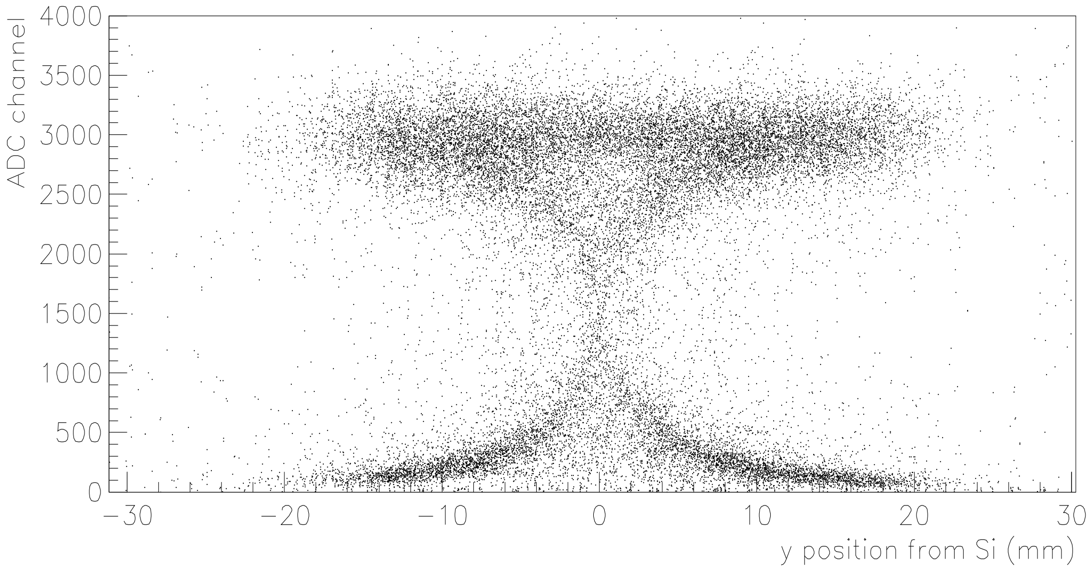

Figure 18: *Scatter plot of calorimeter ADC channel signals Up and Down versus vertical impact point Y measured by the silicon detector. Data are taken with 30 GeV electrons.*

The calorimeter has also a good energy linearity and resolution, see fig. 20 and 21. The relative non-linearity is about 1%. The energy resolution was obtained by fitting first the CERN testbeam data (6-40 GeV energy of positron) alone, as well a combined CERN and DESY testbeam 1-6 GeV [1] data.

The energy resolution only with CERN data points is $\sigma/\mathrm{E} \sim 24\%/\mathrm{sqrt(E)}$ with a constant term of 5% added in quadrature , with E in GeV. In case of fitting with CERN and DESY testbeam, the resolution is σ/E $\sim$ 25%/sqrt(E) with a constant term of 5% (CERN) and 3% (DESY) added in quadrature. The small discrepancy arises from different test beam setups and signal processing chains like beam energy calibrations, PMT gains, ADC boards etc. The beam energy spread (3.5% in CERN and 5% in DESY) has been taken into account for both linearity and resolution analysis. The obtained numbers are consistent the previous CERN test beam results ($\sigma/sqrt(E) = 23 - 24\%$, Relative non-linearity $< 1\%$) and the preradiator accounts for the observed small degradation of the energy resolution.

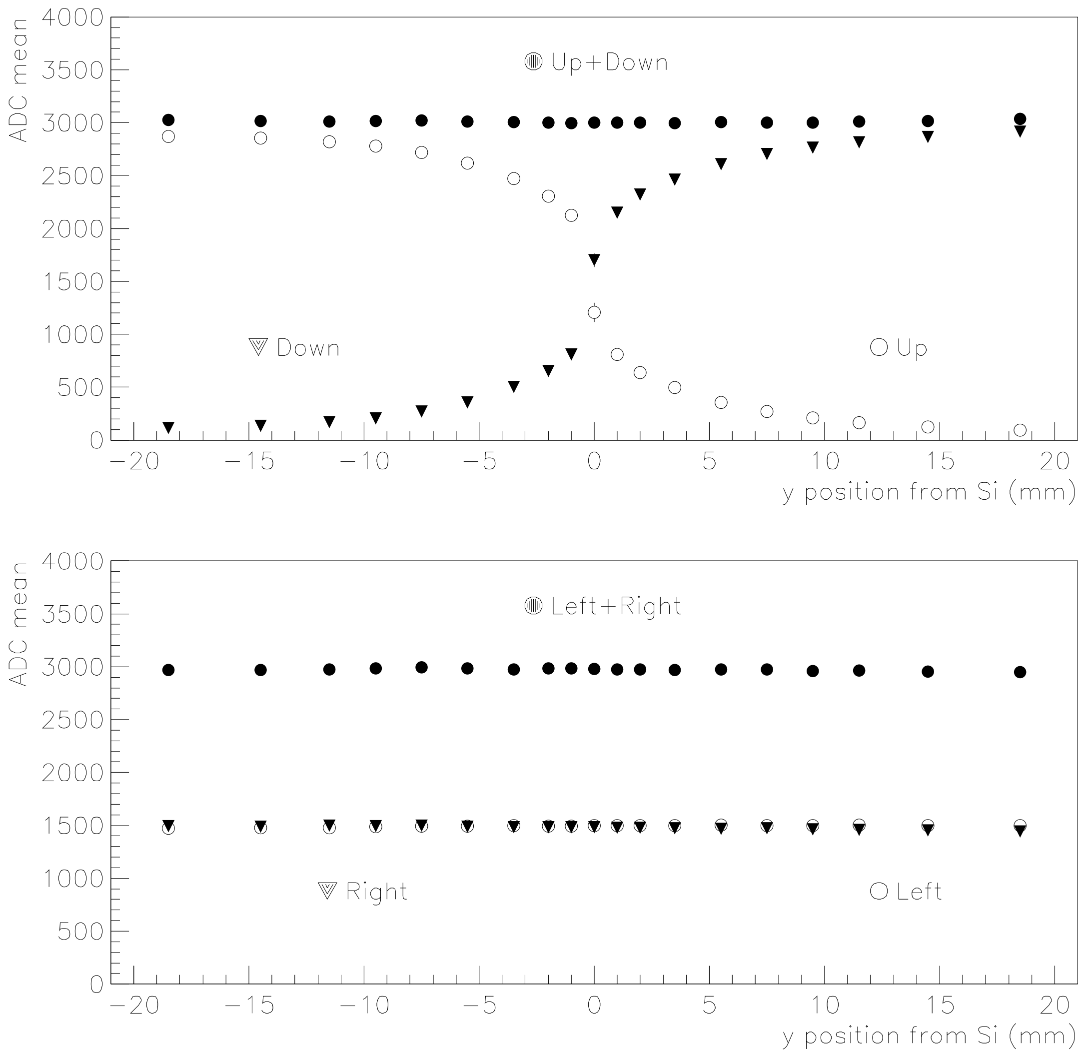

Figure 19: *Mean ADC channel values versus vertical impact point Y measured by the silicon detector (30 GeV electrons). Top plot, mean ADC channel value Up+Down (black dots), Up (inverted black triangles), and Down (open circles), versus Y. Lower plot, mean ADC channel value Left+Right (black dots), Left (inverted black triangles), and Right (open circles), versus Y.*

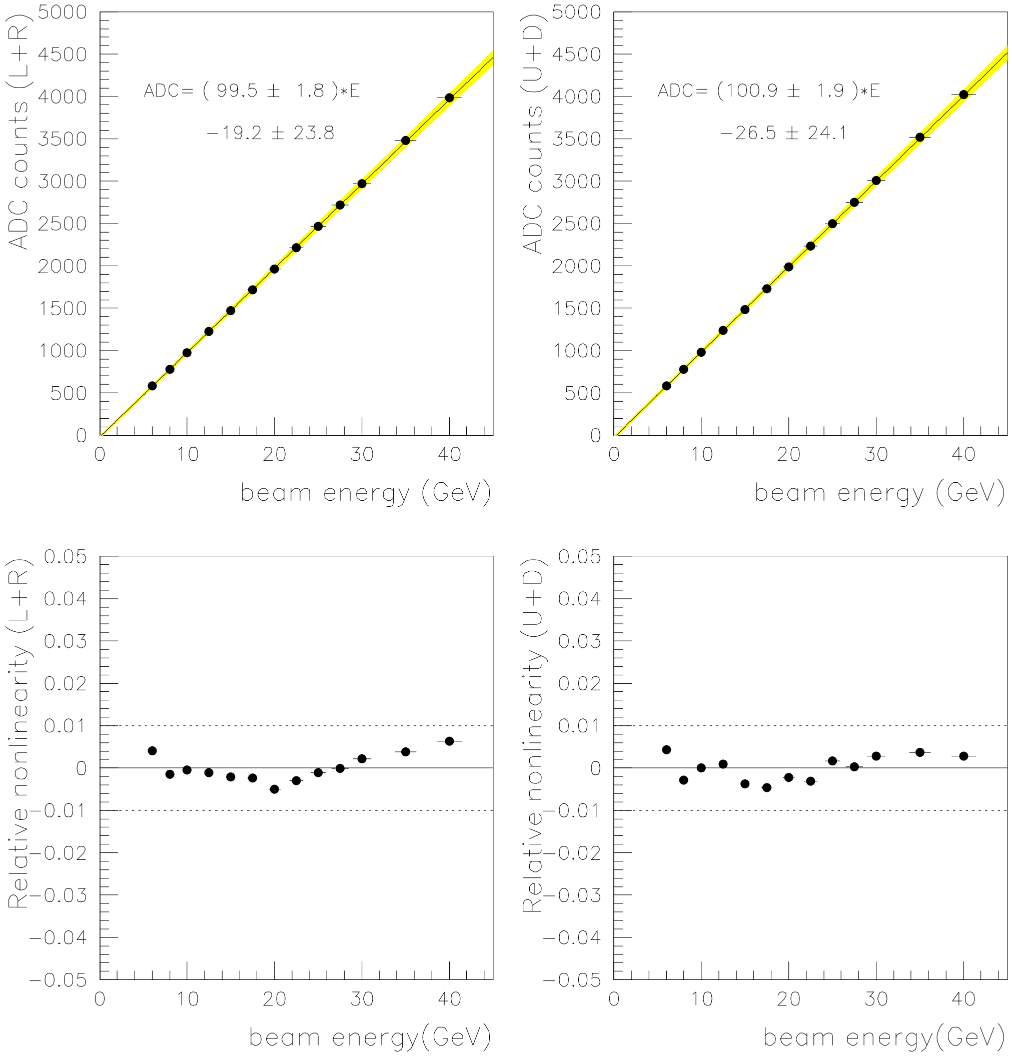

Figure 20: *Calorimeter energy linearity. Beam energy spread of 3.5% is included. The data are fitted with a linear function y=ax+b. Yellow band shows errors from the fit.*

Fig. 22 displays the $\eta - y$ correlation, where $\eta = (E_{up} - E_{down})/(E_{up} + E_{down})$, E_{up} and E_{down} are mean energy deposits of the incident particles (positron) in up and down calorimeter respectively, and y is the vertical position by the Si detector. The data are collected at 10 GeV energy of positron beam.

The η distribution slices by every 320 μm are approximated by Gaussians and a resulting 1D distribution is fitted by a 7 parameter function as displayed in upper plot of Fig. 23. The lower plot in Fig. 23 shows fit residuals. One can observe noticeable deviations around the central part. The fit imperfections are coming from a non-Gaussian nature of

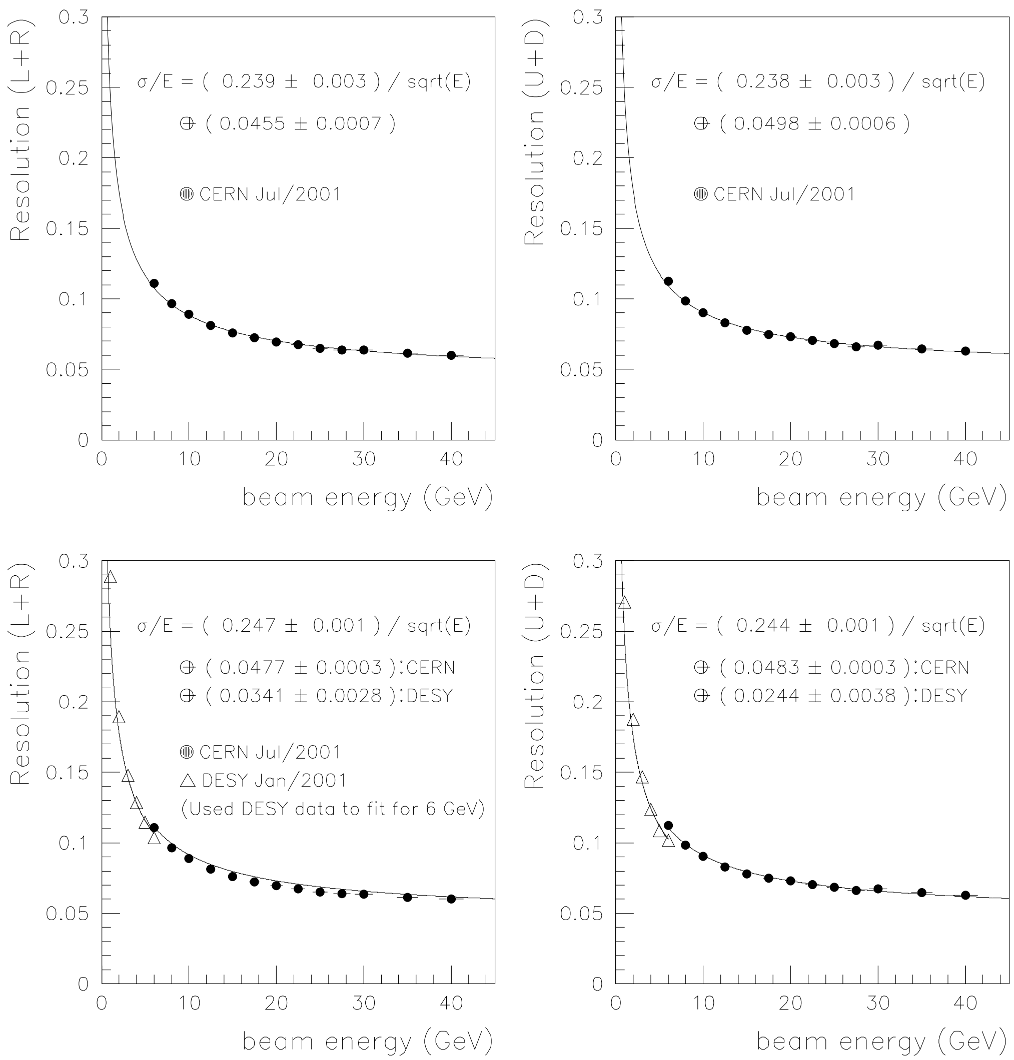

Figure 21: *Calorimeter energy resolution. The beam energy spread 5% for DESY and 3% for CERN is included. The fit was done using only CERN data (upper plots) and DESY, CERN data points (lower plots). At 6 GeV the DESY data are used since the beam energy calibration for that energy is less reliable in case of CERN data.*

the η slices which is more significant as impact point approaches the calorimeter center.

Utilizing the fitted function, a position resolution of the calorimeter as a function of the particle incident position can be calculated. The spatial resolution of the calorimeter is shown in Fig. 24, $sigma = 0.3mm$ at $y = 0$.

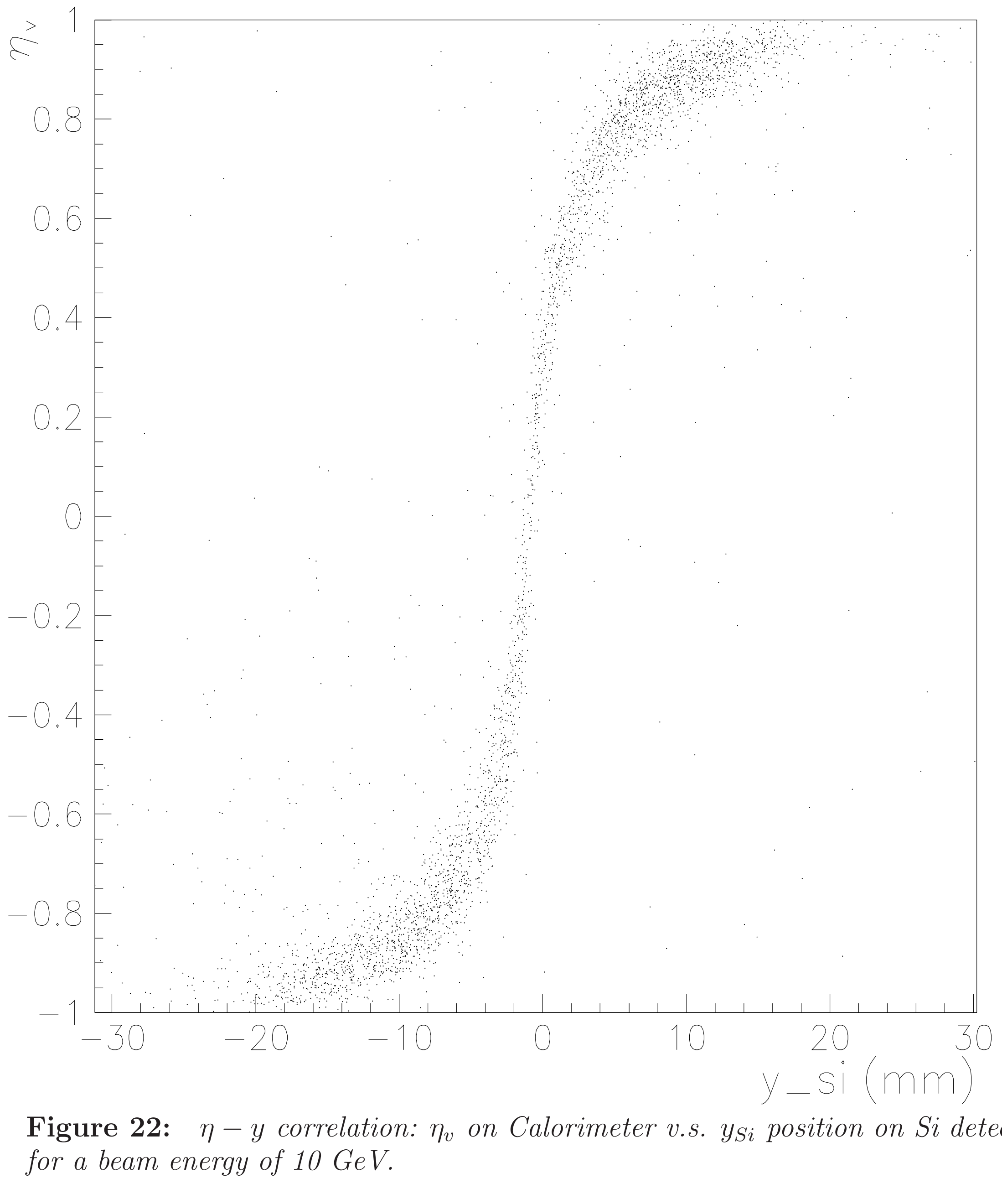

Figure 22: *$\eta - y$ correlation: η_v on Calorimeter v.s. y_{Si} position on Si detector for a beam energy of 10 GeV.*

To resume, the CERN testbeam results show good linearity and spatial uniformity of the calorimeter with energy resolution $\sigma/sqrt(E) = 24-25\%$ and spatial resolution of $0.3mm$ at $y = 0$ for 10 GeV positrons.

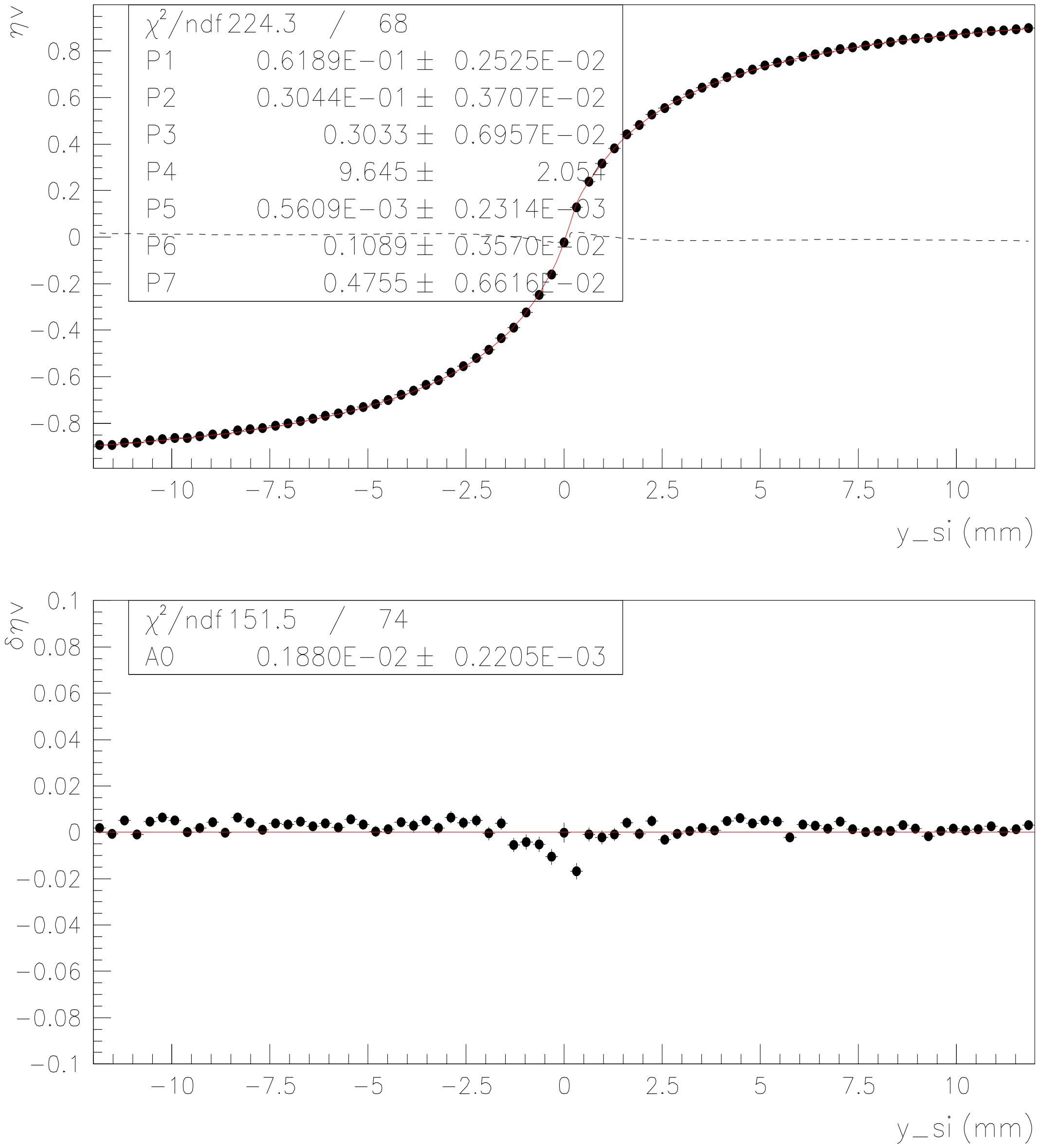

Figure 23: *$\eta - y$ transformation: η on Calorimeter v.s. y position on Si detector for a beam energy of 6 GeV. Also shown a fit by the parameterization $\eta_v(y) = \frac{|y|}{y}(1.0 + (p_1 + p_2 + p_3 + 1.0)e^{-\frac{|y|}{p_7}} - p_1 e^{-\frac{|y|}{p_4}} - p_2 e^{-\frac{|y|}{p_5}} - p_3 e^{-\frac{|y|}{p_6}})$ The residuals (lower plot) are fitted by a constant. The dashed line on the upper plot is a difference between the fit and previous CERN-96 test beam 11 GeV parameterization.*

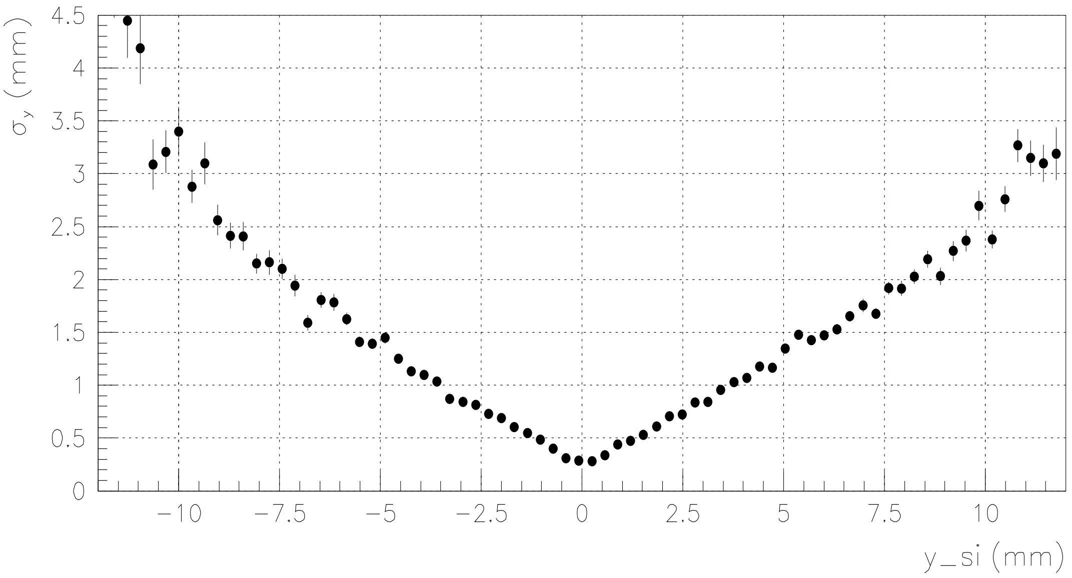

Figure 24: *Vertical position resolution σ_y as a function of the vertical position y_{Si} on Si detector.*

9 The Silicon Data Analysis and Results

9.1 The Silicon Raw Data Structure

Each silicon raw data event consists of 6*150=900 ADC numbers. There are six APV25s [2] and to each APV25 correspond 150 ADC channel numbers. These 150 numbers can be divided in 4 groups: APV25 Header numbers, APV25 analogue channel numbers, end-marker number, and the baseline numbers (see fig.25, 26). Each APV25 readout output frame has the Header part, corresponding to the first 12 numbers, which contains useful APV25 information. The Header numbers, called also digital header numbers, can have only two values: high(=1, logic 1) or low (=0, logic 0).

The first 3 Header numbers are always high (logic 1) and they are needed for the *FED Header Finding Mode*. In this operation mode, the FED recognizes the arrival of an APV25 readout output frame by receiving 3 high (logic 1) numbers in a row. Once the APV25 Header is recognized the FED captures the whole APV25 frame for digitization. The Header numbers 4-11 correspond to the APV25 pipeline digital address. The digital address is an 8 bit number (MSB first, which is the fourth number in the Header), corresponding to the APV25 pipeline address that is used to store the signal when the chip is triggered. The pipeline is 192 storage cells deep, labeled 0 to 191. The number obtained by the Header digital address is a code number (varies between 1 and 255) for the pipeline number, and it does not correspond to the pipeline position number, (see fig.26). The pipeline address is used to monitor the synchronicity of the 6 APV25 chips. That is, for a given event all 6 APV25s must have the same pipeline number in the Header, because the APV25s are triggered for readout synchronously. Header number 12 is the error bit. If an error is detected by the APV25 internal logic, the bit is set to logic 0 (low), otherwise it is always in the logic state 1 (high).

The analogue channel data is stored in the ADC numbers 13-140, corresponding to 128 APV25 analogue channels. The 768 silicon detector chip channels are readout by the 6 APV25s (768=6*128) which are bonded to the silicon.

The end-marker number (number 141) which marks the end of the analogue data region is always in logic state 1 (high). The next 9 numbers (142-150) correspond to the baseline values between two successive APV25 output frames. The baseline values have been include to monitor the baseline between successive APV25 frames.

[2] In this analysis the 6 APV25s are labeled from 1 to 6 as in the CERN test beam ntuple, however to get the proper physical strip ordering the APV25s have to be inverted: APV1 with APV2, APV3 with APV4, APV5 with APV6, i.e. APV2 in the ntuple actually corresponds physically to APV1, and the same is valid with the other 4 APV25s. The APV25 inversion is a result of how the TPOLDAQ stored the silicon FED data (ntuples) during the CERN test beam.

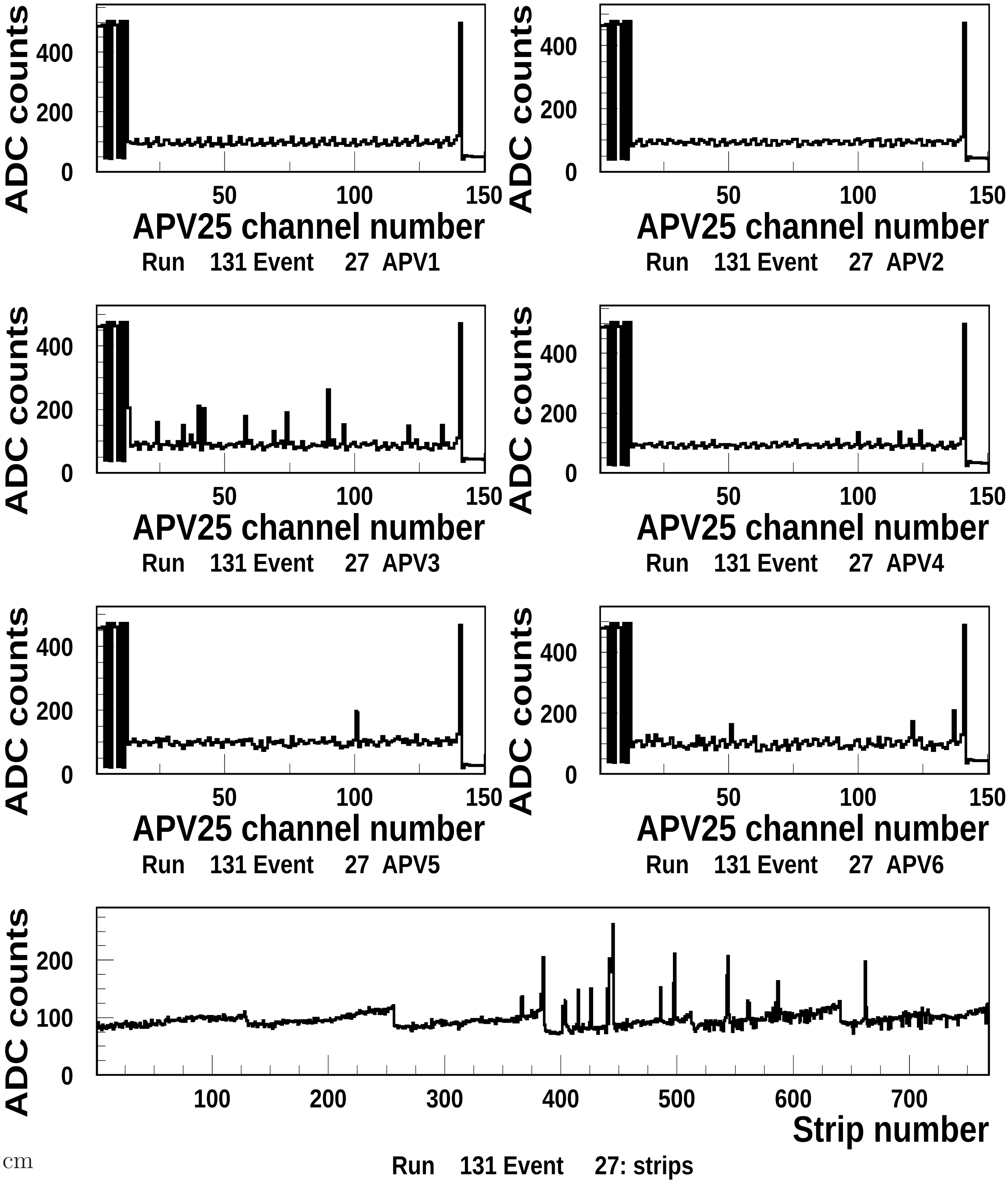

cm

Figure 25: *The typical APV25 output frames for all 6 APV25s is displayed for a signal event. The four regions can clearly be seen: APV25 Header, APV25 analogue channels, end-marker, and baseline. The lowest plot corresponds to the physical silicon chip strip ordering obtained by re-ordering the 6 APV25s. The peaks are signals corresponding to hits in the silicon.*

In the data analysis, the Header part is first checked for any errors. If an error is found the event is discarded. The possible errors are: the error bit (12) is low, or the APV25s have different pipeline numbers which would mean a dis-synchronicity of the APV25 chips. In the CERN data I have found no such errors. The silicon detector system is setup such that one would not expect to obtain such errors unless there is some hardware malfunction in the system.

The event display plots, which correspond to the APV25 output frames, for all 6 APV25 is shown in fig.25, for a given event. The four regions mentioned above can clearly be seen: APV25 Header, APV25 analogue channels, end-marker, and baseline. Signals from test beam particles incident on the silicon detector chip can bee seen in the APV25s analogue channel region (13-140); which in this case corresponds to a shower of particles. The lowest plot, displays the event display plot for the same event according to the silicon detector chip physical strip ordering obtained from the 6 APV25s after re-ordering. The raw readout from the APV25s has an internal channel ordering which does not correspond to the physical strip ordering. The see-saw structure corresponds to the 6 APV25 analogue channel areas which have been strip-wise re-ordered and plotted one next to another according to their physical position with respect to the silicon detector chip.

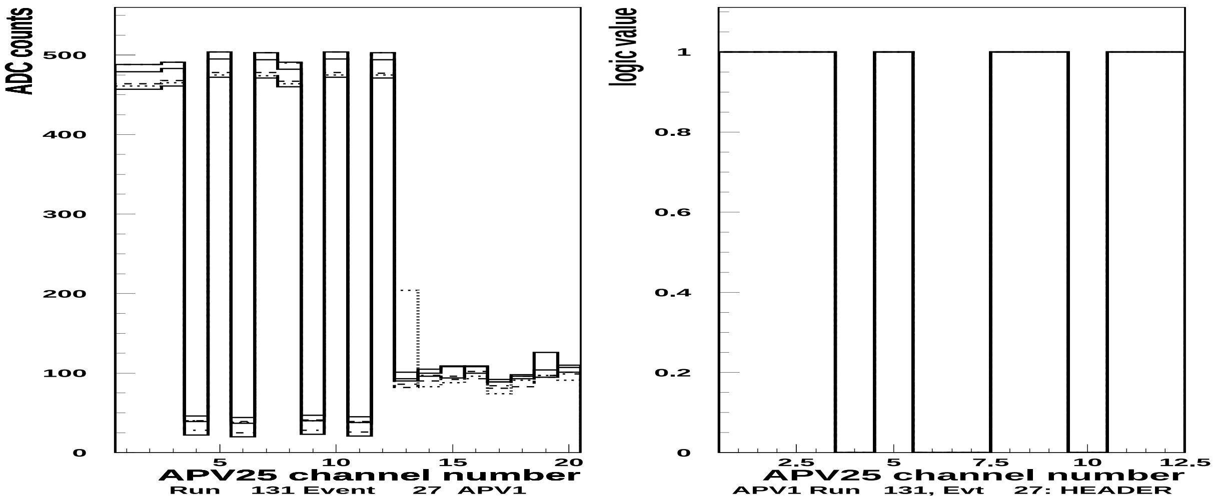

Figure 26: *Left plot, close up of the Header region. A few analogue channels are also displayed, in fact the first analogue channel (channel 13) has a signal in one of the APV25s. The Header regions of the 6 APV25s are superimposed for the same event; APV25s are synchronous and the error bit is high (no error). The Headers have the same structure,as expected for a good event. The right plot shows only the Header region for the same event with its corresponding logic values, for all 6 APV25s superimposed.*

A close up of the Header region is displayed in fig.26. The Header regions for all 6 APV25s have been superimposed (left plot); for a good given event the Header region structure is the same for the 6 APV25s. There are minor differences in the amplitudes because the APV25s output is analogue, however the corresponding digital values are identical for all 6 APV25s (right plot).

The APV25s readout parameters have been adjusted such that the APV25 analogue channel region baseline offset is positioned at about 1/5 (about 100 ADC counts) of the total end-marker or Header high (logic 1) height, which is about 500 ADC counts, for each APV25 (see fig.27). By setting the baseline offset to a small value there is enough dynamic range for the signal. A MIP corresponds to about 1/7 of the total end-marker height and the ADC range varies from 0-511 ADC counts. The APV25s analogue output frame maximum amplitude have been set, via driver board amplification (see section 5), to span the complete ADC range.

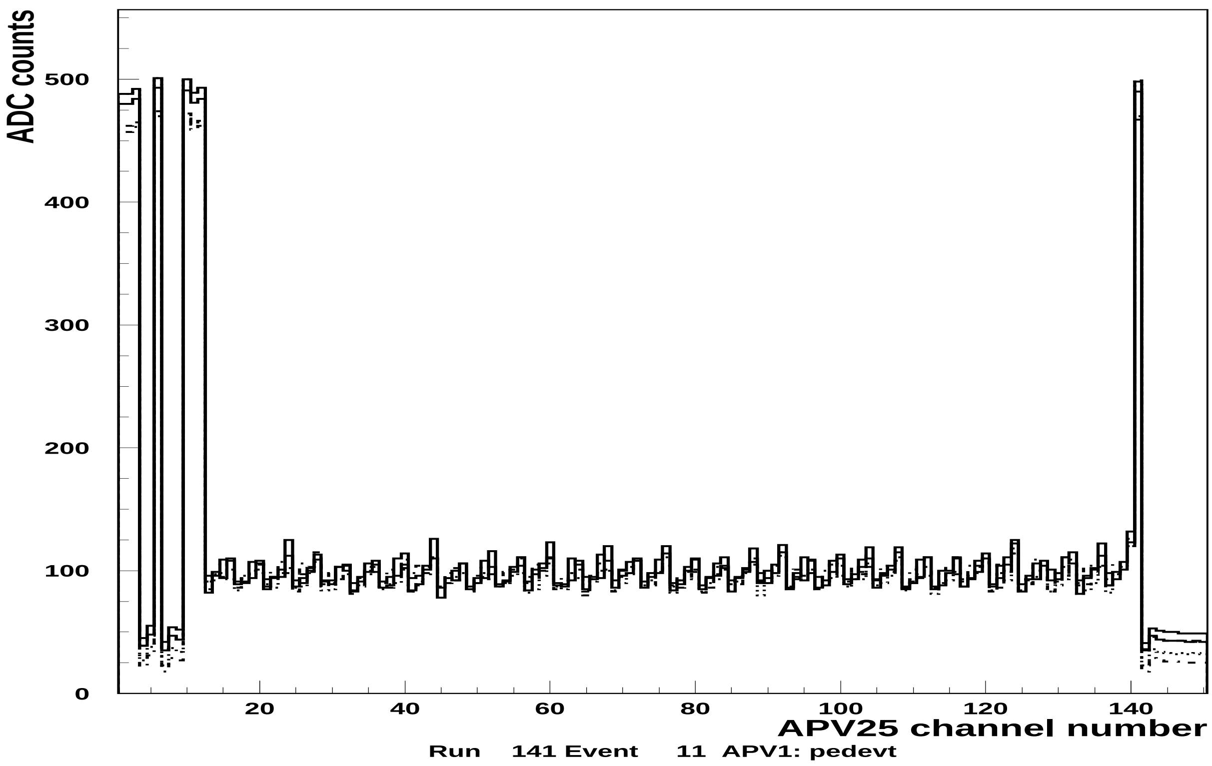

Figure 27: *The 6 APV25 readout output frames superimposed for a given pedestal event. The APV25 analogue channel region baseline offset is set at about 1/5 of the total ADC range.*

9.2 Silicon Latency

The silicon latency was calculated by taking a set of latency runs (see section 5.2). The trigger signal sent by the SEQSI to the APV25s for readout must have the correct SEQSI clock timing (clock number) to match the latency (cabling and electronics) of the silicon detector system. The correct SEQSI sequence clock number value was obtained by doing a latency scan, which meant varying the SEQSI clock number; each SEQSI clock number step corresponds to 25 nsec step. The approximate silicon latency (approximate SEQSI clock number) was calculated beforehand from the total cable lengths and delays in the silicon detector system and from previous experience. Several data runs with the same number of signal events but with different SEQSI clock number values (latencies) around the approximate SEQSI clock number were then collected. For simplicity, a 3RMS cut was used to select signal events. All signals in a given run (latency interval of 25 nsec) were summed up. The run with the highest signal was the one with the correct clock sequence number i.e. the SEQSI clock latency for the silicon detector was thus found. This clock sequence number was used in the SEQSI sequence, to send correctly timed trigger signals to the APV25s for readout, for all test-beam runs. The latency number was 60048 (SEQSI program clock numbering).

9.3 Data Runs

In this section the following data runs were used in the analysis. The table position is in millimeters.

- Runs 131 to 142: 10 GeV electrons, table position x=-7.4, y=18.7 fiber scan
- Runs 143 to 151: 10 GeV electrons, table position x=-7.4, y=(-2.7 to 38.7) table scan
- Runs 218 to 226: 20 GeV electrons, table position x=-7.6, y=(-2.7 to 38.7) table scan
- Runs 305 to 319: 10 GeV positrons, table position x=-3.7, y=20.3 fiber scan
- Runs 342 to 365: 10 GeV positrons, table position x=-3.6, y=20.3 fine fiber scan (run 346 excluded because fiber motor on which produces large noise in the silicon)
- Run 273: 27.5 GeV positrons, table position x=-5.1, y=20.3
- Run 323: 10.0 GeV positrons, table position x=-3.6, y=30.3
- Run 372: 40.0 GeV positrons, table position x=-4.1, y=20.3

9.4 Pedestals and Raw Noise

The pedestals are calculated from the pedestal events present in each data run (random pedestal trigger, see section 3 and section 5); about 1-2% of the events in a data run.

The mean *pedestal* value for a given channel is obtained by averaging over all pedestal events in a data run(s) corresponding to the channel.

The *raw noise* of a given channel is defined as the RMS of the pedestal pulse height distribution for the channel.

Below, in fig. 28 and fig. 29 the mean pedestal and raw noise versus the APV25 channel number (0 to 150) is plotted. It is calculated over a large set of runs, runs 133 to 151, corresponding to about 13 k pedestal events. The mean pedestal value for the APV25 analogue channels (13-140) is around 100 ADC counts for all 6 APV25s. The APV25 analogue channel region offset (channels 13-140) has been adjusted to this pedestal value ($\sim$100 ADC counts) for all 6 APV25s (see section 9.1).

The first 12 APV25 channels correspond to the Header part. These channels have high RMS values because only two possible values are possible (digital header): low or high. The last 10 channels (end-marker and baseline) are expected to be very stable, resulting in low RMS values. The raw noise is somewhat high because of contamination with physics events of the pedestal sample. The raw noise value may reach high values (up to $\sim$35 ADC counts) typically for the dead strips, also because of stray noise pickup. There is contamination with physics events in the pedestal due to the fact that the pedestal trigger electronics which was used, was not completely safe; sometimes a pedestal trigger actually contains a physics event.

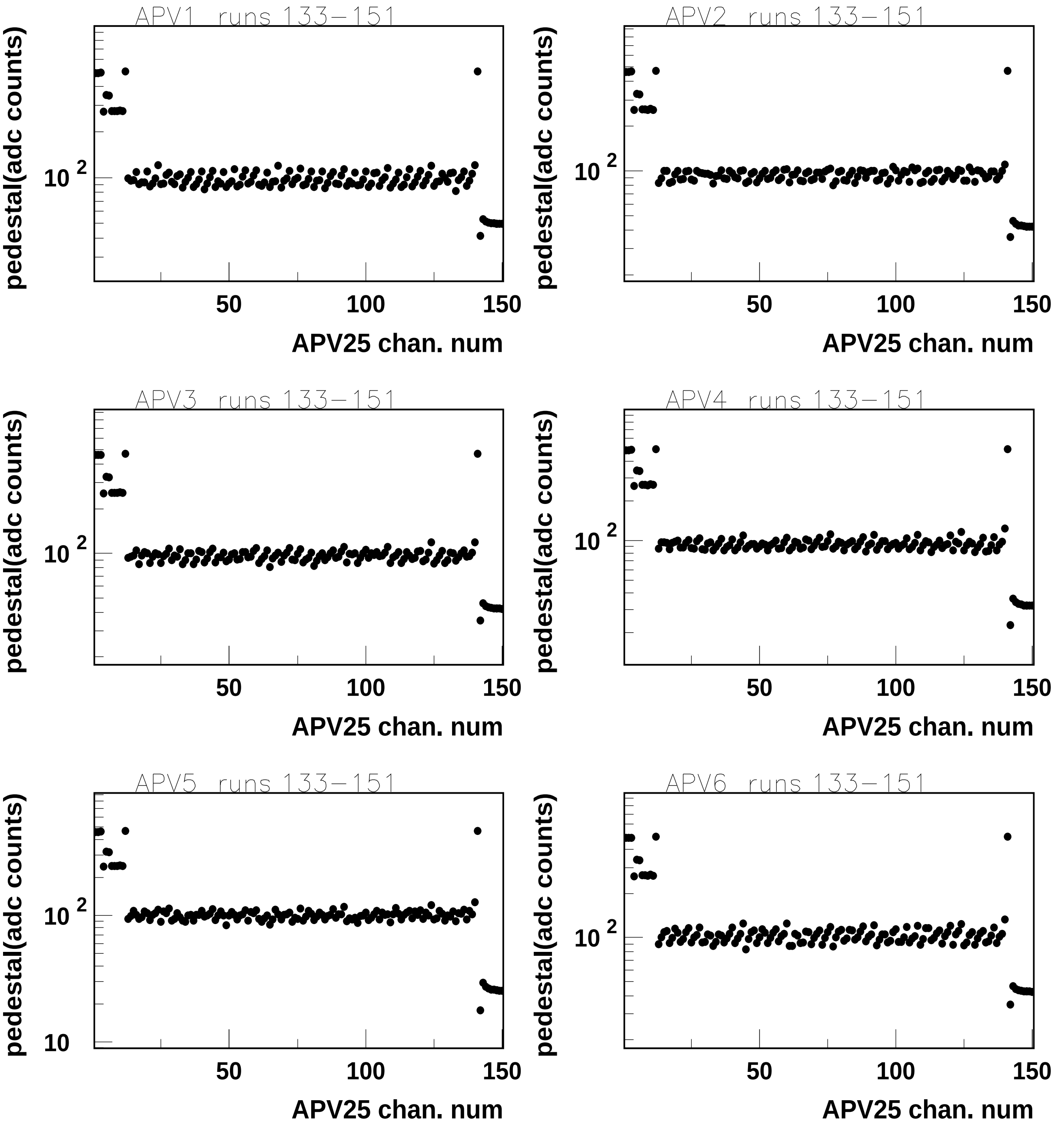

Figure 28: *The mean pedestal value versus the APV25 channel number (0 to 150), for all 6 APV25s. The first 12 APV25 channels correspond to the Header part, while the last 10 APV25 channels correspond to the end-marker and baseline. The pedestal is calculated over a large set of runs, runs 133 to 151, containing about ∼13 k pedestal events.*

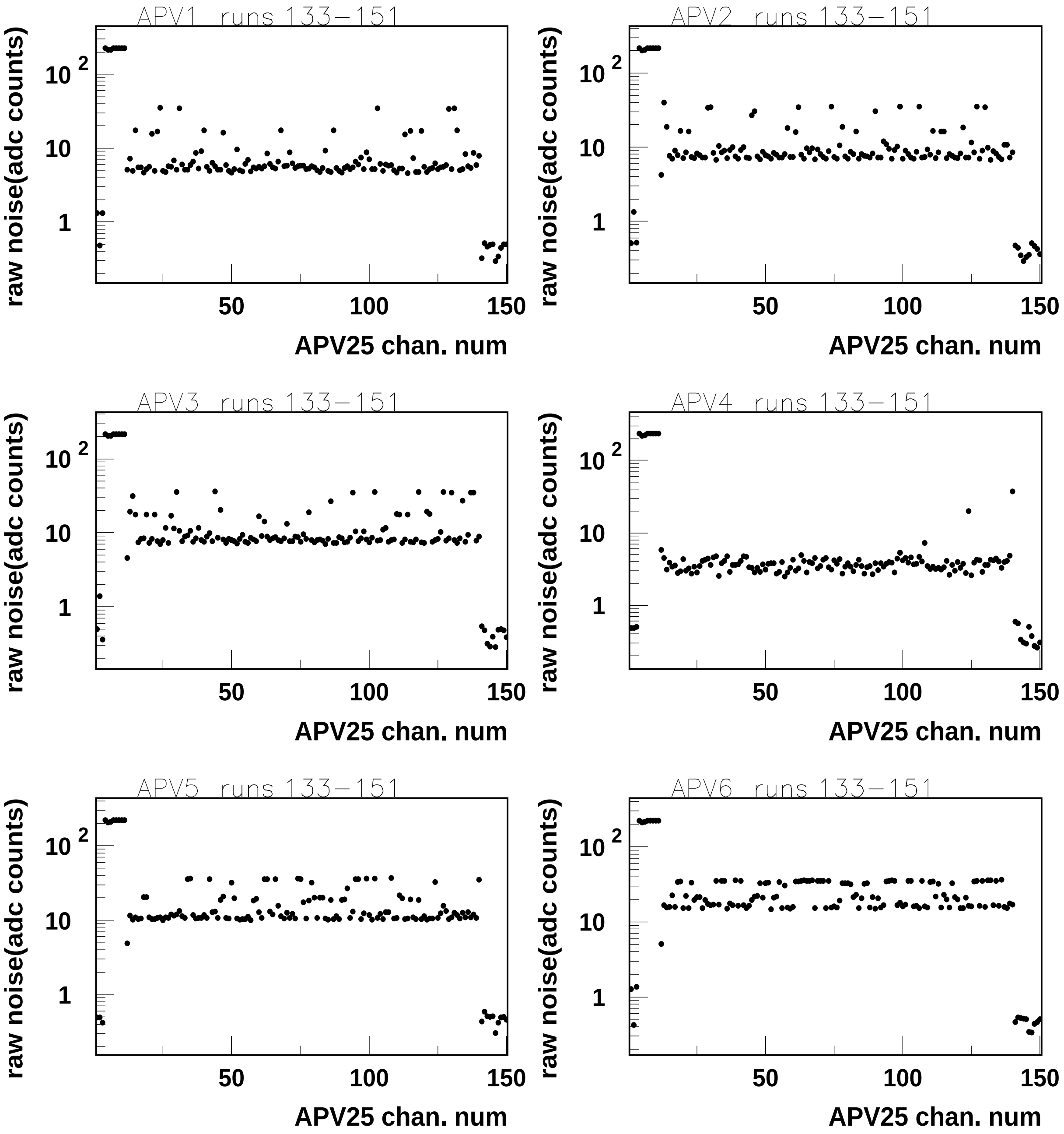

Figure 29: *The raw noise value versus the APV25 channel number (0 to 150), for all 6 APV25s. The first 12 APV25 channels correspond to the Header part, while the last 10 APV25 channels correspond to the end-marker and baseline. The raw noise is calculated over a large set of runs, runs 133 to 151, containing ∼13 k pedestal events.*

The contamination percentage is low, $\sim$1% of the pedestal sample. This contamination is removed later on, when calculating the Common Mode, noise and signals, by introducing a cut which eliminates the high ADC count events from the pedestal and RMS calculation i.e. if greater then the mean pedestal value plus a given number of ADC counts, which corresponds to events out of the pedestal area. There can still be, a little contamination of physics events with this cut, but the high ADC count (physics events) events which give rise to a high RMS value, are eliminated from the pedestal and noise calculation. In fig. 30 one can clearly see that the large RMS value is due to physics contamination. The upper two plots show the pulse height distribution for pedestal events for two typical APV25 channels (APV1 channel 84 and APV4 channel 59, which are live channels) for the large set of runs (runs 133 to 151); the two lower plots are the same but only for one run (run 372). In this case (run 372) there is little physics contamination for the two APV25 channels, because the data set is much smaller, lowering the probability of finding some contamination.

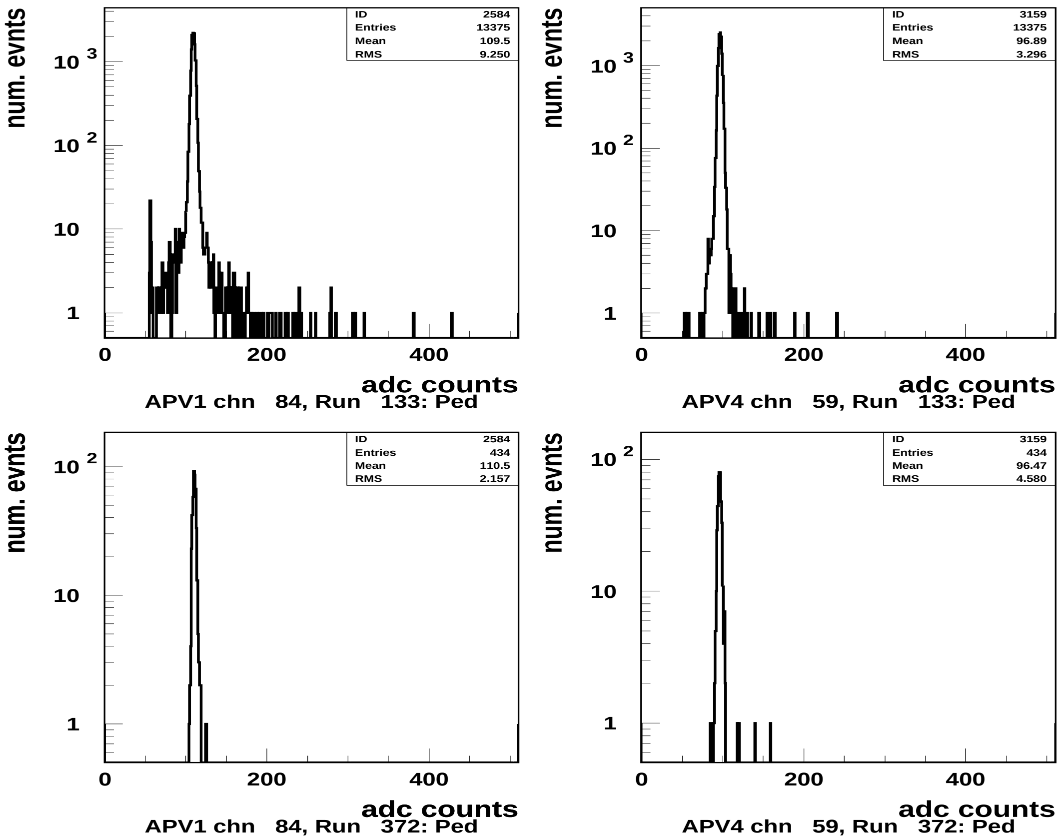

Figure 30: *The pulse height distribution for pedestal events; for two APV25 channels. The two top plots correspond to the large set of runs, runs 133 to 151 (only the first run number is written) while the two lower plots to run 372.*

A zoom-in plot of the mean pedestal value versus the APV25 channel number, for four different pedestal data sets, is shown in fig. 31 and fig. 32, for APV25 1 to 6. The APV25 channel number is limited to the APV25 channel analogue region which corresponds to channels 13 to 140. The runs have been chosen to span the complete data range collected during the test beam, which corresponds to runs taken some days apart.

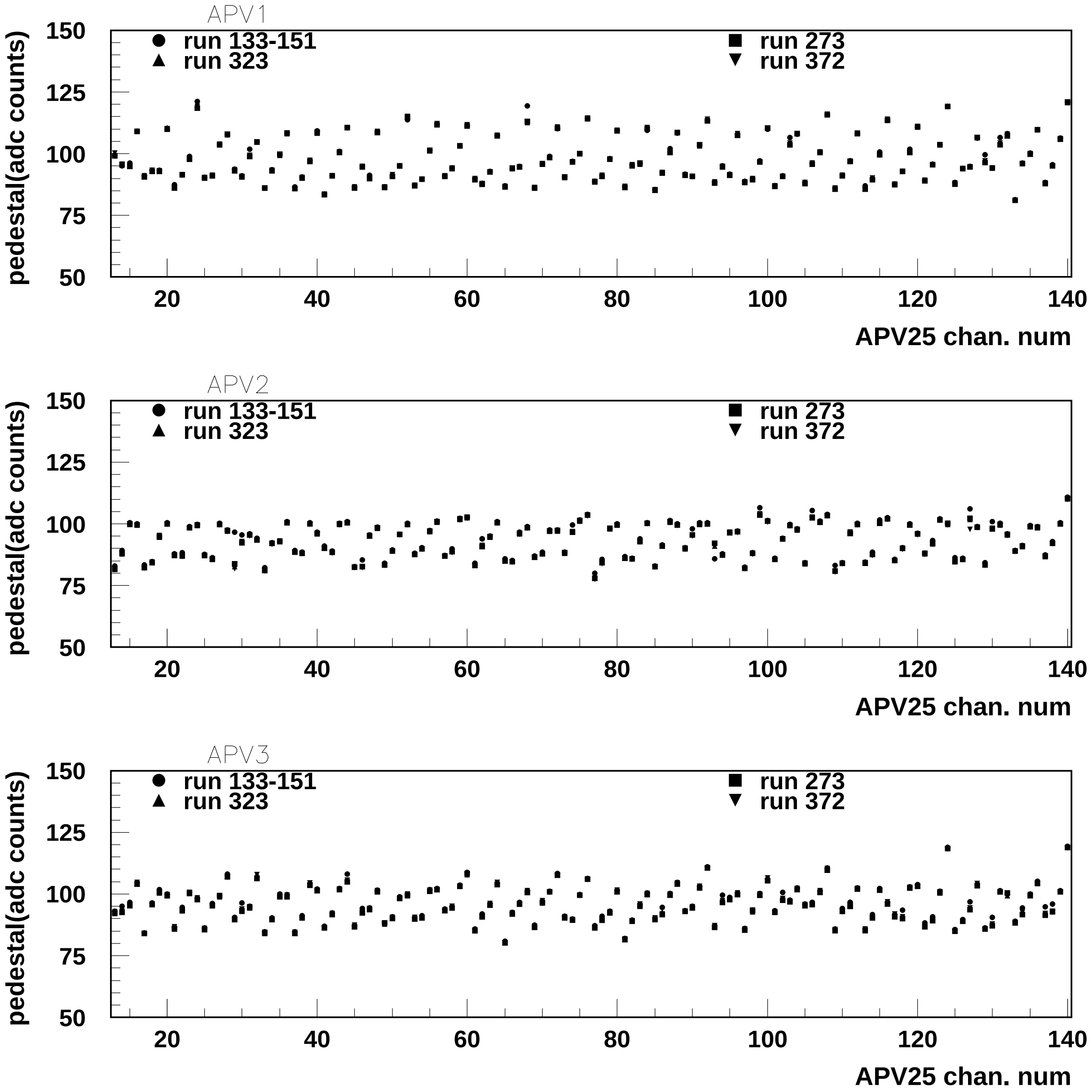

Figure 31: *The mean pedestal value versus the APV25 channel number, for APV25 1 to 3. The APV25 channel number range varies only from 13 to 140, corresponding to the APV25 channel analogue region. Four data run sets are plotted.*

Runs 273, 323, and 372, are typical test beam runs containing between 20k and 50k events (pedestal + physics). For comparison also a large data set is included, runs 133 to 151, about 565k events (pedestal + physics). The mean pedestal value varies little from run to run, indicating that the pedestal is quite stable, over the whole test beam period.

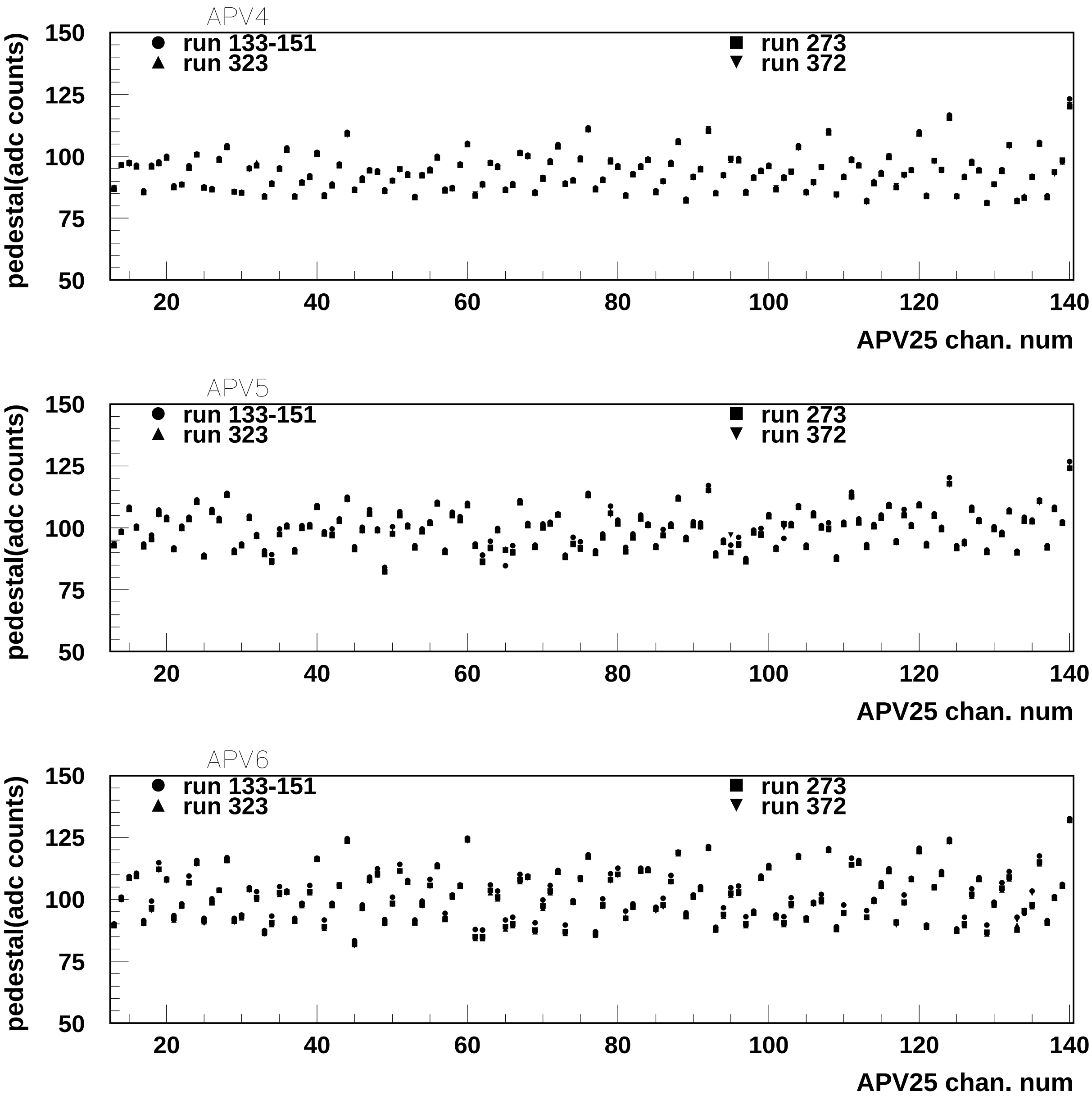

Figure 32: *The mean pedestal value versus the APV25 channel number, for APV25 4 to 6. The APV25 channel number range varies only from 13 to 140, corresponding to the APV25 channel analogue region. Four data run sets are plotted.*

The raw noise value versus the APV25 channel number, for all 6 APV25s and for the four data run sets is shown in fig. 33. The larger RMS values correspond mainly to the large runs data set (runs 133 to 151), typically for the dead strips. Typically the dead strips have the higher raw noise values. The raw noise is on average higher for APV25 6, which is also the APV25 with the highest number of dead strips, instead APV4 which contains only one dead strip (channel 140) has on average the lowest raw noise values (see section 10 on dead strip study).

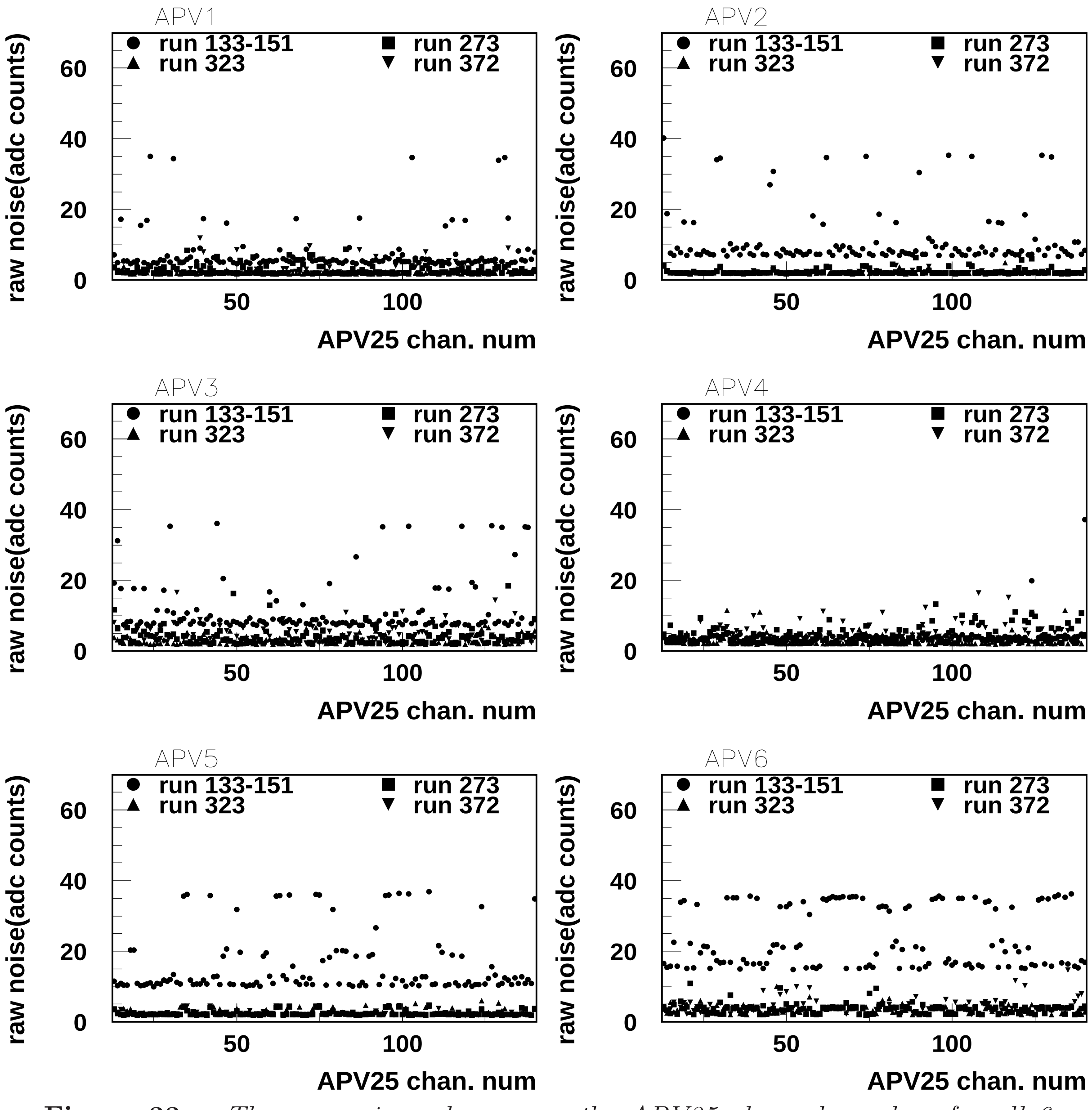

Figure 33: *The raw noise value versus the APV25 channel number, for all 6 APV25s. The APV25 channel number range varies only from 13 to 140, corresponding to the APV25 channel analogue region. Four data run sets are plotted.*

In the plots of fig. 34 the mean pedestal and raw noise are plotted versus the silicon strip number, for the 4 data sets superimposed. The mean pedestal value increases with the strip number, for each APV25; producing a see-saw structure. This is a normal characteristic of the APV25 readout chips. One can clearly see the structure for the 6 APV25s. The APV25s are plotted according to the physical strip order (APV25: 2,1,4,3,6,5). The mean pedestal value is quite stable over time. The raw noise versus silicon strip number has a more complicated structure due to the physics contamination in the sample and dead strips (noise pickup), already discussed previously.

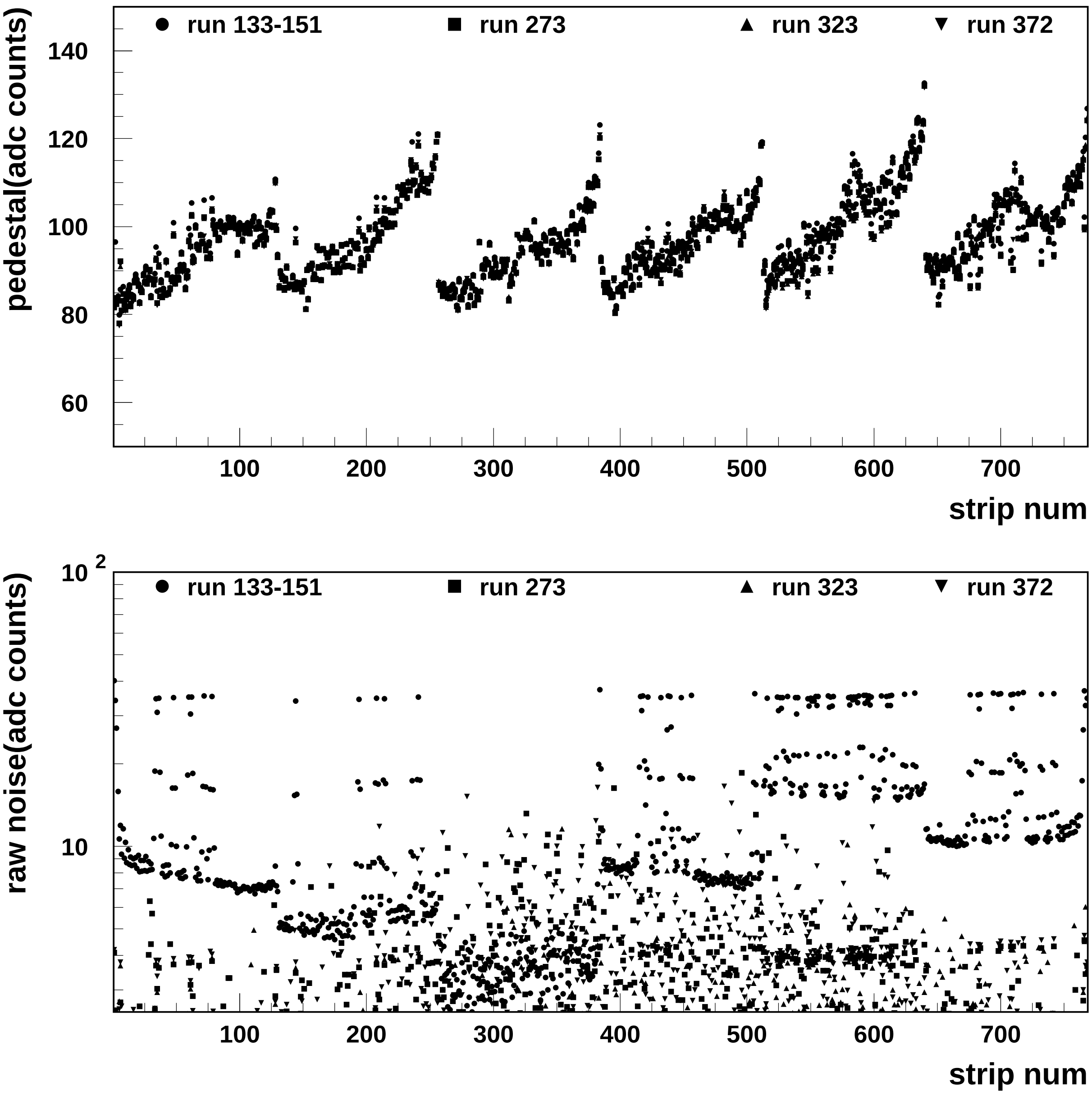

Figure 34: *The mean pedestal value and raw noise value in ADC counts plotted versus the silicon strip number, for the four data sets.*

The typical mean pedestal, raw noise, and raw noise versus mean pedestal distributions are displayed in figs. 35, 36, and 37. The distributions for all 6 APV25s are plotted. A typical run was chosen i.e. run 273. The mean pedestal distribution is centered around 100 ADC counts as expected.

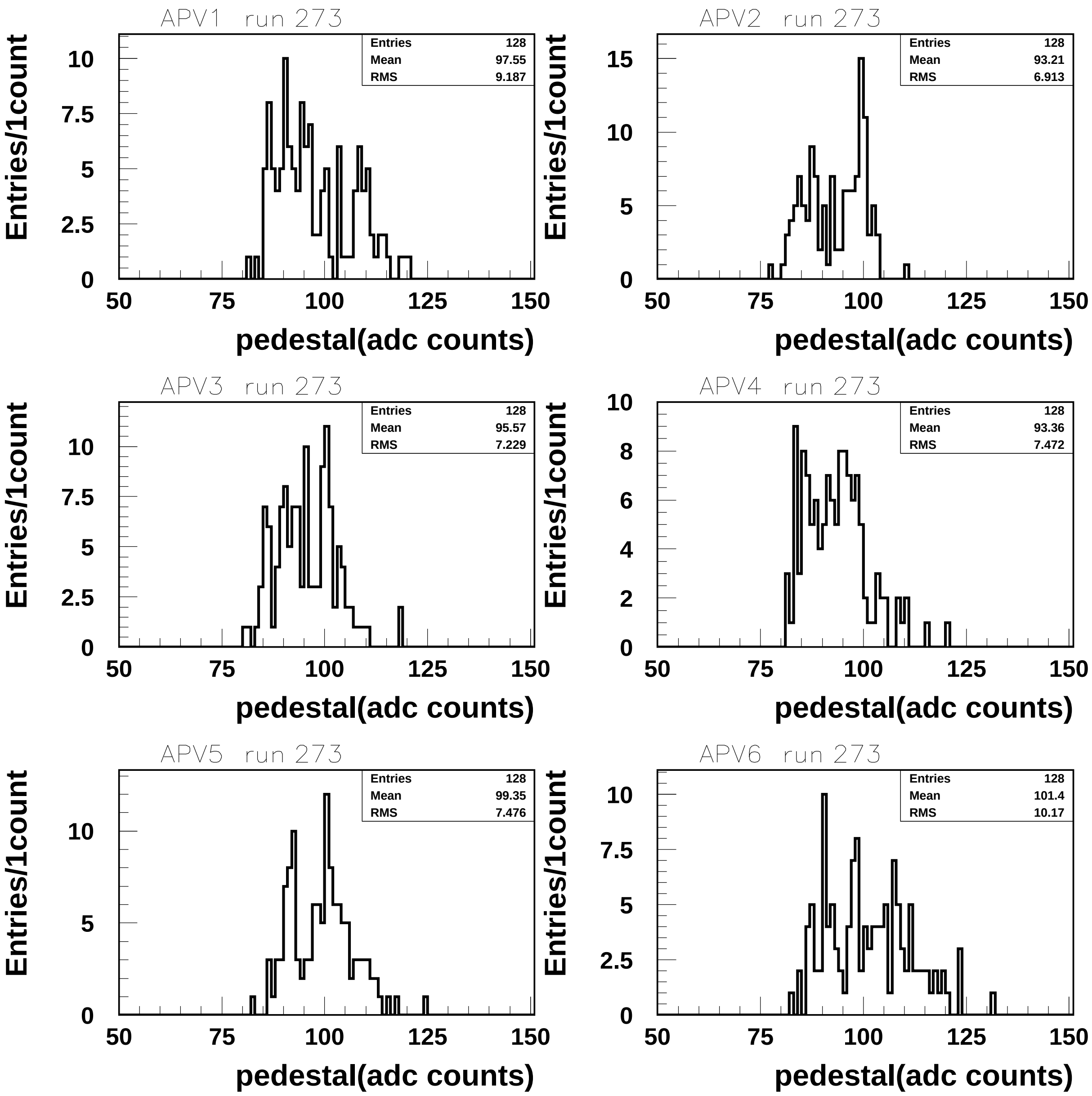

Figure 35: *The typical mean pedestal distribution for all 6 APV25s, for a typical run: run 273 with 50k events (physics + pedestal). The pedestal sample is 1% of the total data sample.*

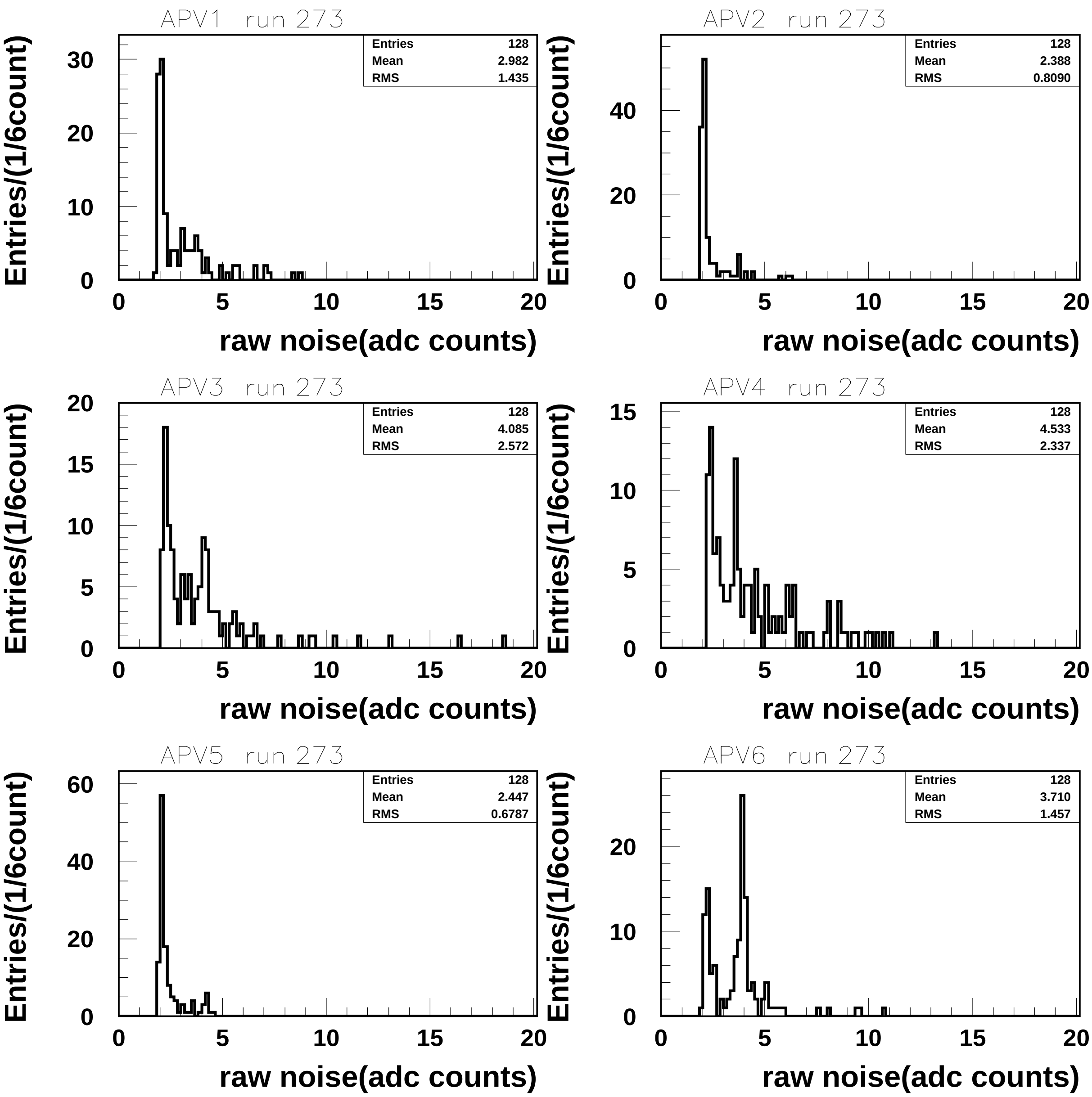

Figure 36: *The typical raw noise distribution for all 6 APV25s, for a typical run: run 273 with 50k events (physics + pedestal). The pedestal sample is 1% of the total data sample.*

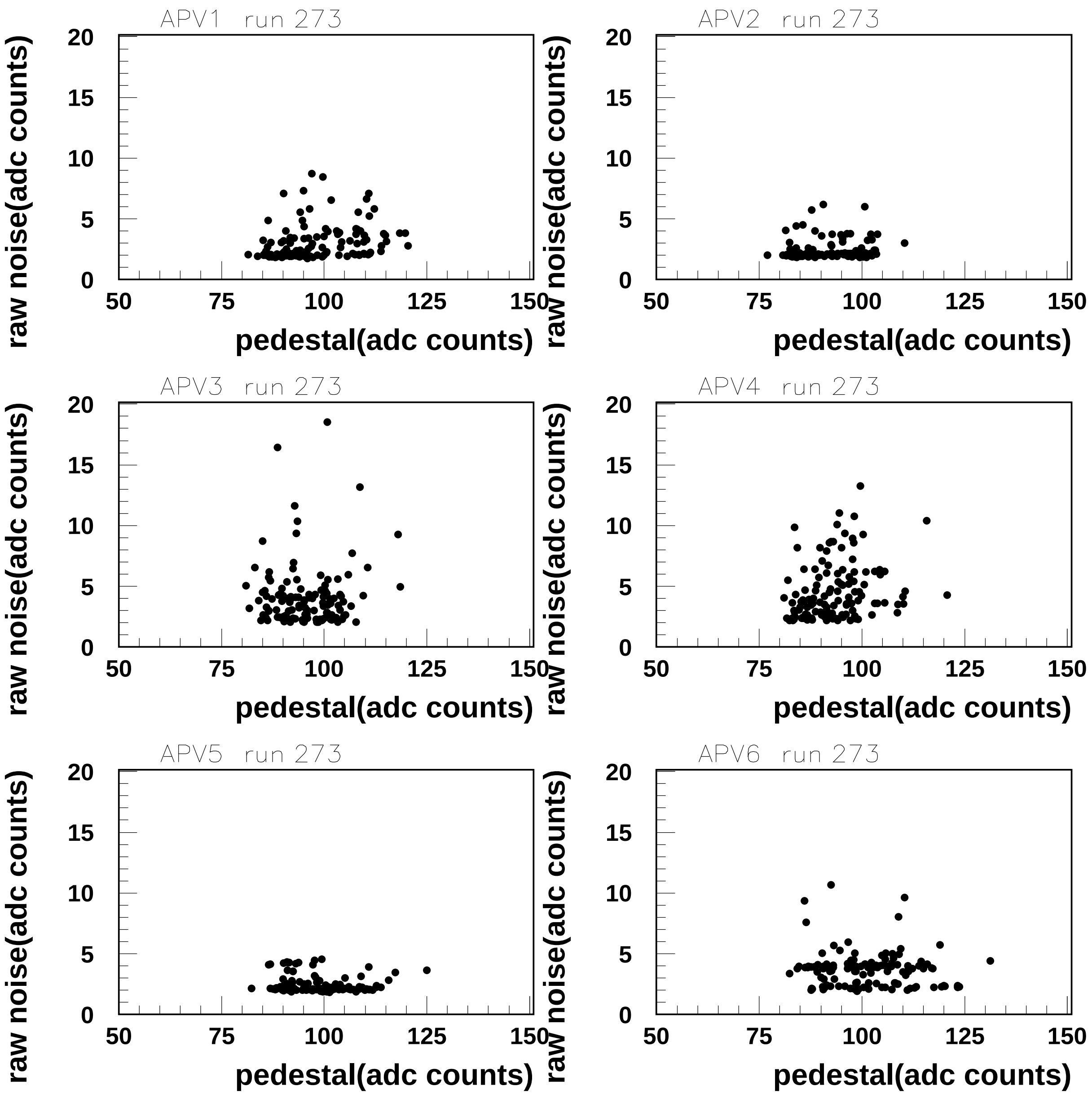

Figure 37: *The typical raw noise versus mean pedestal distribution for all 6 APV25s, for a typical run: run 273 with 50k events (physics + pedestal). The pedestal sample is 1% of the total data sample.*

9.5 Common Mode Correction

A common mode subtraction (symbolized by CM) is applied to correct for the baseline shift of the whole APV25 analogue output frame. The baseline fluctuation is mainly due to power supply variations and noise pickup. The CM correction is calculated for each APV25, considering all 128 strips. The dead strips are also included for simplicity, and because they are also affected by the baseline fluctuation. The CM is calculated by finding for each event the average raw ADC value of all strips that do not have a signal, but are within the noise limit. All strips that have a raw ADC count value within 4 RMS of the mean pedestal value are considered in the CM calculation. In fig. 38 the typical CM distribution (baseline shift) is shown for a pedestal sample of events (large data set, runs 133 to 151). The CM distribution is approximately Gaussian when considering the central part of the distribution. A physics contamination cut is applied on the pedestal sample before calculating the Common Mode to remove physics events from the pedestal sample, see section 9.4.

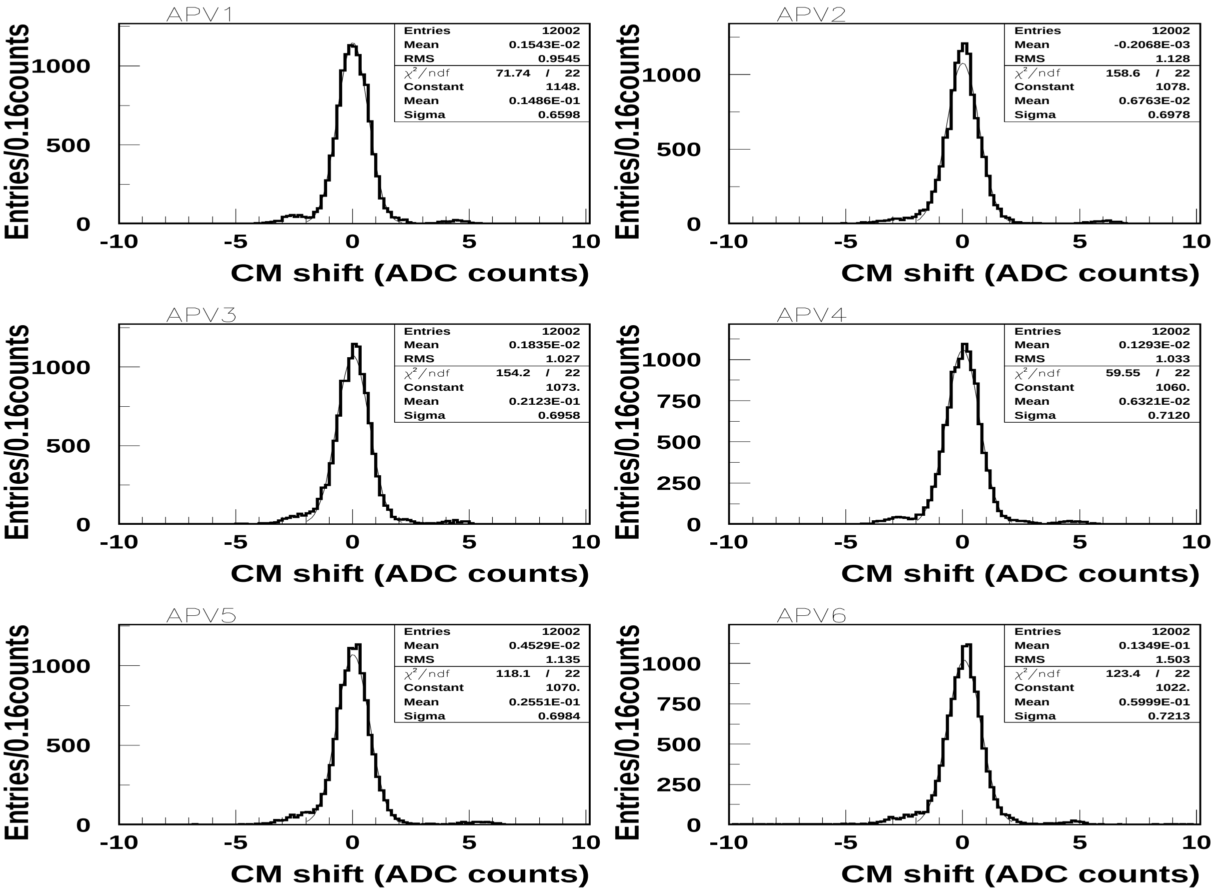

Figure 38: *The common mode baseline shift (CM) for all 6 APV25, for runs 133 to 151.*

9.6 Noise

First we present and define some terminology regarding silicon pulse height, noise and signals, which will be used throughout the next sections. The terminology is referred to strips (physical order) rather than channels (APV25 order). From now on the pedestal sample has the physics contamination cut applied.

Strip Pulse Height PH_i: For each data event in a run the pulse height PH_i for strip i is calculated from the following equation:

$$PH_i = ADC_i - PED_i - CM \tag{12}$$

where:
ADC_i = raw ADC counts in strip i;
PED_i = mean pedestal value in ADC counts, averaged over all pedestal events in the run, for strip i;
CM = Common Mode baseline shift correction for the event.

Strip Noise Definition N_i: The noise of a given strip i.e. strip noise N_i, is calculated as the RMS of PH_i for pedestal events i.e. the RMS of the strip i pedestal pulse height distribution:

$$N_i = RMS(PH_i) \tag{13}$$

where $PH_i = ADC_i - PED_i - CM$ for pedestal events.
The strip noise has the pedestal and CM shift is subtracted from the raw ADC counts, when calculating it.

Signal Definition S_i: For a given event, strip i is considered to have a signal S_i, if the PH_i value is greater the four times the RMS of the strip noise N_i:

$$S_i = PH_i > 4 * N_i. \tag{14}$$

In fig. 39 the raw pedestal distributions (no physics contamination cut) and the corrected pedestal (contamination cut, CM subtraction and mean pedestal subtraction applied) samples is shown, for two typical APV25 channels. The RMS clearly improves when the contamination cut, CM and mean pedestal subtraction are applied. The RMS of the raw pedestal distribution corresponds to the raw noise of the channel, while the RMS of the corrected pedestal distribution corresponds to the noise of the channel, in the present terminology. The corrected pedestal distributions are centered around 0 as expected. The corrected pedestal distributions are quite well fitted by a Gaussian.

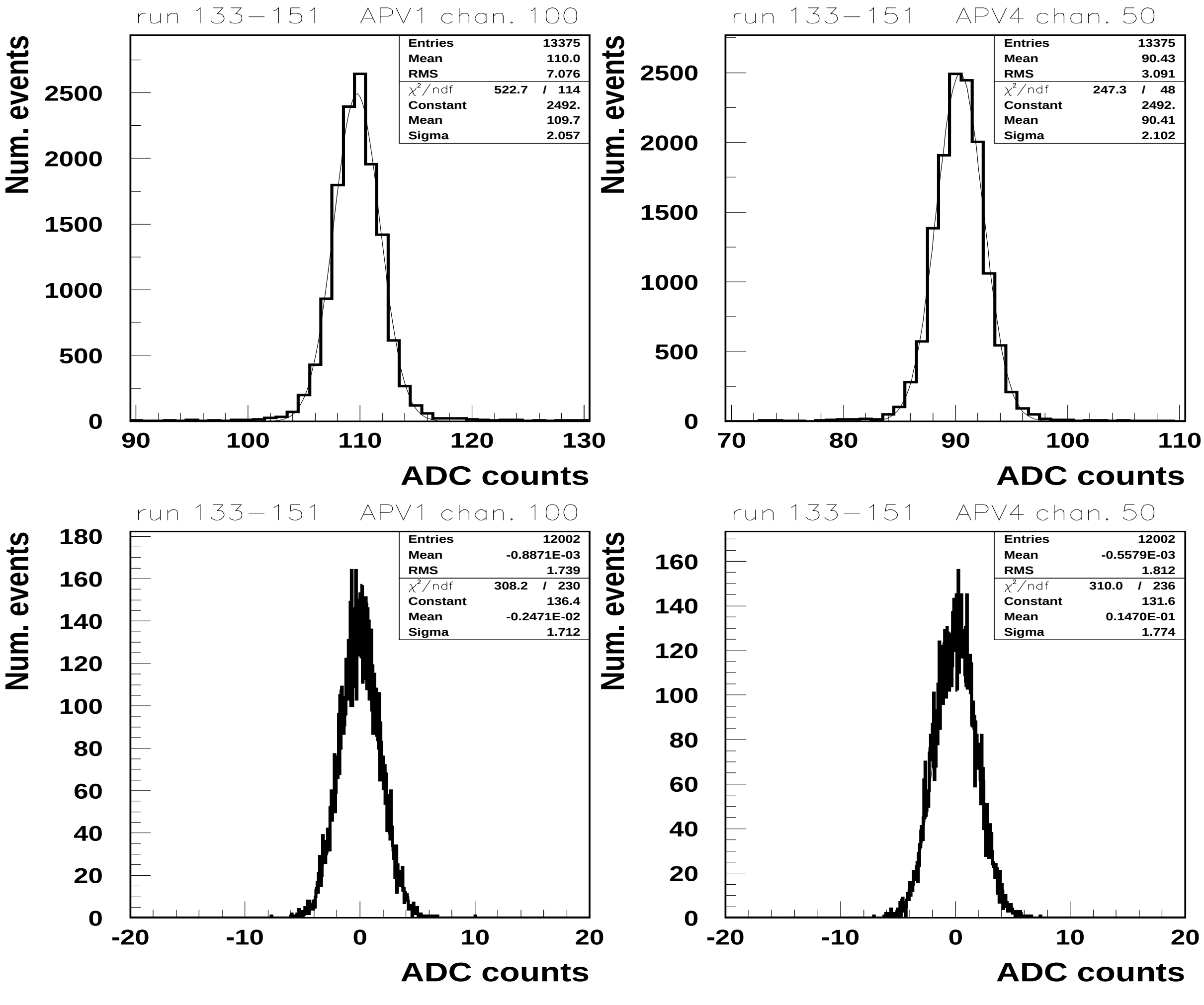

Figure 39: *The two top plots correspond to the typical raw pedestal distribution, with no cut applied, for two typical APV25 channels. The two lower plots correspond to the typical corrected pedestal distribution for the same two APV25 channels, with the contamination cut, CM, and mean pedestal subtraction applied. The data set used is the large data set run (runs 133 to 151). A Gaussian is fitted on the complete pedestal distributions for comparison.*

In the plots of fig. 40 the mean pedestal (contamination cut applied) and noise are plotted versus the silicon strip number. The pedestal plot is for the 4 data sets superimposed, while for the noise there are two plots, for clarity. The mean pedestal value increases with the strip number, for each APV25; producing a see-saw structure as expected and is quite stable over time. The APV25s are plotted according to the physical strip order (APV25: 2,1,4,3,6,5). From the plot noise versus strip number, one can see that the typical strip noise is around 2 ADC counts, except for the dead strips where the strip noise rises to values around 4 ADC counts. One can easily identify the dead strips by looking at the high strip noise values in the plot. The plot noise versus strip number for the large data set run (runs 133 to 151) has been plotted separetly from the other three data sets for clarity. Also in this plot the strip noise is around 2 ADC counts, except for the dead strips where the strip noise rises to values up to 6 ADC counts. This is because the data set is much larger, with some of its runs containing dead strips which picked up more noise.

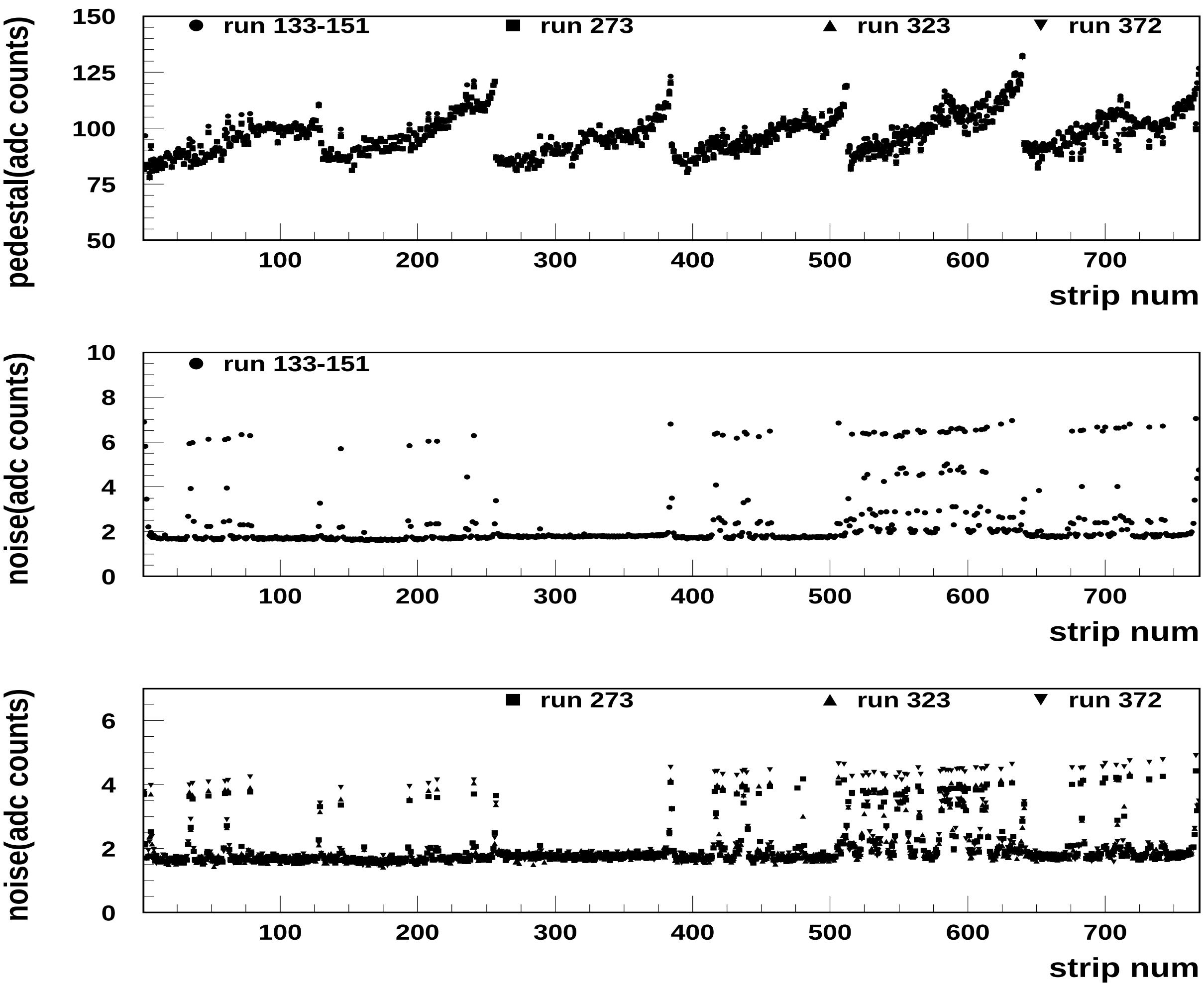

Figure 40: *The mean pedestal value and noise value in ADC counts plotted versus the silicon strip number, for the four data sets.*

The typical noise, and noise versus mean pedestal distributions are displayed in figs. 41 and 42. The distributions for all 6 APV25s are plotted. A typical run was chosen i.e. run 273. The high RMS values correspond to dead strips. APV25 number 6 (physical order 5 in fig. 40) has the highest number of dead strips. The mean strip noise for the 6 APV25s is around 2 ADC counts.

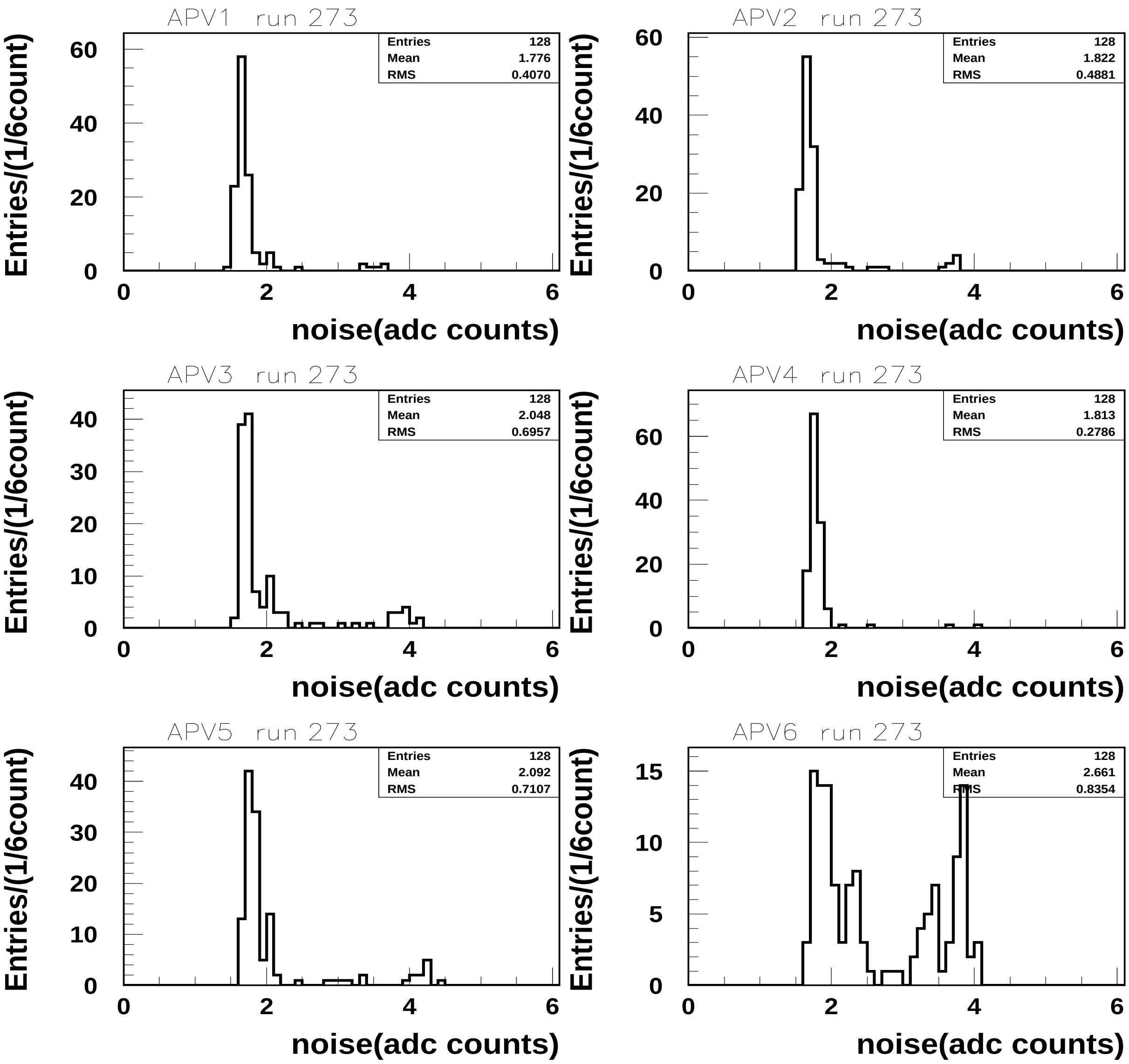

Figure 41: *The typical noise distribution for all 6 APV25s, for a typical run: run 273 with 50k events (physics + pedestal). The pedestal sample is 1% of the total data sample.The high RMS values correspond to dead strips.*

The noise versus pedestal distribution is tendentially flat, where it not for the dead strips which have a higher strip noise value.

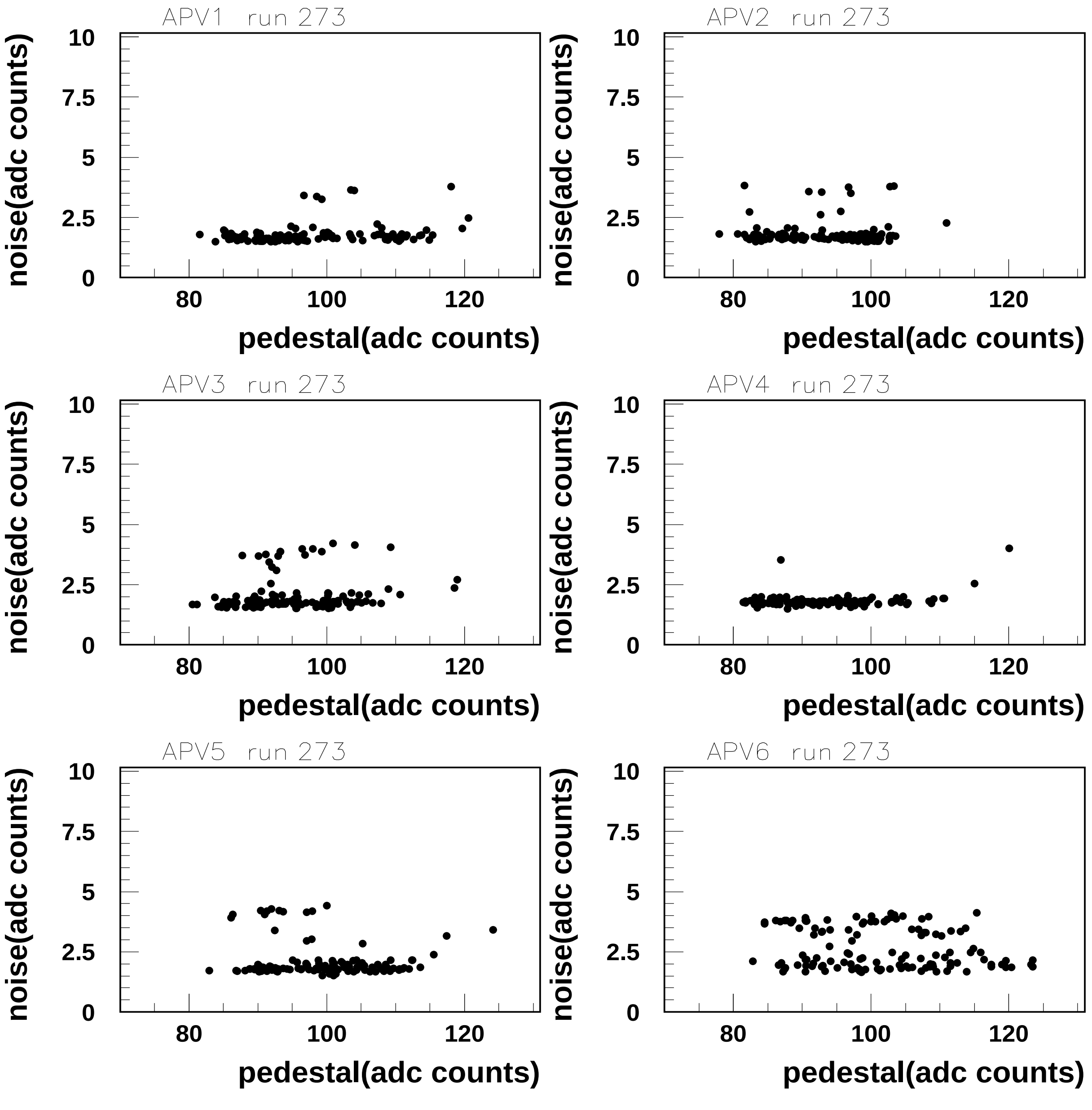

Figure 42: *The typical noise versus pedestal distribution for all 6 APV25s, for a typical run: run 273 with 50k events (physics + pedestal). The pedestal sample is 1% of the total data sample.*

9.7 Signals

In this section physics events will be considered i.e. events that are triggered by the scintillator trigger counters (physics trigger), and not by the pedestal artificial trigger (pedestal trigger).

The APV25 digital header pipeline number is approximately uniformly distributed over all 192 possible pipeline numbers, which is to be expected, if the events are randomly distributed with respect to the pipeline clock counter. The pipeline is 192 pipeline storage cells deep (see section 5.1). The pipeline numbers obtained from the digital header range between 32 to 127, and 160 to 255, giving a total of 192 numbers. The number obtained by the Header digital address is a code number for the pipeline number, and it does not correspond to the pipeline position number. In fig. 43 the digital header pipeline numbers are displayed for the long data set run (runs 133 to 151) for physics events and for all 6 APV25s superimposed. The APV25s must have the same pipeline numbers for a given event, because they are readout simultaneously, if not then there is a readout error, and the event should be discarded. No such cases have been seen in the CERN test beam data; each event is checked for that all 6 APV25s have the same pipeline number.

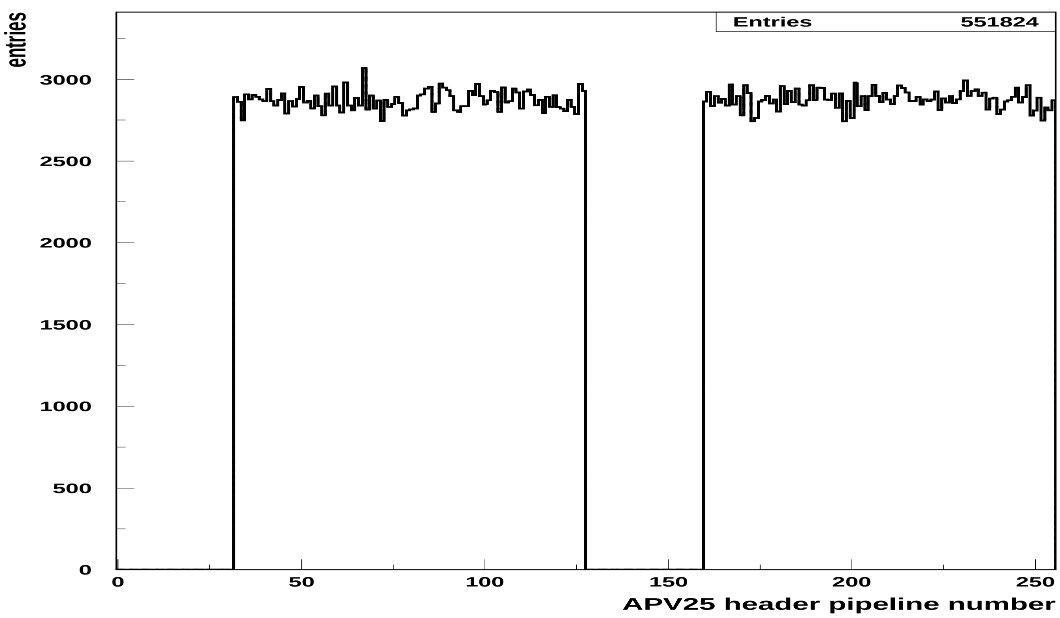

Figure 43: *The APV25 Header pipeline numbers are plotted for all 6 APV25s superimposed, for runs 133 to 151 for physics events. The plot displays the number of entries per one integer unit pipeline number.*

The typical raw pulse height distribution for physics events is shown in fig. 44 for two APV25 channels. The pedestal peak is centered around 100 ADC counts. The pedestal peak contains many more events then the rest of the raw pulse height distribution, because a hit in the silicon will give rise to signals only in a few strips, so that for a given strip only some very small fraction of its physics data raw pulse height distribution events will correspond to a hit (i.e. signal in the strip), most events will fall in the pedestal region, because some other strips are hit. Also some strips will have more signals (hits) on average, than other strips depending on the beam profile and beam position, with respect to the strip position.

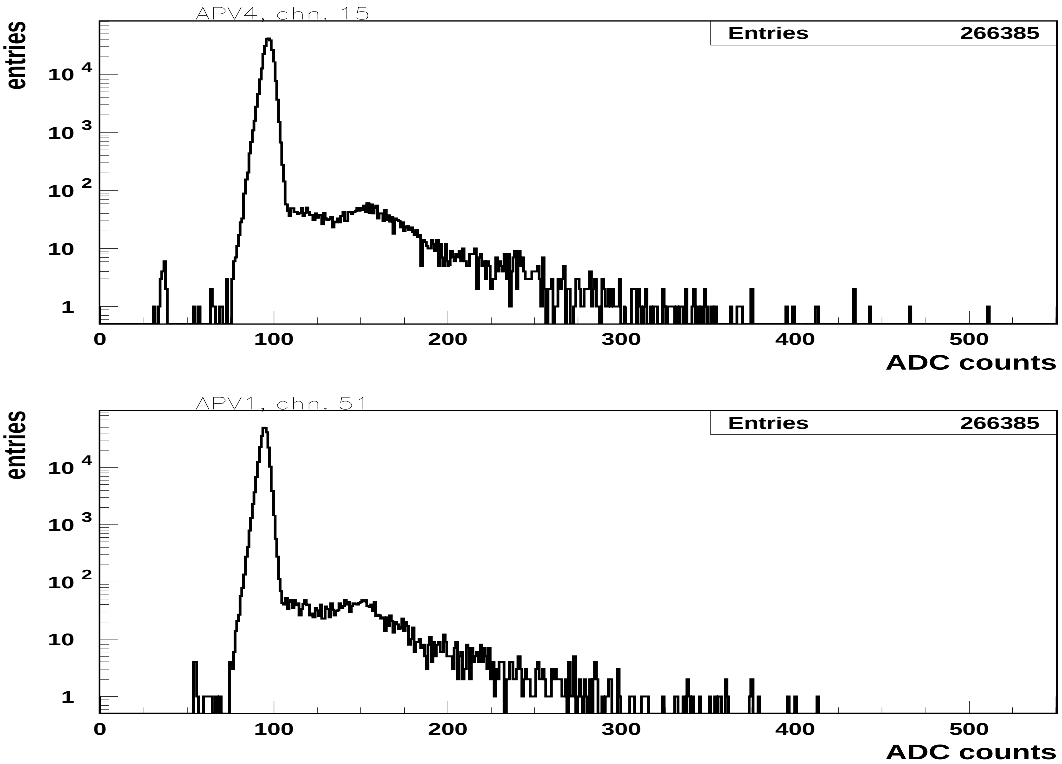

Figure 44: *The raw pulse height distribution for physics events for two different APV channels: APV4 channel 15 and APV1 channel 51 (runs 218 to 226).*

To calculate the gain for the silicon strips, single strip clusters events should be used. This was possible in the previous DESY test beam [1] were data was collected also without the preshower in front of the silicon. In the CERN test beam the preshower was always present, giving rise to very single strip clusters events. Typically the events with preshower have wider clusters and the clusters are more numerous (multi-particle hit). The charge is shared differently between strips, depending on whether it is a single or multi-particle hit. In a single particle hit the charge is seen by only one, at most two strips, thus giving a more peaked pulse height distribution, allowing to obtain the gain for a given strip, by selecting only single strip clusters events. The strip gain is calculated as the average value of the strip's signal pulse height distribution for all single strip cluster events. For the CERN data this is not feasible, because of the preshower presence. Therefore the average value of the strip's signal pulse height distribution is used to obtain a rough value for the strip gain. Below in fig. 45, the typical average signal value in ADC counts for each strip is shown. The table scan run set (runs 218 to 226) has been chosen to have signals (hits) distributed along the whole silicon area. The dead strips can easily be identified, as dips in the average signal value with respect to neighboring strips. The dead strips are not always completely dead, there might be some signal or noise pick up as can be seen in the two lower plots of fig. 45. However dead strips have a much lower signal average than live strips and for dead strips very few events pass the signal cut criteria when compared to live strips.

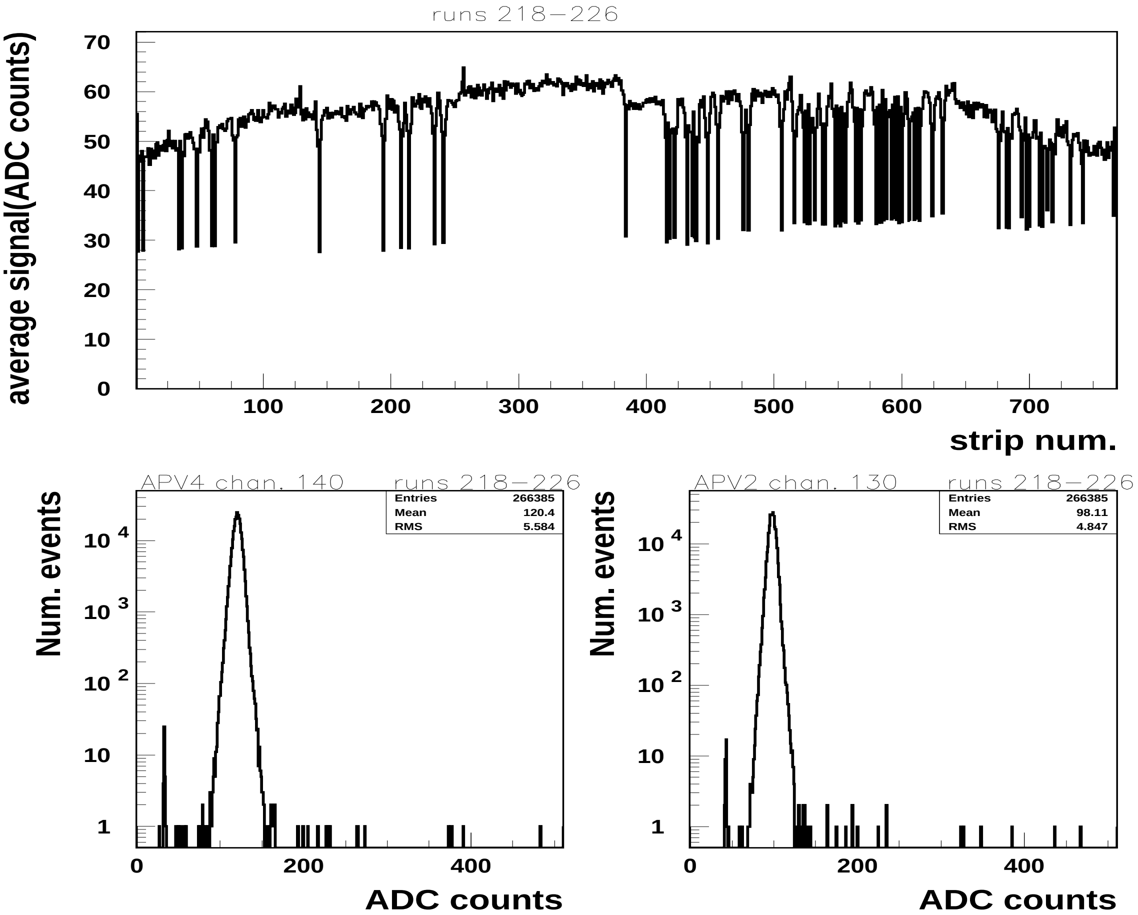

Figure 45: *The top plot is the average signal value (in ADC counts) for each strip, for the table scan run set (runs 218 to 226). The dead-faulty strips can clearly be seen. The two lower plots are the raw pulse height distribution for two typical dead strips: APV4 APV25 channel 140 and APV2 APV25 channel 130.*

The beam-profile measured by the silicon is plotted in fig. 46. The beam-profile is given by plotting the total number of signals (hits) in a given strip versus the strip number. The top plot is flatter because it corresponds to a table scan, resulting in the beam moving with respect to the silicon. The middle plot shows the typical CERN test beam profile, the table was not moved, a fiber scan was done. A close up view of a dead strip region is shown in the lower plot. Typically the strips neighboring a dead strip have an increased number of signals hits. These are the spikes seen in the beam-profile, near a dead strip. The dead strips affect the neighboring live strips i.e. increase in signal hits.

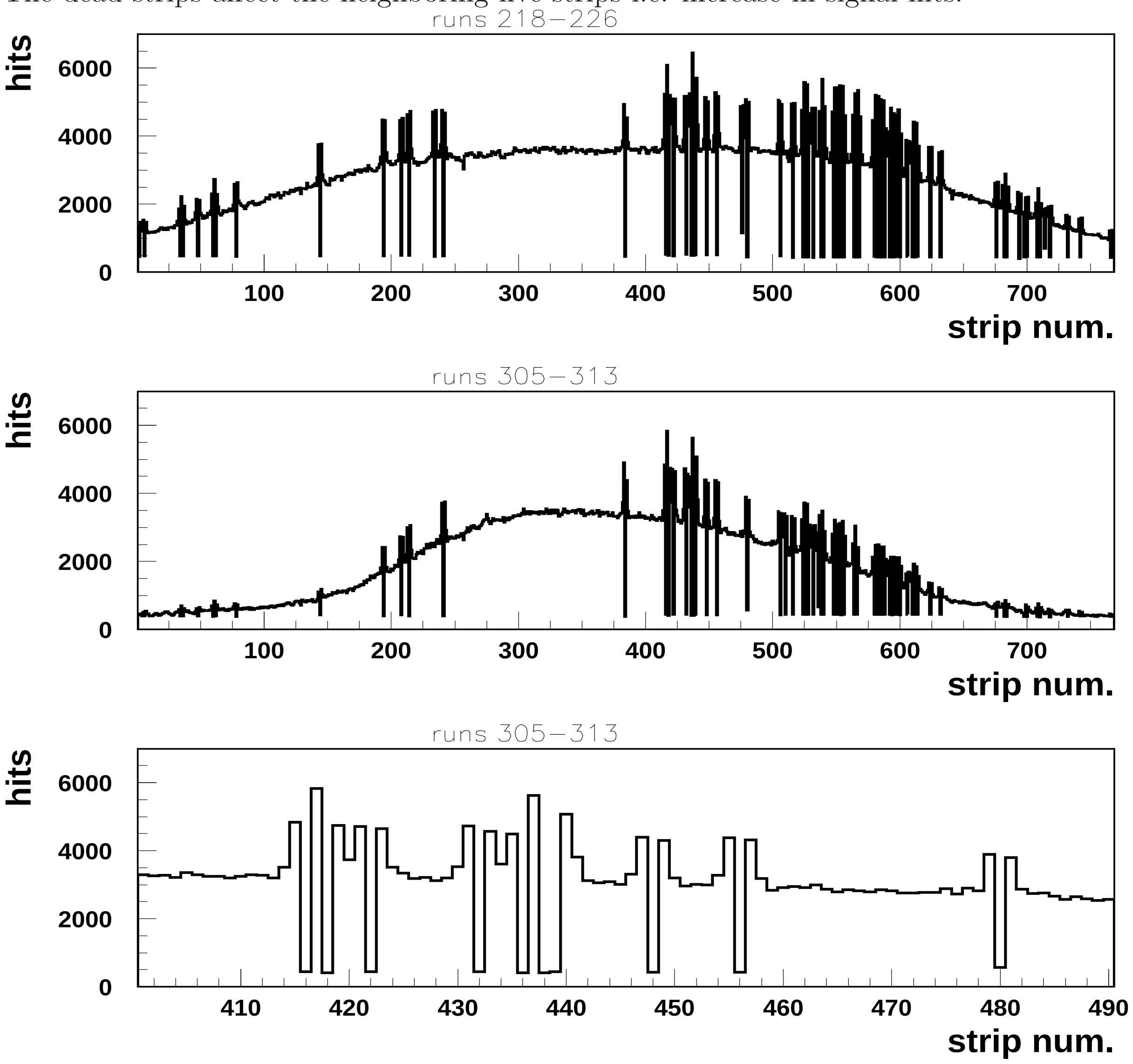

Figure 46: *The total number of signals (hits) in a given strip versus the strip number i.e. the beam-profile. Top plot for the table scan run set (runs 218 to 226), middle plot for runs 305-313 (table in fixed position) and lower plot close up view strips 400 to 490 where there are several dead strips (runs 305-313).*

The ratio between, the total number of events that produce a signal in a given strip ,and the total number of physics events in the run which correspond to a the total number of physics triggers in the run, is called strip occupancy (hit ratio). The strip occupancy is strongly dependent on the beam profile. From figure 47 the average strip occupancy is around 1.5% for strips that are in the beam.

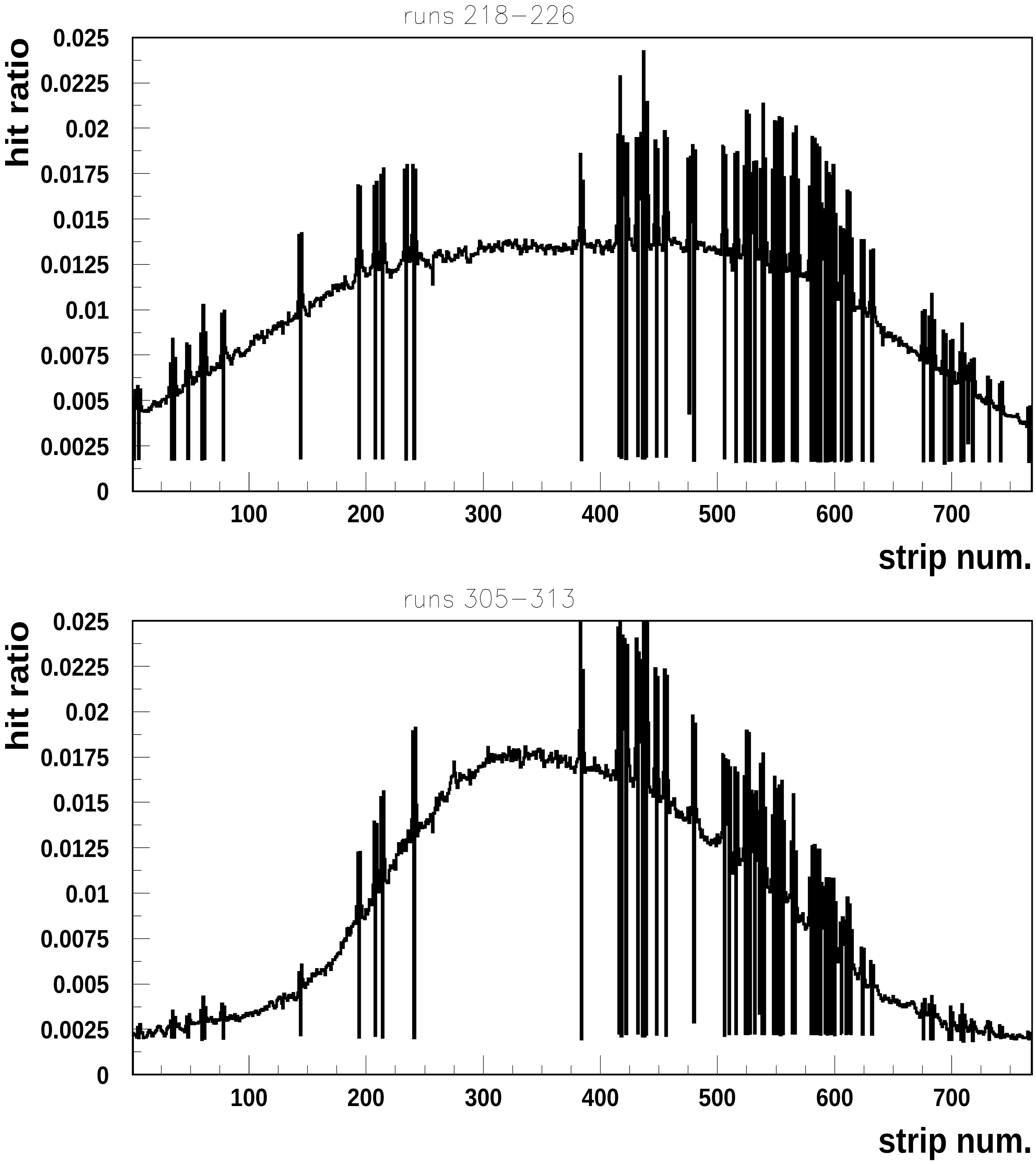

Figure 47: *The strip occupancy for two different data sets; runs 305-313 for table in fixed position and runs 218 to 226 for the table scan.*

The signal to noise ratio S/N, is calculated for each strip as the ratio between the average strip signal value and the strip noise. In reality to calculate the S/N ratio one would use the strip gain and not the average strip signal; but anyhow an approximate value can be obtained for S/N. The average S/N for all the strips is shown in fig. 48. The top plot shows that the average S/N ratio is between 30 and 35. The dead strips have a low value S/N ratio value varying between 5 and 25. The S/N ratio distribution and average signal distribution is displayed in the two lower plots of fig. 48. The dead strips can be easily identified: they have a low S/N ratio and a low average signal value.

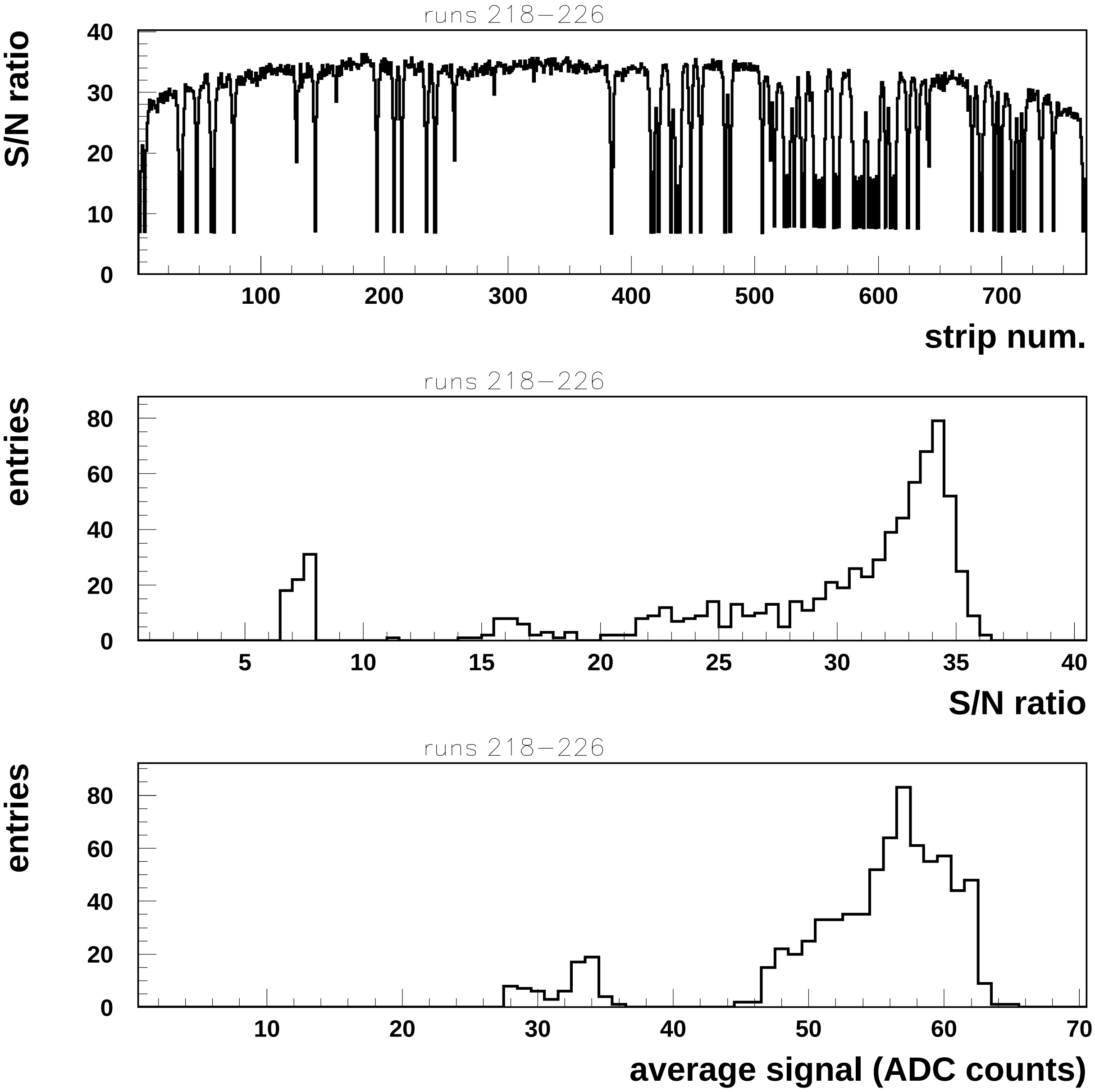

Figure 48: *Top plot: the S/N ratio for all strips. Middle plot: S/N ratio distribution. Lower plot: average signal distribution. Run set: runs 218 to 226.*

The average signal versus noise and average signal versus pedestal, and also the S/N ratio versus noise and S/N ratio versus pedestal are plotted in fig. 49 for all silicon strips. The dead strips can easily be identified, they correspond to strips with higher noise and lower average signal and S/N values.

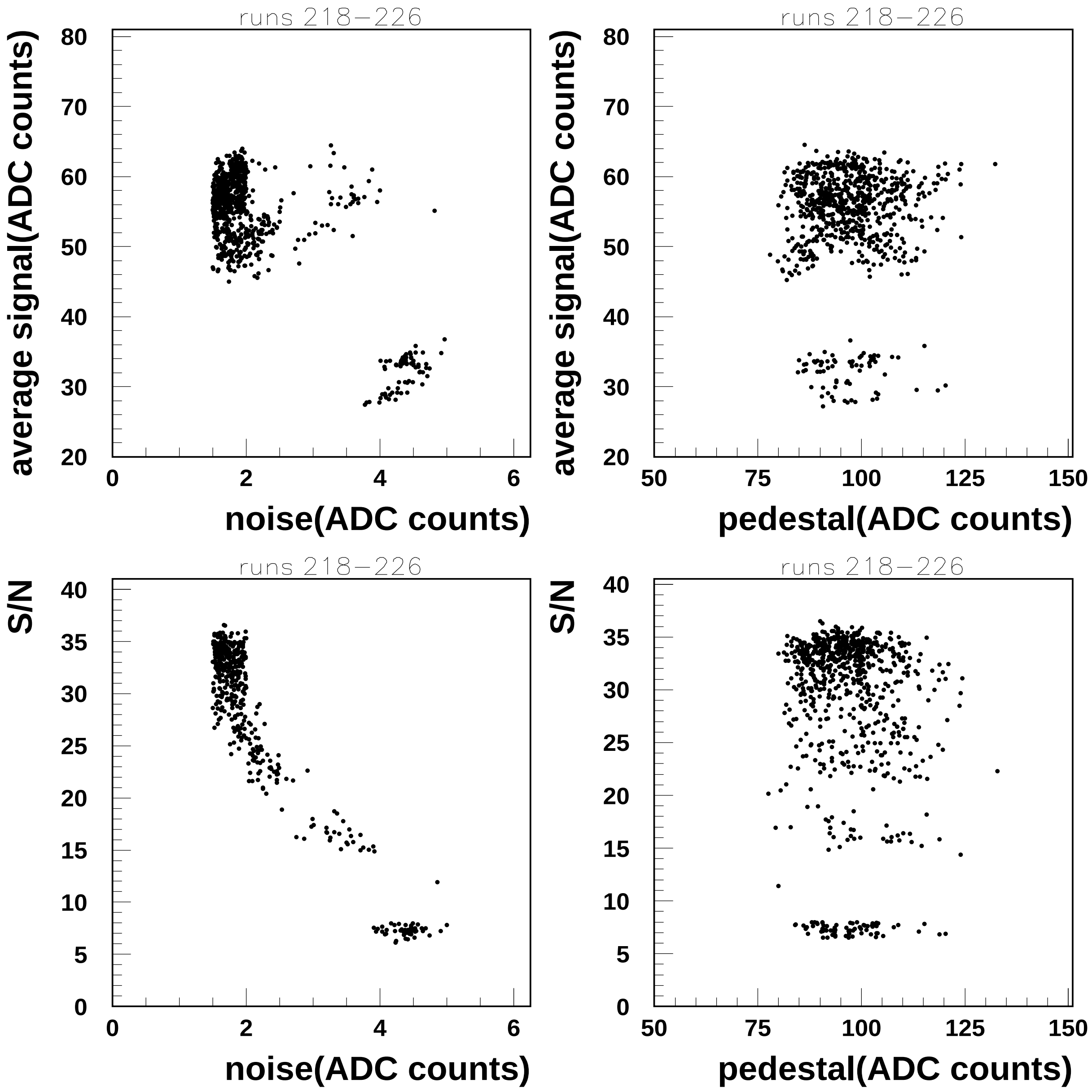

Figure 49: *Top two plots: average signal versus noise and average signal versus pedestal. Lower two plots: S/N ratio versus noise and S/N ratio versus noise pedestal. Run set: runs 218 to 226.*

9.8 Clusters

Clusters are built from several adjacent strips, which share between them the charge deposited by the particle crossing the silicon. To obtain the $\eta - y$ transformation (see sections 4, and **??**) one needs to reconstruct good single clusters in the silicon; where $\eta = (E_{up} - E_{down})/(E_{up} + E_{down})$, E_{up} and E_{down} are mean energy deposits of the incident test beam particles in UP and DOWN calorimeter respectively, and y is the vertical position by the Si detector.

Events with more than one cluster in the silicon are not useful for the $\eta - y$ transformation, because for each η value there must correspond only a single reconstructed y silicon value (single cluster). Multiple silicon clusters (multiple y values) correspond to wide multi particle hits (wide showers) on the silicon; these events are discarded when calculating the $\eta - y$ transformation.

A cluster algorithm has been implemented to find and build good single clusters in the silicon. When reconstructing the silicon clusters one needs to take in account also the large number of silicon dead strips (see section 10). The dead strip problem is due to the defective Kapton pitch adaptor, which bonds the silicon strips to the APV25 readout chips. Dead strips can become live strips, and live strips can become dead strips, over time. This change (dead/live) has been observed only in a few percent of the silicon total strip number. The strip change (dead/live) occurs because the Kapton pitch adaptor bonds can slightly move as a result of thermal and mechanical stress, changing the conductivity of the bond.

The silicon cluster algorithm goes through the following steps listed below.

Cluster Algorithm:

- Find the dead strips. A noise and signal cut is used to separate dead strips from live strips. A strip is considered dead if its noise is greater than 3.5 ADC counts and its average signal is lower than 40 ADC counts (see fig. 49). With such a cut one can clearly differentiate the dead strips from live strips.

- Scan the 768 silicon strips to find the cluster peaks, called also cluster seeds. The dead strips are jumped in this scan, and also the two adjacent live strips, adjacent left and adjacent right of the dead strip. This is done because the live adjacent strips are somewhat affected by the dead strip (extra number of hits see fig. 46) and also because cluster seeds should not be adjacent to a dead strip if one wants to reduce the dead strip bias on the reconstructed the cluster parameters. The condition for a strip i to have a cluster seed is:

$$PH_i = ADC_i - PED_i - CM > 15 * Ni \tag{15}$$

  where PH_i is the pulse height in the strip and Ni is the strip noise, see sections 9.6 and 9.7. For live strips, the average strip noise is about 2 ADC counts, while the average strip signal value is around 55 ADC counts. The 15 RMS cut corresponds to a strip signal value cut of ~30 ADC counts. This RMS cut has been chosen to select only cluster peaks with a significant strip signal.

- Calculate distance between the different cluster seeds i.e. $CLUDIST$ is the number of strips between the two cluster seeds. The minimum distance between two clusters is taken to be $CLUDIST = 6$, i.e. there are minimum of 6 strips between the two cluster seeds, otherwise the two cluster seeds are considered to belong to the same cluster. For example if a cluster seed is at strip 187 and another at strip 180, then CLUDIST=6, and there are 6 strips between the two cluster seeds.

- Select events with only one cluster seed. About 22% of the silicon events are one cluster events.

- Find the cluster strips. Check the PH_i value of the adjacent strips left and right of the cluster seed (-$CLUDIST$ + cluster-seed-position, +$CLUDIST$ + cluster-seed-position). If the strip satisfies $PH_i > 4 * Ni$ (signal in strip) add the strip to the cluster seed. In this calculation all adjacent live strips are considered, also live strips adjacent a dead strip, but not the dead strips. Most clusters are only some strips wide.

The cluster seed with the added strips will constitute a cluster. Various parameters (cluster seed signal value, CLUDIST, number of cluster strips, etc.) for the cluster reconstruction have been varied and tested; the above values have proven to give good results.

We first present and define some cluster terminology, that will be used for the reconstructed silicon clusters.

Cluster Signal S_{cl}

The cluster signal S_{cl} is defined as the signal sum of all strips belonging to the cluster:

$$S_{cl} = \sum_{j}^{Nstrips} S_j \tag{16}$$

where:
S_j: is the signal value in strip j;
$Nstrips$: is the number of strips belonging to the cluster.

Cluster Noise N_{cl}

The cluster noise N_{cl} is defined as the quadratic mean of the strip noise for all strips in the cluster:

$$N_{cl} = \sqrt{\sum_{j}^{Nstrips} (N_j)^2/(Nstrips)} \tag{17}$$

where:
N_j: strip noise of strip j;
$Nstrips$: is the number of strips belonging to the cluster.

Cluster Signal to Noise Ratio S/N_{CL}

The cluster signal to noise ratio S/N_{CL} is defined as the ratio between the cluster signal S_{cl} and the cluster noise N_{cl}:

$$S/N_{CL} = \frac{S_{cl}}{N_{cl}} \tag{18}$$

Cluster Position P_{cl}

The cluster position P_{cl} is defined as the signal center of gravity of the cluster:

$$P_{cl} = \frac{\sum_{j}^{Nstrips} S_j j}{\sum_{j}^{Nstrips} S_j}. \tag{19}$$

The particle position is reconstructed using the simple hypothesis that there is a linear charge sharing between the strips. This assumption is valid only as a first approximation.

Figure 50 shows the event displays in the silicon for some typical silicon single clusters.

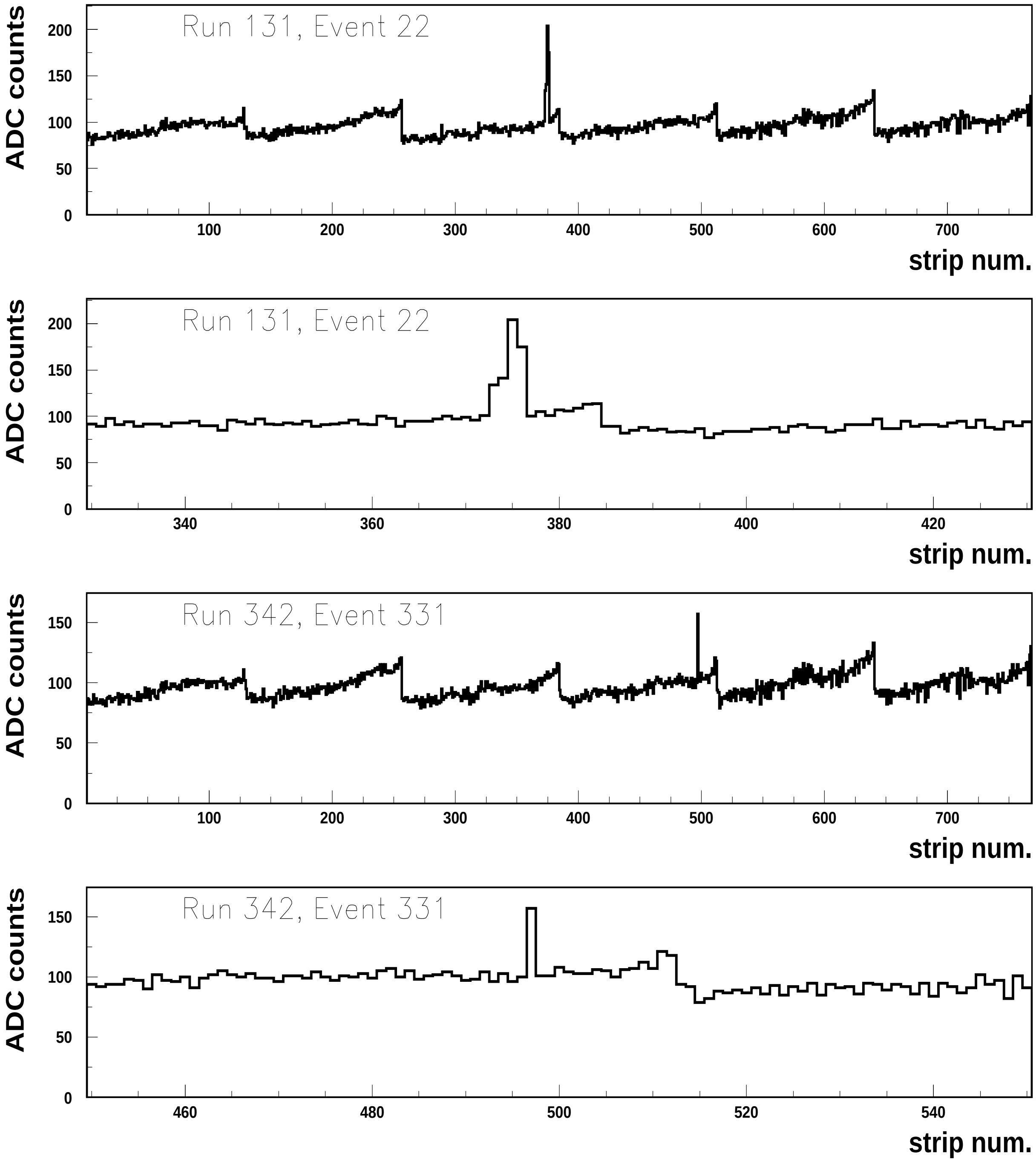

Figure 50: *Typical cluster event displays, with all 768 strips displayed and also for a limited number of strips around the cluster. Top two plots: cluster four strips wide. Bottom two plots: single strip cluster.*

The typical cluster variables distributions are displayed in figures 51, 52, and 53.

- **Cluster Signal**: The cluster signal without the preshower presence should generally follow a Landau distribution as would be expected for a charged particle crossing a thin layer of matter (one particle hit, see [1]). But during the CERN test beam the preshower was always present; the cluster signal distribution does not follow a Landau distribution. The tail has a peak centered around 200 ADC counts. With the preshower present clusters tend to be larger and with more energy deposited in the silicon detector, (multi-particle hits).

- **Cluster Noise**: The cluster noise has a mean value of ~ 1.8 ADC-counts. The tail at higher cluster noise values comes from the noisier strips.

- **Cluster Signal/Noise Ratio**: The mean value for the cluster S/N ratio distribution is ~ 68.

- **Number of cluster strips**: Most single cluster events have clusters consisting of a few strips.

- **Reconstructed Cluster Position**: The beam profile is obtained from the reconstructed single cluster events. The dead strip areas can clearly be seen as dips in the beam profile distribution. In proximity to dead strips one can not properly reconstruct the cluster position because of lack of reliable strip information. The dead strip areas contain also some live strips, but few clusters will be reconstructed for these live strips if there are several dead strips in the neighborhood, as a result of the clustering algorithm.

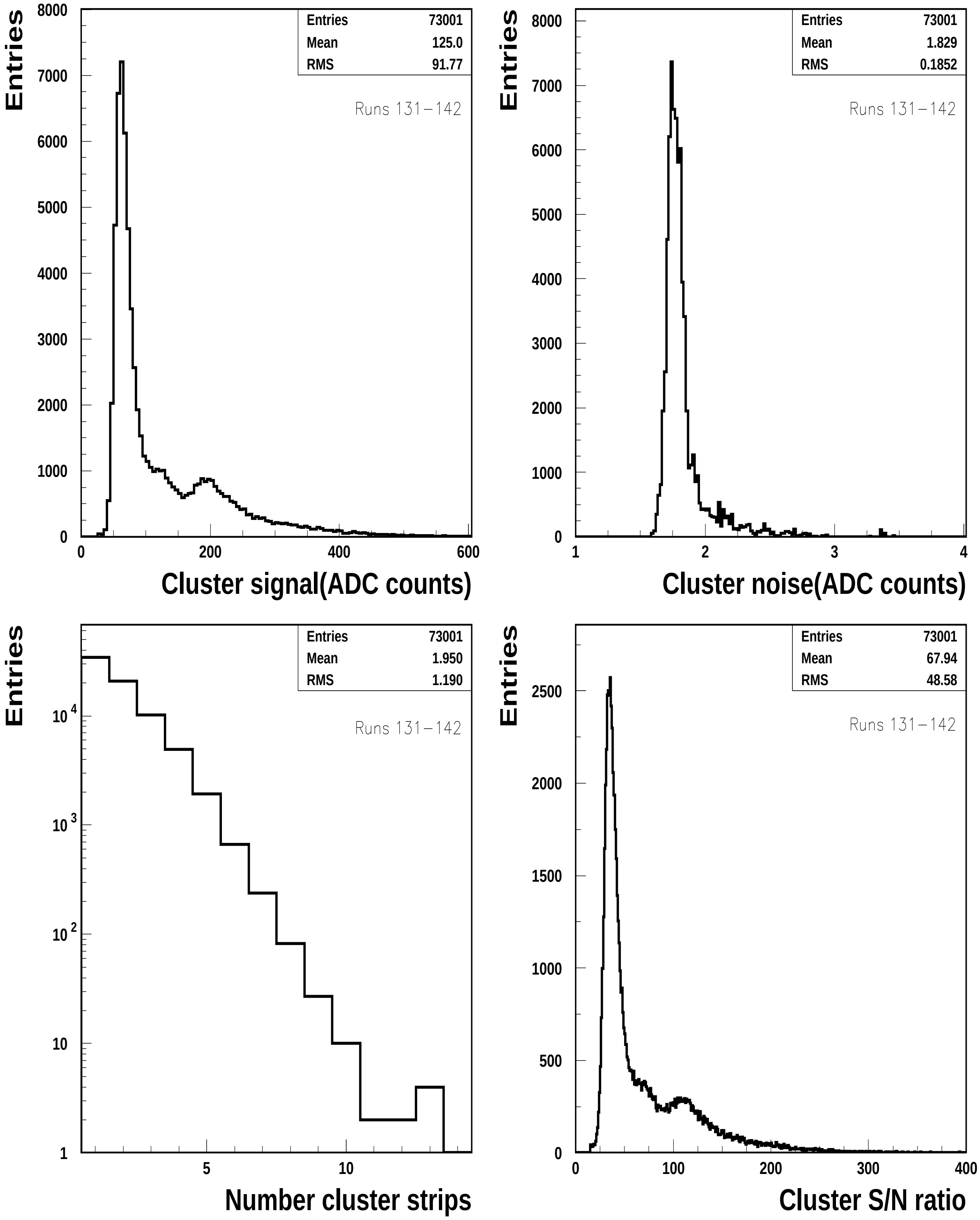

Figure 51: *The four cluster variables, for the case of single cluster events. The run set is runs 131 to 142.*

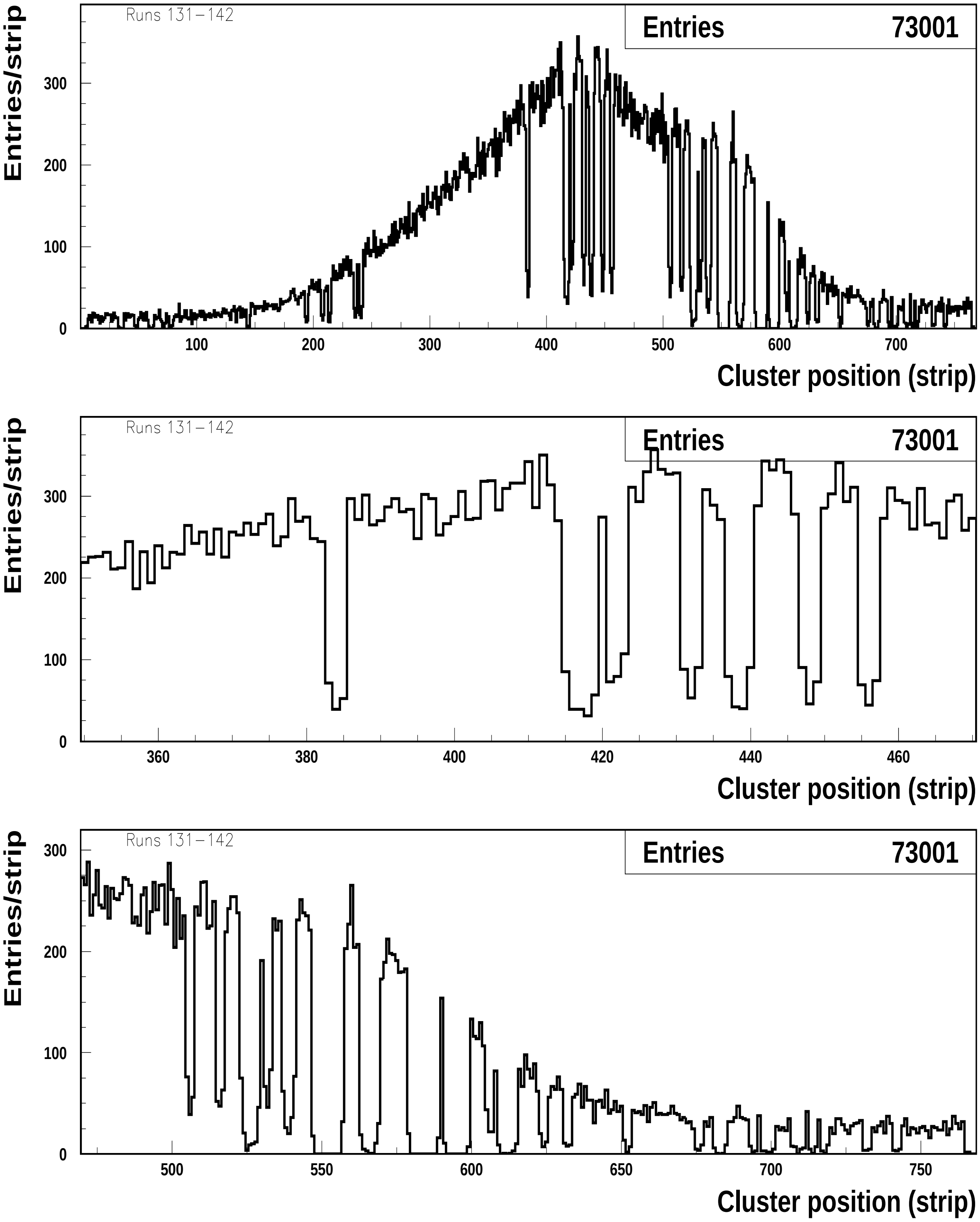

Figure 52: *The reconstructed cluster position for single cluster events. Top plot shows the beam profile. The two lower plots shows an expanded view of the dead strip areas. The run set is runs 131 to 142, the TPOL table was not moved.*

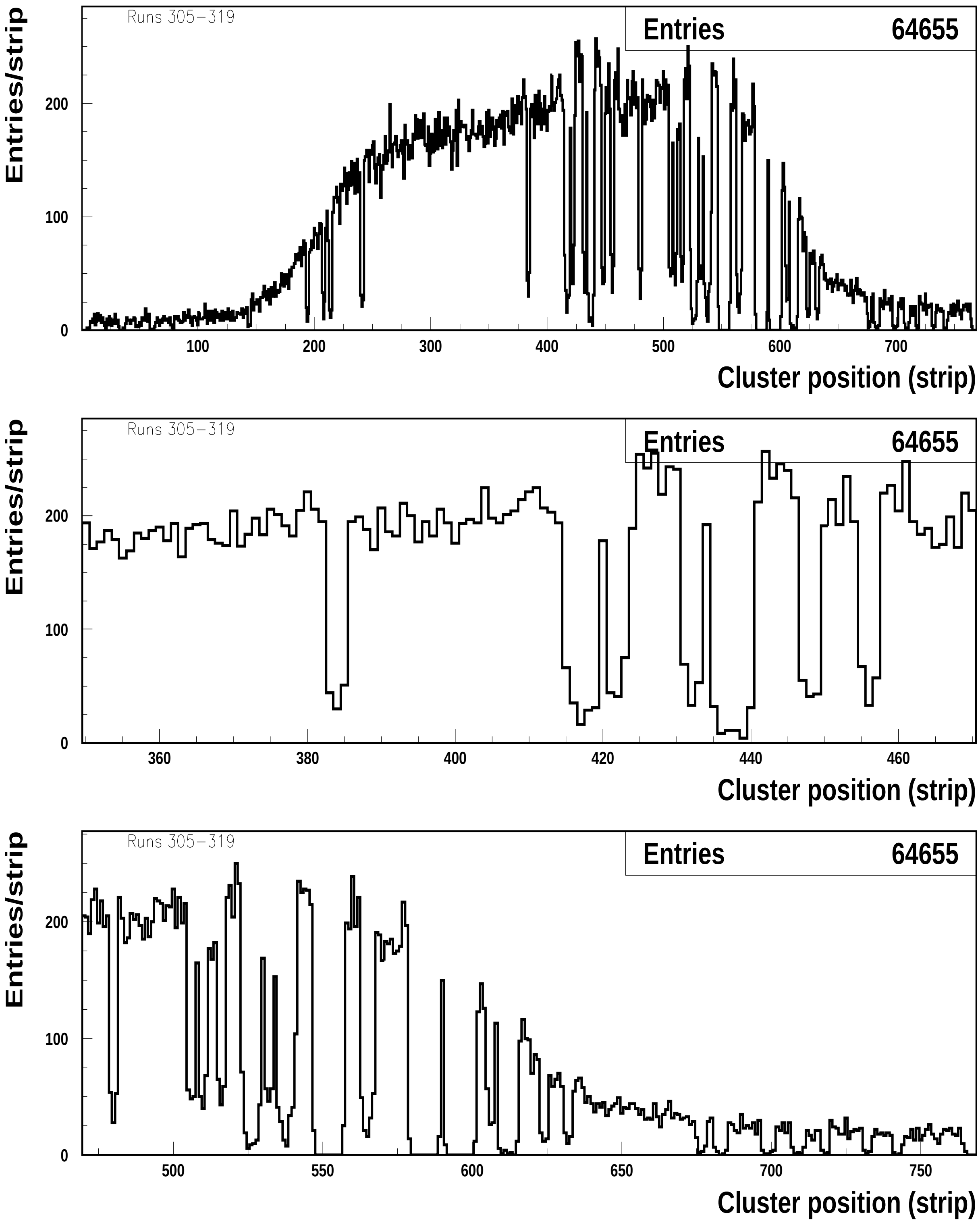

Figure 53: *The reconstructed cluster position for single cluster events. Top plot shows the beam profile. The two lower plots shows an expanded view of the dead strip areas. The run set is runs 305 to 319, the TPOL table was not moved.*

9.9 The Eta-Y Transformation

The precise determination of the η-y transformation is of primary importance for improving the accuracy of the transverse polarization measurement (see section 4 and [1]). The purpose of the silicon microstrip detector is to determine accurately the η-y transformation in situ, during data-taking, without having to rely on test-beam data. In section 8 the the calorimeter data analysis is presented, including an η-y study (different clustering and parameterization).

The eta (η) variable is obtained from the calorimeter measurement and is defined as (see section 4):

$$\eta = \frac{E_u - E_d}{E_u + E_d} \tag{20}$$

where E_u and E_d are the measured energy deposits in the upper (UP module) and lower module (DOWN module) of the TPOL calorimeter, respectively.

The y variable is the vertical coordinate of the incident particle hit position measured by the silicon microstrip detector. The η-y plots are obtained by requiring that there is only one reconstructed cluster in the silicon, a lower threshold cut is applied to the cluster signal and calorimeter signal values i.e. the silicon clustering algorithm is described in 9.8, and the calorimeter total energy must be greater than 5 GeV.

Figure 54, shows the η-y scatter plot for four data sets. The data sets are for different test beam energies and table positions. The dead strip areas can clearly be seen as vertical white lines in the η-y scatter plot. The strip number, which is directly related to the y position of the cluster, is used in these scatter plots.

The silicon strip number is converted into millimeters to obtain y, where y is centered with respect to the calorimeter vertical center i.e. y=0 for η =0.

Figures 55 and 56 display the fitted η-y profile histograms, for different data run sets. The fitted function is of the type (y is the vertical coordinate):

$$\eta(y) = \frac{|y|}{y}\left[1 - e^{-|y|/P_3} + P_1(e^{-|y|/P_3} - e^{-|y|/P_2})\right] \tag{21}$$

The slices in y are Δy=80μm; the η means for each slice is plotted as a profile histogram and then fitted. The semi-continuous line is the η-y transformation at 8 GeV, for the old CERN test-beam data. This old CERN test-beam data η-y transformation is plotted for comparison. It is expected to differ from the newly measured η-y transformations, because of the different setup between the two test beams. In the old CERN test beam no preshower was used. The presence of the preshower modifies the η-y transformation. The η-y transformation is flatter than the old CERN η-y transformation. This is a typical effect of the preshower material; the more material the more flattened out the η-y transformation, because the showers incident on the calorimeter face become larger.

The η-y profile histograms (figs. 55 and 56) have been fitted for a limited y region (± 10 mm or ± 15) corresponding to the central region of the η-y transformation, which is of major interest ($-0.8 < \eta < 0.8$), and also there is enough data to make the fit. The fit has been extended to the whole y range for the data run set 218 to 226 (table scan) which has enough data points also for large η. The test beam energy range of interest is around 10 GeV for η-y, which corresponds to the average incident Compton photon energy.

The fits are somewhat worsened by the effect of the dead strips, which give rise to no eta values for some regions in y or shift the η to lower values with respect to the general η-y curve. However η-y fits are reasonably good.

Two new silicon detectors, one to measure y (the vertical impact point), and the other to measure x (the horizontal impact point) with a new pitch adaptor, (aluminium on glass pitch adaptor), are being prepared and tested at IC London. The new pitch adaptor would prevent the dead strip problem from happening again. These detectors will be installed in the HERA tunnel during the next long HERA shutdown (March 2003). It is expected to obtain a improved η-y measurement (no dead strip problem) with these new silicon detectors.

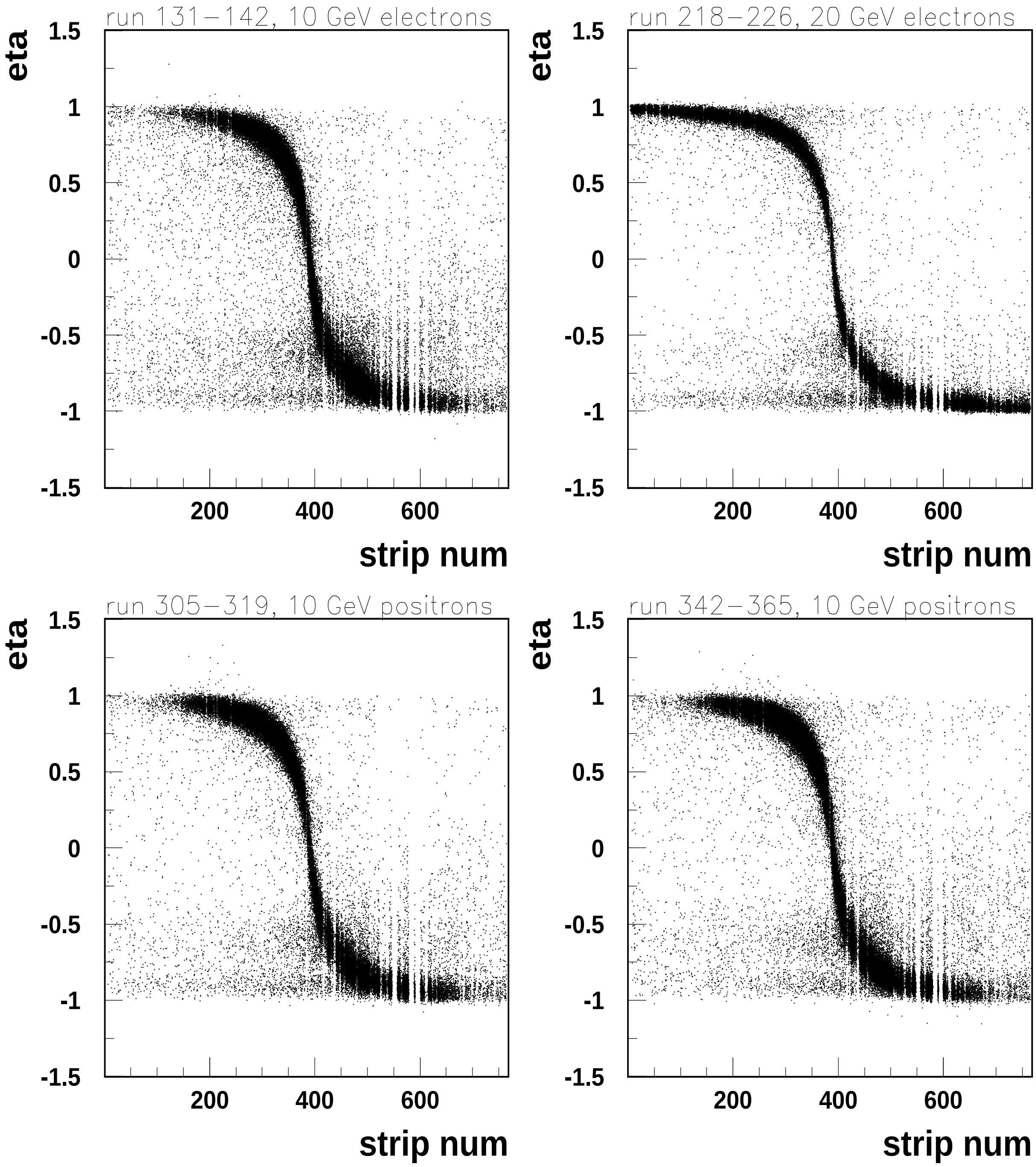

Figure 54: *The η-y scatter plot for four data sets. Instead of y in mm the strip number is plotted. The dead strip areas correspond to the vertical white lines in the η-y scatter plot. Runs 131 to 142, 10 GeV electrons, table centered, 65k eta-y events. Runs 218 to 226, with 10 GeV positrons, table scan, 55k eta-y events. Runs 305 to 319, with 10 GeV positrons, table centered, 58k eta-y events. Runs 342 to 365, with 10 GeV positrons, table centered, 71k eta-y events.*

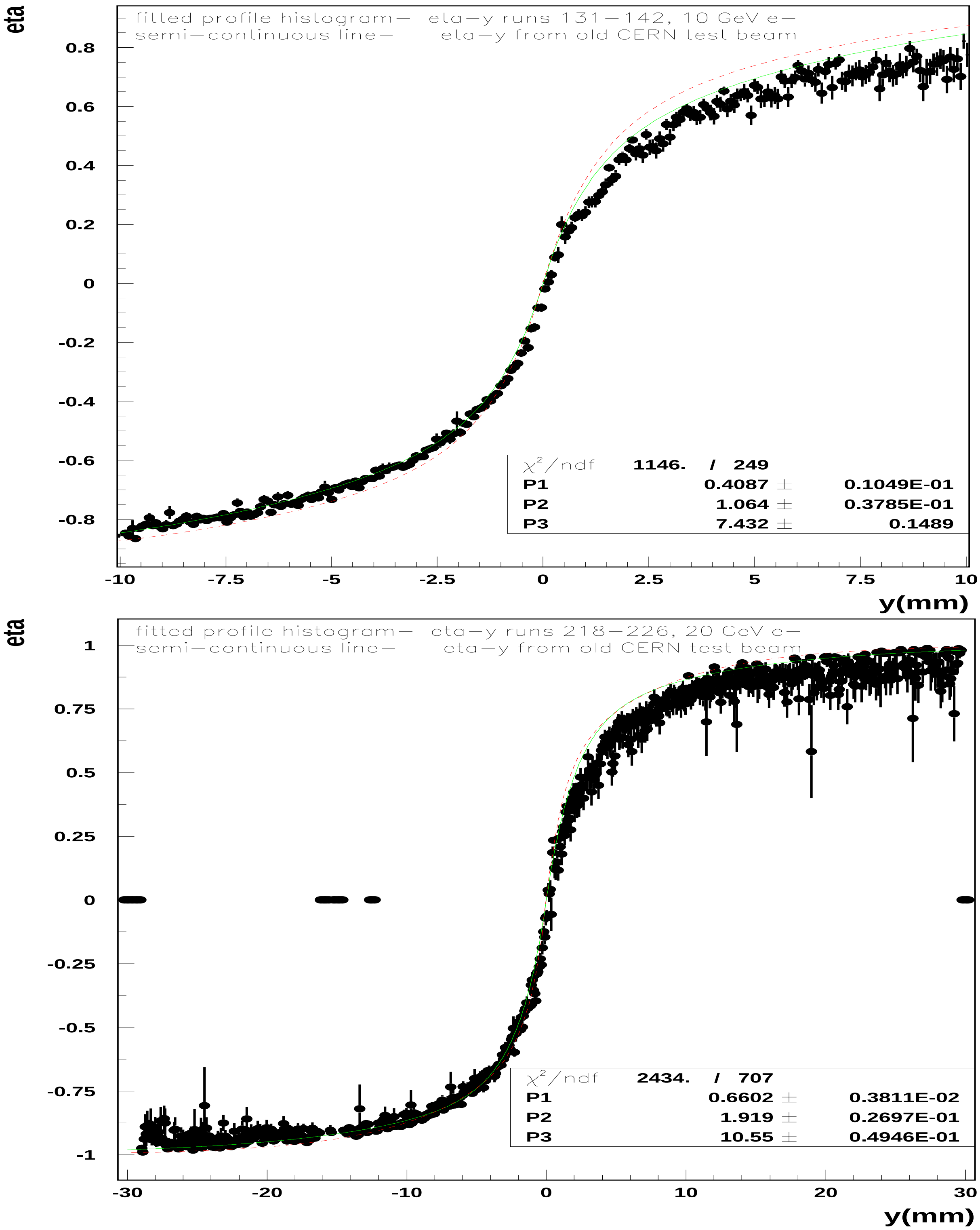

Figure 55: *The fitted η-y profile histograms for the data run set 131 to 142, 10 GeV electrons, table centered, 65k eta-y events (top plot); and the data run set 218 to 226, 10 GeV positrons, table scan, 55k eta-y events (lower plot). The old CERN test-beam η-y transformation function is plotted for comparison.*

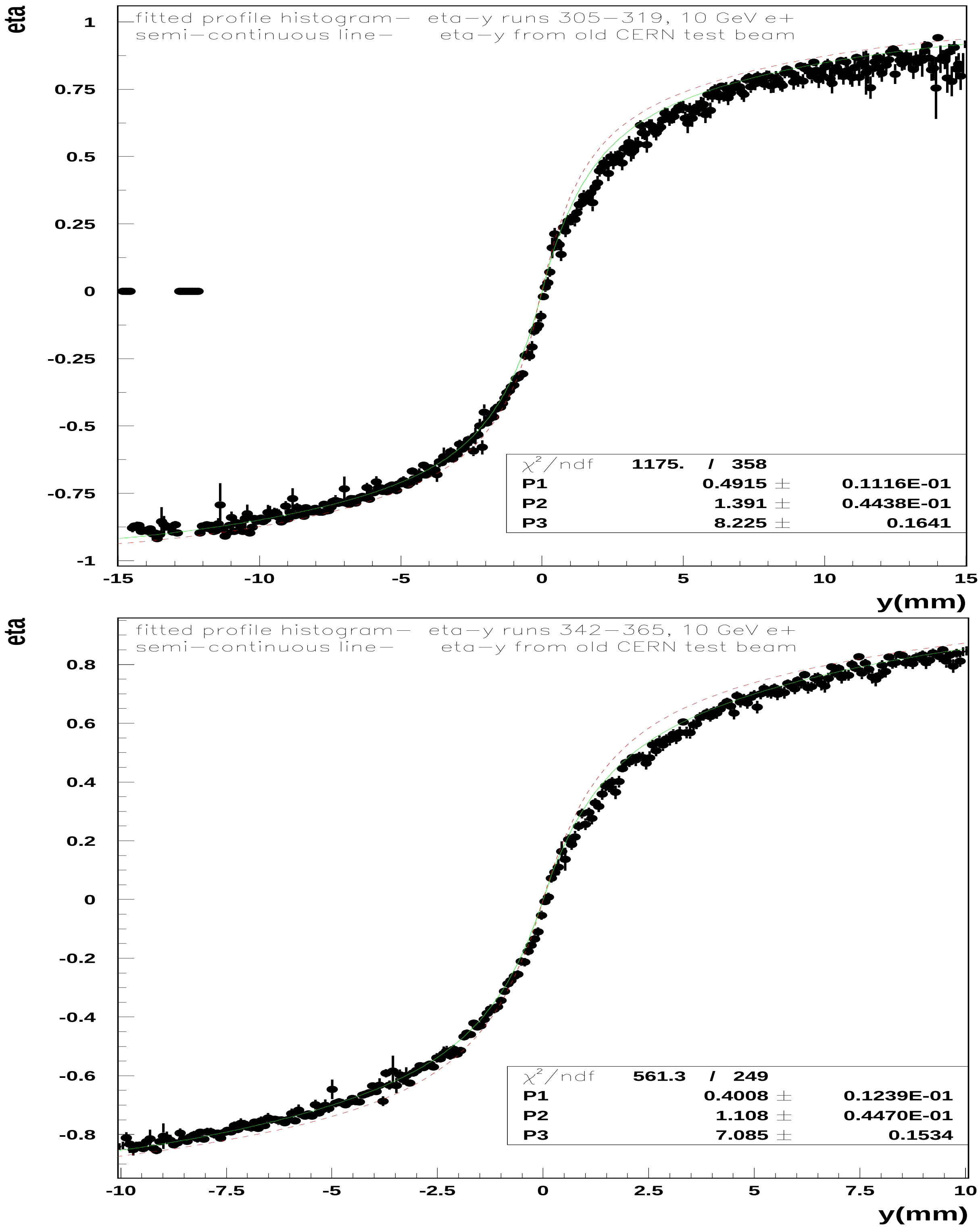

Figure 56: *The fitted η-y profile histograms for the data run set 305 to 319, 10 GeV positrons, table centered, 58k eta-y events (top plot); and the data run set 342 to 365, 10 GeV positrons, table centered, 71k eta-y events (lower plot). The old CERN test-beam η-y transformation function is plotted for comparison.*

10 Silicon Defective Strip Study

Whilst performing online analysis of the data obtained from the CERN test beam, it was noticed that some of the Silicon strips appeared to give little or no signal. Worse still, a subset of these strips gave intermittent signals. The detector was again analysed upon its return to DESY (in the T22 test beam[3]), prior to installation in the HERA tunnel.

The beams at CERN and DESY T22 were not diffuse enough to cover the whole detector in just one run, so several runs were made at different heights relative to the beam. A set of runs which fully illuminated the detector was called a 'Table Scan'.

At CERN, three suitable Table Scans were made, and are referred to as CERN1,2,3 respectively. At DESY, just one Scan was made. The details of the scans and run numbers contained therein can be found in Table 1.

10.1 Strip Analysis

The strip responses (in ADC counts) were analysed using pedestal events to separate the signal from the background. In the case of the CERN scans, pedestal events were taken during the run by means of a random trigger. In the DESY scan, a separate pedestal run was performed with no beam (see Table 1). The Common Mode was also taken into account in determining whether or not the response constituted a signal. The Common Mode is calculated for each APV by summing (for each strip) the difference between the pedestal mean (mean strip response for all pedestal events) and the strip value (excluding strips with signal). The average difference for the event (between pedestal mean and strip value) is the Common Mode. Then, the response was considered to be a signal for the i^{th} strip if:

$$Strip_i \ - \ Ped_i \ - \ CM \ > \ 8 \times RMS_i \tag{22}$$

For the purposes of the dead strip study, a 'signal' was classified as a strip response over $8 \times$ pedestal RMS. Plots of strip responses, such as Figure 57 show how the removal of strip responses below $8 \times$ RMS removes only a small amount of signal from a healthy strip, whilst eliminating almost all of the pedestal responses.

The $8 \times$ RMS cut enables an easy distinction to be made between strips which are 'dead' and those which are 'alive'.

As mentioned in §10, the beam did not illuminate the detector evenly. A typical run is depicted in Figure 58. The plot shows (for each strip) the number of times a signal was registered over $8 \times$ RMS. To determine the strips which were not responding, a 'local

[3] Reference [1] contains a description of the T22 area.

Table Scan	Run Nr.	Date	Energy (GeV)	Table ‘y’ Pos (mm)
CERN 1	128	27-Jul	20	-11.4
	127	27-Jul	20	-1.4
	126	27-Jul	20	8.6
	129	27-Jul	20	28.7
	130	27-Jul	20	38.7
CERN 2	179	29-Jul	15	-2.7
	180	29-Jul	15	3.7
	181	29-Jul	15	8.7
	182	29-Jul	15	13.7
	183	29-Jul	15	18.7
	184	29-Jul	15	23.7
	185	29-Jul	15	28.7
	186	29-Jul	15	33.7
	187	29-Jul	15	38.7
CERN 3	218	29-Jul	20	-2.7
	219	29-Jul	20	3.7
	220	29-Jul	20	8.7
	221	29-Jul	20	13.7
	222	29-Jul	20	18.7
	223	29-Jul	20	23.7
	224	29-Jul	20	28.9
	225	29-Jul	20	33.7
	226	29-Jul	20	38.7
DESYT22	1050	14-Nov	1	-9.3
	1049	14-Nov	1	0.7
	1048	14-Nov	1	10.7
	1047	14-Nov	1	20.7
	1043	14-Nov	1	30.7
	1044	14-Nov	1	40.7
	1045	14-Nov	1	50.7
	1046	14-Nov	1	60.7

Table 1: *The data used in the investigation into dead strips. The DESY scan used run 1042 for calibration.*

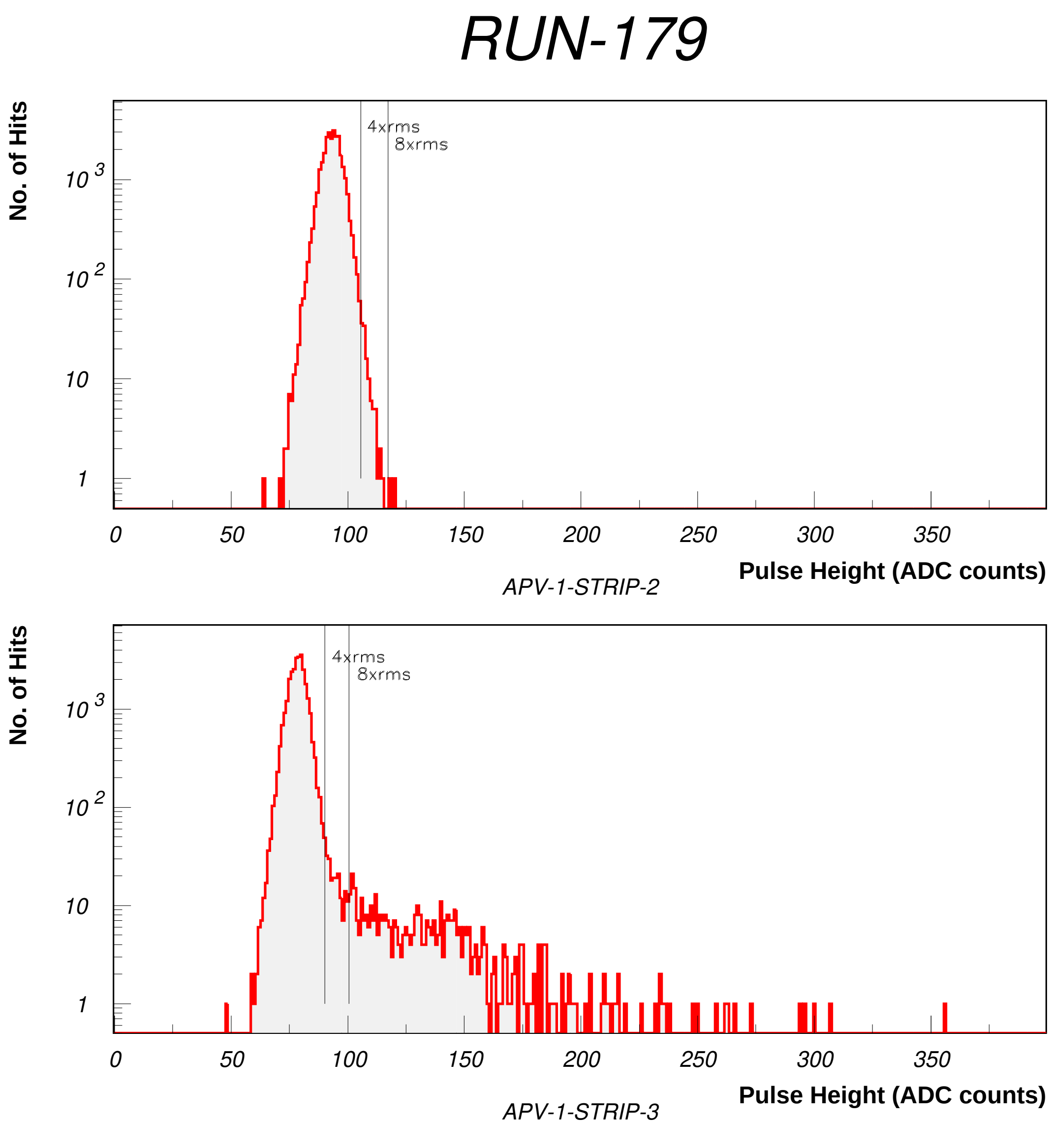

Figure 57: *(Top): Response from a typical 'dead' strip. (Bottom): Response for a 'healthy' strip. The lines show 4 and 8 × the RMS of the pedestal events.*

average' was constructed for each strip. This consisted of the average number of hits registered on the nearest 20 strips to the strip in question. The local average did not contain more strips because it was found that the typical beam profile (see Figure 58) varied too greatly over larger distances, making the local average response less meaningful.

Due to the uneven illumination, the local average number of hits was only used in the 'high statistics' region of the beam profile - where the local average was greater than 50.0 or $\frac{1}{6}\times$ Maximum No. of Hits in Beam Profile, whichever is the greater.

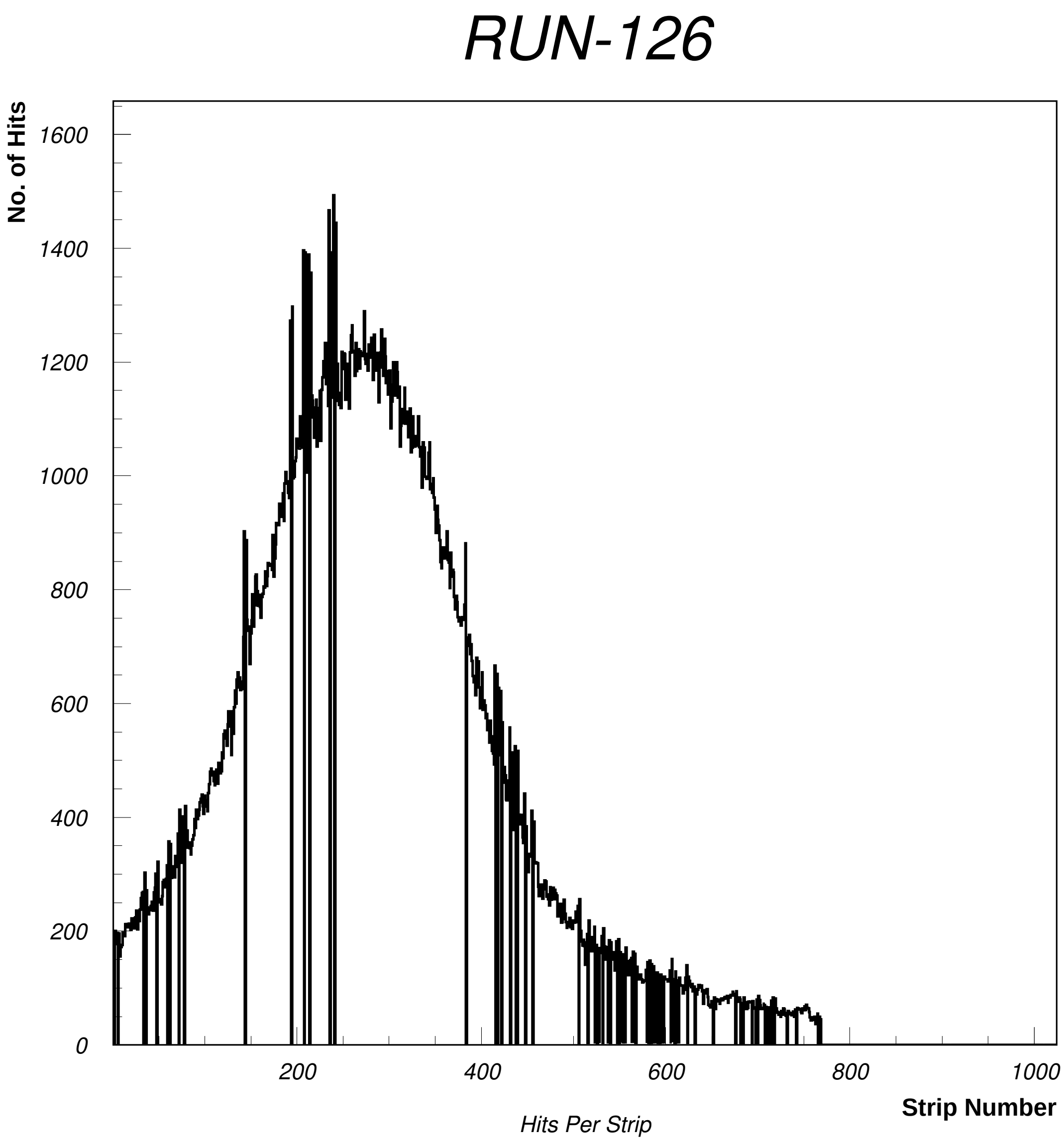

Figure 58: *Number of 'Hits' for each strip in run 126. The beam does not illuminate the detector evenly.*

If in any run, a strip responded significantly less than its local average response ($< 25\%$ of local average), the strip was flagged as possibly defective, and then the strip watched for the analysis of the entire data set. Typically, a 'dead' strip had response levels of less than 5% of the local average response, so the 25% watch threshold is a very loose 'cut', yet it is quite effective at highlighting the defective strips.

For the sake of completeness, the other checks applied were:

- The error bit on all APV25 responses was 'high' (over 200 ADC counts).
- The pipelines for each APV25 were the same.
- Events with > 100 channels of signal excluded (from experience sometimes there are occasional events where the response is 511 or 256 ADC counts for all channels).

10.2 Strip Results

Identification of Dead Strips:
Strips which were consistently dead for all four Table Scans are tabulated with no colour. Strips which appeared to give inconsistent responses *between* Table Scans are coloured yellow. These strips were either alive or dead for all the runs in any Table Scan, but at least one Table Scan did not match the others.
Strips which appeared to be inconsistent *inside* a Table Scan (between runs) are labelled red. For these strips, individual runs in the table scan did not correspond to each other. This only occurred for seven strips in one Table Scan.
Every defective/intermittent strip has three numbers in Figure 59:

- Strip Number.
- Number of Hits.
- Value of Local Average.

It is worthwhile noting that there are 87 dead and intermittent strips out of a total of 768. This represents a figure of about 11%.

CERN RUN 1	CERN RUN 2	CERN RUN 3	DESY
APV1:strip,value,ave> 2 0.000000 325.5500	APV1:strip,value,ave> 2 3.000000 495.0000	APV1:strip,value,ave> 2 1.000000 185.6000	
APV1:strip,value,ave> 6 9.000000 330.7500	APV1:strip,value,ave> 6 2.000000 530.0500	APV1:strip,value,ave> 6 0.000000 201.5000	APV1:strip,value,ave> 6 1.000000 53.80000
			APV1:strip,value,ave> 16 2.000000 53.75000
APV1:strip,value,ave> 34 0.000000 313.5000	APV1:strip,value,ave> 34 3.000000 566.8000	APV1:strip,value,ave> 34 1.000000 251.3500	
APV1:strip,value,ave> 36 0.000000 313.5000	APV1:strip,value,ave> 36 3.000000 573.9000	APV1:strip,value,ave> 36 1.000000 262.1000	APV1:strip,value,ave> 36 1.000000 91.85001
APV1:strip,value,ave> 48 0.000000 330.0500	APV1:strip,value,ave> 48 4.000000 626.8500	APV1:strip,value,ave> 48 0.000000 320.5000	APV1:strip,value,ave> 48 2.000000 101.0000
			APV1:strip,value,ave> 54 1.000000 105.2500
APV1:strip,value,ave> 60 0.000000 308.3499	APV1:strip,value,ave> 60 2.000000 639.6501	APV1:strip,value,ave> 60 0.000000 356.2500	APV1:strip,value,ave> 60 2.000000 106.6000
APV1:strip,value,ave> 62 0.000000 296.2500	APV1:strip,value,ave> 62 2.000000 643.1500	APV1:strip,value,ave> 62 1.000000 364.3000	APV1:strip,value,ave> 62 2.000000 107.2500
APV1:strip,value,ave> 72 0.000000 285.1000			
APV1:strip,value,ave> 78 1.000000 288.6000	APV1:strip,value,ave> 78 3.000000 680.8000	APV1:strip,value,ave> 78 0.000000 452.0500	APV1:strip,value,ave> 78 2.000000 115.6500
			APV1:strip,value,ave> 96 2.000000 121.5500
APV2:strip,value,ave> 16 0.000000 169.6000	APV2:strip,value,ave> 16 1.000000 688.3500	APV2:strip,value,ave> 16 0.000000 708.8500	
APV2:strip,value,ave> 66 0.000000 103.9500	APV2:strip,value,ave> 66 1.000000 538.4000	APV2:strip,value,ave> 66 0.000000 785.0000	APV2:strip,value,ave> 66 2.000000 105.3500
APV2:strip,value,ave> 80 0.000000 79.74999	APV2:strip,value,ave> 80 2.000000 489.5000	APV2:strip,value,ave> 80 0.000000 757.6000	APV2:strip,value,ave> 80 2.000000 98.15001
APV2:strip,value,ave> 86 0.000000 74.75000	APV2:strip,value,ave> 86 1.000000 475.3000	APV2:strip,value,ave> 86 0.000000 741.8000	APV2:strip,value,ave> 86 2.000000 95.05000
	APV2:strip,value,ave> 106 1.000000 394.6000	APV2:strip,value,ave> 106 0.000000 679.0501	APV2:strip,value,ave> 106 2.000000 85.35000
APV2:strip,value,ave> 108 0.000000 1157.550			
APV2:strip,value,ave> 113 0.000000 1163.600	APV2:strip,value,ave> 113 0.000000 361.9500	APV2:strip,value,ave> 113 0.000000 658.6499	APV2:strip,value,ave> 113 2.000000 85.30000
			APV3:strip,value,ave> 114 1.000000 97.49999
APV3:strip,value,ave> 128 0.000000 720.4000	APV3:strip,value,ave> 128 0.000000 397.1000	APV3:strip,value,ave> 128 1.000000 606.5001	APV3:strip,value,ave> 128 2.000000 97.50000
APV4:strip,value,ave> 32 1.000000 496.7500	APV4:strip,value,ave> 32 2.000000 276.6500	APV4:strip,value,ave> 32 2.000000 484.0500	APV4:strip,value,ave> 32 2.000000 89.99999
APV4:strip,value,ave> 34 1.000000 483.1000	APV4:strip,value,ave> 34 2.000000 268.3500	APV4:strip,value,ave> 34 2.000000 468.8000	APV4:strip,value,ave> 34 1.000000 89.70000
APV4:strip,value,ave> 38 0.000000 446.4000	APV4:strip,value,ave> 38 3.000000 248.9000	APV4:strip,value,ave> 38 1.000000 434.2000	APV4:strip,value,ave> 38 2.000000 89.60000
APV4:strip,value,ave> 48 2.000000 393.5000	APV4:strip,value,ave> 48 3.000000 232.8500	APV4:strip,value,ave> 48 3.000000 366.6500	APV4:strip,value,ave> 48 2.000000 85.50001
		APV4:strip,value,ave> 52 1.000000 365.6500	APV4:strip,value,ave> 52 2.000000 85.20000
APV4:strip,value,ave> 54 1.000000 370.4500	APV4:strip,value,ave> 54 2.000000 219.4500	APV4:strip,value,ave> 54 2.000000 347.9500	APV4:strip,value,ave> 54 2.000000 82.20000
APV4:strip,value,ave> 55 1.000000 368.1500	APV4:strip,value,ave> 55 0.000000 219.8000	APV4:strip,value,ave> 55 3.000000 347.6500	APV4:strip,value,ave> 55 2.000000 83.89999
			APV4:strip,value,ave> 56 3.000000 83.14999
APV4:strip,value,ave> 64 1.000000 320.4500	APV4:strip,value,ave> 64 2.000000 186.4500	APV4:strip,value,ave> 64 2.000000 319.0000	APV4:strip,value,ave> 64 2.000000 70.20000
APV4:strip,value,ave> 72 2.000000 313.2500	APV4:strip,value,ave> 72 4.000000 183.5000	APV4:strip,value,ave> 72 3.000000 320.0500	
			APV4:strip,value,ave> 84 0.000000 80.35000
	APV4:strip,value,ave> 92 1.000000 515.1000	APV4:strip,value,ave> 92 16.00000 240.7500	APV4:strip,value,ave> 92 2.000000 76.15000
	APV4:strip,value,ave> 96 1.000000 500.7000	APV4:strip,value,ave> 96 2.000000 227.1500	
APV4:strip,value,ave> 122 1.000000 459.1000	APV4:strip,value,ave> 122 1.000000 398.5500	APV4:strip,value,ave> 122 2.000000 163.1000	
			APV4:strip,value,ave> 126 2.000000 63.90000
APV5:strip,value,ave> 4 2.000000 429.3500	APV5:strip,value,ave> 4 13.00000 338.9000	APV5:strip,value,ave> 4 10.00000 133.3500	APV5:strip,value,ave> 4 2.000000 58.15000
APV5:strip,value,ave> 12 4.000000 420.5500	APV5:strip,value,ave> 12 7.000000 305.0000	APV5:strip,value,ave> 12 12.00000 507.1000	APV5:strip,value,ave> 12 2.000000 56.75000
APV5:strip,value,ave> 14 4.000000 413.0999	APV5:strip,value,ave> 14 9.000000 295.9000	APV5:strip,value,ave> 14 12.00000 484.7000	APV5:strip,value,ave> 14 2.000000 54.30000
APV5:strip,value,ave> 16 4.000000 409.5500	APV5:strip,value,ave> 16 10.00000 293.9000	APV5:strip,value,ave> 16 11.00000 481.7500	APV5:strip,value,ave> 16 2.000000 54.00000
APV5:strip,value,ave> 20 2.000000 394.0500	APV5:strip,value,ave> 20 7.000000 270.7000	APV5:strip,value,ave> 20 13.00000 445.3000	APV5:strip,value,ave> 20 2.000000 53.84999
APV5:strip,value,ave> 26 3.000000 399.1000	APV5:strip,value,ave> 26 11.00000 261.9000	APV5:strip,value,ave> 26 13.00000 429.1500	APV5:strip,value,ave> 26 2.000000 50.89999
APV5:strip,value,ave> 28 3.000000 405.5500	APV5:strip,value,ave> 28 7.000000 259.2000	APV5:strip,value,ave> 28 13.00000 426.7500	
			APV5:strip,value,ave> 30 5.000000 97.59999
APV5:strip,value,ave> 36 3.000000 369.6000	APV5:strip,value,ave> 36 9.000000 216.2500	APV5:strip,value,ave> 36 11.00000 366.5500	APV5:strip,value,ave> 36 4.000000 100.6500
APV5:strip,value,ave> 38 2.000000 380.9000	APV5:strip,value,ave> 38 9.000000 220.5500	APV5:strip,value,ave> 38 10.00000 376.8500	
APV5:strip,value,ave> 40 3.000000 396.2500	APV5:strip,value,ave> 40 16.00000 226.6000	APV5:strip,value,ave> 40 12.00000 386.6500	APV5:strip,value,ave> 40 6.000000 100.8000
APV5:strip,value,ave> 42 3.000000 376.3500	APV5:strip,value,ave> 42 7.000000 213.6500	APV5:strip,value,ave> 42 11.00000 364.9500	APV5:strip,value,ave> 42 5.000000 103.3500
APV5:strip,value,ave> 44 3.000000 361.9000	APV5:strip,value,ave> 44 6.000000 199.3500	APV5:strip,value,ave> 44 10.00000 344.5000	APV5:strip,value,ave> 44 8.000000 101.9500
			APV5:strip,value,ave> 48 6.000000 101.6500
APV5:strip,value,ave> 52 3.000000 385.8500	APV5:strip,value,ave> 52 10.00000 196.6500	APV5:strip,value,ave> 52 9.000000 345.4000	
APV5:strip,value,ave> 54 2.000000 397.4000	APV5:strip,value,ave> 54 9.000000 200.9000	APV5:strip,value,ave> 54 10.00000 353.2500	APV5:strip,value,ave> 54 5.000000 102.1000
APV5:strip,value,ave> 56 3.000000 410.0500	APV5:strip,value,ave> 56 9.000000 205.6000	APV5:strip,value,ave> 56 14.00000 360.0000	APV5:strip,value,ave> 56 6.000000 104.0500
APV5:strip,value,ave> 68 3.000000 362.6500	APV5:strip,value,ave> 68 12.00000 166.2500	APV5:strip,value,ave> 68 11.00000 306.1000	APV5:strip,value,ave> 68 6.000000 112.6000
APV5:strip,value,ave> 70 3.000000 343.2000	APV5:strip,value,ave> 70 6.000000 154.6000	APV5:strip,value,ave> 70 10.00000 286.7000	APV5:strip,value,ave> 70 5.000000 111.8000
APV5:strip,value,ave> 72 3.000000 323.6500	APV5:strip,value,ave> 72 6.000000 143.9000	APV5:strip,value,ave> 72 11.00000 269.2000	APV5:strip,value,ave> 72 4.000000 113.0500
APV5:strip,value,ave> 74 4.000000 306.7000	APV5:strip,value,ave> 74 9.000000 457.9000	APV5:strip,value,ave> 74 14.00000 246.7500	APV5:strip,value,ave> 74 5.000000 113.0500
APV5:strip,value,ave> 76 4.000000 286.4000	APV5:strip,value,ave> 76 9.000000 434.1500	APV5:strip,value,ave> 76 11.00000 227.9000	APV5:strip,value,ave> 76 6.000000 114.3500
APV5:strip,value,ave> 80 4.000000 296.8500	APV5:strip,value,ave> 80 10.00000 414.3500	APV5:strip,value,ave> 80 11.00000 205.1500	APV5:strip,value,ave> 80 6.000000 112.5500
APV5:strip,value,ave> 82 3.000000 304.5000	APV5:strip,value,ave> 82 12.00000 426.5000	APV5:strip,value,ave> 82 11.00000 206.6000	APV5:strip,value,ave> 82 4.000000 113.0500
APV5:strip,value,ave> 84 4.000000 303.5500	APV5:strip,value,ave> 84 10.00000 426.2500	APV5:strip,value,ave> 84 12.00000 201.3000	APV5:strip,value,ave> 84 3.000000 111.3000
APV5:strip,value,ave> 86 4.000000 316.5000	APV5:strip,value,ave> 86 10.00000 446.3000	APV5:strip,value,ave> 86 11.00000 205.9000	APV5:strip,value,ave> 86 6.000000 114.1000
	APV5:strip,value,ave> 88 12.00000 443.1500	APV5:strip,value,ave> 88 9.000000 198.0500	
APV5:strip,value,ave> 94 3.000000 304.0500	APV5:strip,value,ave> 94 9.000000 431.0000	APV5:strip,value,ave> 94 10.00000 181.7000	APV5:strip,value,ave> 94 3.000000 111.6500

Figure 59: *Dead (white) and intermittent (red/yellow) strips. Yellow rows indicate the strip was consistent between runs in a Table Scan, however at least one Table Scan did not match the others. Red rows indicate a strip performing inconsistently between runs inside a Table Scan. NB: in black and white output, the yellow rows appear light grey, and the red rows appear dark grey. The values in each cell are Strip number, Number of Responses and the Local Average.*

CERN RUN 1	CERN RUN 2	CERN RUN 3	DESY
APV5:strip,value,ave> 98 4.000000 321.7000	APV5:strip,value,ave> 98 11.00000 453.8999	APV5:strip,value,ave> 98 11.00000 184.8500	APV5:strip,value,ave> 98 6.000000 113.2000
APV5:strip,value,ave> 100 4.000000 316.4000	APV5:strip,value,ave> 100 11.00000 463.8499	APV5:strip,value,ave> 100 12.00000 189.9500	APV5:strip,value,ave> 100 8.000000 114.6500
APV5:strip,value,ave> 102 3.000000 302.6500	APV5:strip,value,ave> 102 9.000000 441.8000	APV5:strip,value,ave> 102 10.00000 180.3500	APV5:strip,value,ave> 102 4.000000 111.2000
APV5:strip,value,ave> 112 3.000000 301.3000	APV5:strip,value,ave> 112 12.00000 431.4500	APV5:strip,value,ave> 112 10.00000 174.8000	APV5:strip,value,ave> 112 5.000000 111.2500
APV5:strip,value,ave> 120 3.000000 284.2000	APV5:strip,value,ave> 120 9.000000 413.2000	APV5:strip,value,ave> 120 14.00000 636.3500	APV5:strip,value,ave> 120 5.000000 115.9500
APV6:strip,value,ave> 12 0.000000 234.4500			APV6:strip,value,ave> 12 1.000000 109.3000
			APV6:strip,value,ave> 30 3.000000 113.0500
			APV6:strip,value,ave> 34 3.000000 107.8500
APV6:strip,value,ave> 36 1.000000 173.9000	APV6:strip,value,ave> 36 2.000000 253.6500	APV6:strip,value,ave> 36 6.000000 475.0001	APV6:strip,value,ave> 36 2.000000 109.9500
			APV6:strip,value,ave> 38 2.000000 108.2500
APV6:strip,value,ave> 42 1.000000 162.9500	APV6:strip,value,ave> 42 3.000000 240.5000	APV6:strip,value,ave> 42 4.000000 441.0001	APV6:strip,value,ave> 42 2.000000 104.5500
APV6:strip,value,ave> 44 1.000000 155.6000	APV6:strip,value,ave> 44 4.000000 227.9500	APV6:strip,value,ave> 44 5.000000 417.2500	APV6:strip,value,ave> 44 3.000000 96.80000
APV6:strip,value,ave> 54 1.000000 137.6500	APV6:strip,value,ave> 54 2.000000 199.7000	APV6:strip,value,ave> 54 2.000000 371.2000	APV6:strip,value,ave> 54 2.000000 86.99999
APV6:strip,value,ave> 58 0.000000 134.2000	APV6:strip,value,ave> 58 4.000000 190.9000	APV6:strip,value,ave> 58 4.000000 354.9500	APV6:strip,value,ave> 58 1.000000 86.40000
APV6:strip,value,ave> 60 0.000000 124.2500	APV6:strip,value,ave> 60 2.000000 183.4000	APV6:strip,value,ave> 60 4.000000 336.6500	APV6:strip,value,ave> 60 1.000000 87.30000
APV6:strip,value,ave> 68 1.000000 358.6500	APV6:strip,value,ave> 68 4.000000 158.5000	APV6:strip,value,ave> 68 6.000000 286.4500	APV6:strip,value,ave> 68 3.000000 86.25001
APV6:strip,value,ave> 70 1.000000 373.9000	APV6:strip,value,ave> 70 2.000000 160.8000	APV6:strip,value,ave> 70 8.000000 297.2000	
APV6:strip,value,ave> 74 0.000000 380.3500	APV6:strip,value,ave> 74 26.00000 158.9000	APV6:strip,value,ave> 74 38.00000 285.4000	APV6:strip,value,ave> 74 3.000000 88.05000
APV6:strip,value,ave> 78 1.000000 370.7500	APV6:strip,value,ave> 78 1.000000 306.4000	APV6:strip,value,ave> 78 7.000000 266.1000	
			APV6:strip,value,ave> 88 2.000000 73.35000
APV6:strip,value,ave> 92 1.000000 359.0000	APV6:strip,value,ave> 92 2.000000 284.0000	APV6:strip,value,ave> 92 5.000000 233.2000	APV6:strip,value,ave> 92 3.000000 66.65000
APV6:strip,value,ave> 102 1.000000 330.8500	APV6:strip,value,ave> 102 1.000000 254.3500	APV6:strip,value,ave> 102 4.000000 210.5000	APV6:strip,value,ave> 102 3.000000 54.55000
APV6:strip,value,ave> 126 1.000000 293.7000	APV6:strip,value,ave> 126 1.000000 224.7500	APV6:strip,value,ave> 126 5.000000 187.9000	

Figure 60: *(Continued from Figure 59) Dead (white) and intermittent (red/yellow) strips. Yellow rows indicate the strip was consistent between runs in a Table Scan, however at least one Table Scan did not match the others. Red rows indicate a strip performing inconsistently between runs inside a Table Scan. NB: in black and white output, the yellow rows appear light grey, and the red rows appear dark grey. The values in each cell are Strip number, Number of Responses and the Local Average.*

Where strips behaved inconsistently between Table Scans (yellow rows in Figures 59 and 60), the responses were generally at or below the 5% level (compared to the local average), and for runs with signals, the signals themselves were low (generally very near to the 8× RMS cutoff).

For the strips labelled red in Figures 59 and 60, an individual analysis is needed.
APV4 strip 92
This strip was observed to be dead in 14 runs, and healthy (though giving weak response) in 3 runs. This strip behaved so unpredictably that it should not be considered for data analysis.
APV5 strip 36,40,42,44
These strips gave signals in only one run (222) of one Table Scan. These strips all fired on exactly the same events of run 222, which certainly suggests that the responses were not physics related. These strips should therefore not be considered for data taking.
APV5 strip 38
This strip was actually giving (weak) signals in the last Table Scan at DESY, but in all previous runs (apart from run 222), the strip was dead. Interestingly, in run 222, the strip registered signals, but only in exactly the same events as APV5 strips 36,40,42,44 (above). The responses in run 222 therefore do not seem to be physics related.
APV6 strip 74
This strip was dead in the first Table scan, registered some (though weak) signal in the 2nd and 3rd Table Scans. In one run (226) on the third table scan, the weak signals actually just managed to pass the 25% of local average threshold, hence the strip is coloured red. Once again the strip was dead in the last Table Scan at DESY.

Extra Responses:
It was noticed that both strips immediately adjacent to the dead strips gave more signals than expected. This effect can be seen in Figure 61.

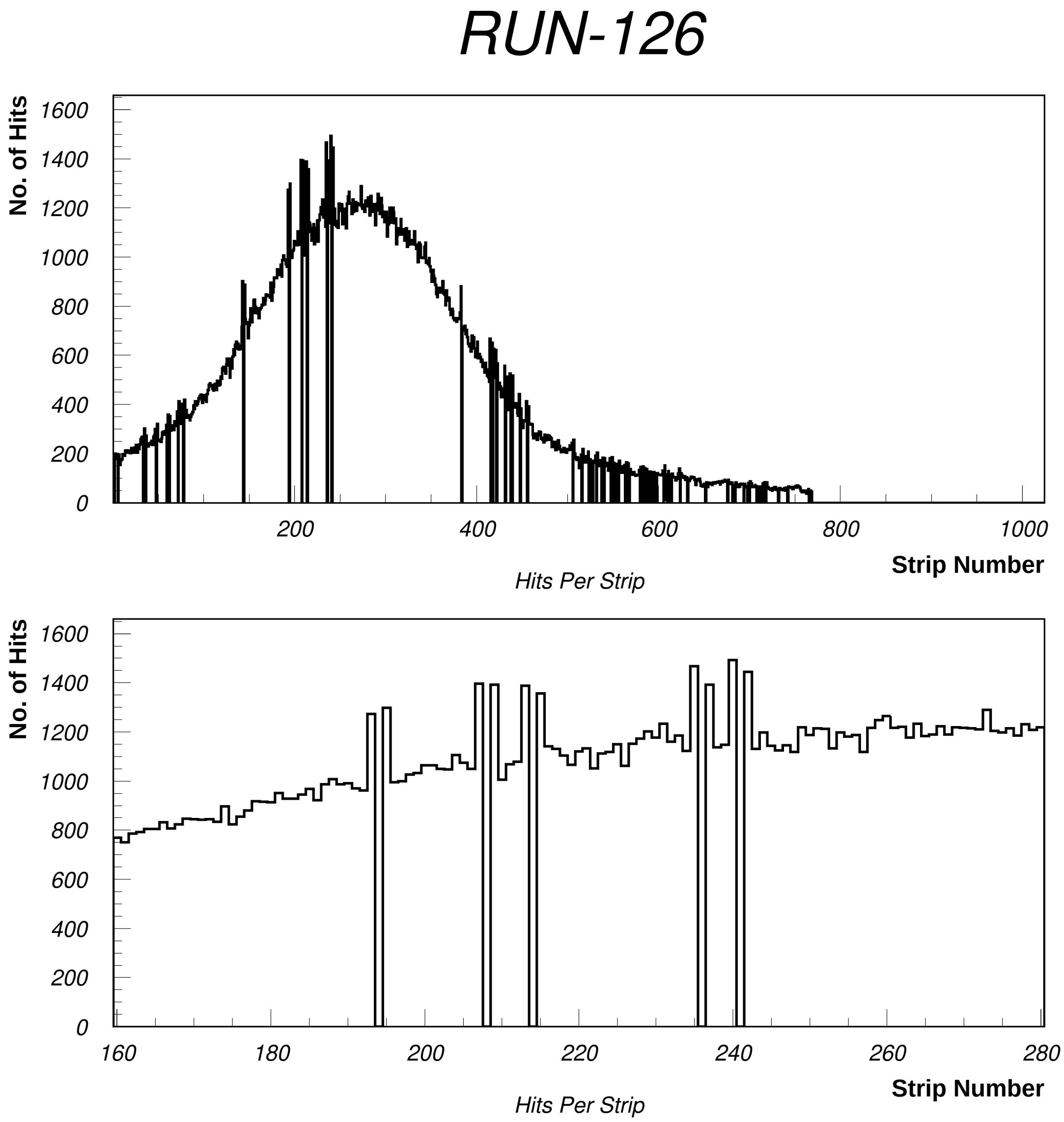

Figure 61: *(Top) Spikes of higher response appear in the beam profile. (Bottom) A magnification of the area between strips 160 and 280 shows five dead strips in this region, and the strips either side giving higher responses.*

All dead strips have been systematically checked and found to exhibit this behaviour, and the ratio of 'local average' to 'extra hits' was reasonably constant, around one third.

10.3 Strip Analysis Conclusions

It is immediately obvious from the results that all the dead strips have even numbers, apart from two strips, one of which, (APV4 strip 55) is known as the only strip on the detector not to be bonded. As the even numbered strips are not adjacent to each other, it does not appear as though faults on the silicon detector itself are to blame (such as scratches, etc.). The APV25 itself has an internal calibration signal, which was completely normal for the unresponsive strips, and therefore the fault does not appear to be caused by anything beyond (or including) the APV25 chips. One possibility is that the bonds between pitch adaptor and silicon are defective for the even strips (which are longer than bonds to the odd strips). This however was felt to be unlikely, as the bonds were analysed visually using a powerful microscope, and also with probing needles. Much more likely, it seems, is that the pitch adaptor connecting the silicon to the APV25 inputs is to blame.

The pitch adaptor is made of Kapton, with etched copper tracks on either side. Crucially, even strips on one side, and odd strips on the other. It would therefore appear that the results are consistent with the pitch adaptor failing to transfer the signal to the APV25. This would mean that the unresponsive strips were effectively "unbonded".

The extra responses from §10.2 are also consistent with the strips not being connected to the APV25 amplifier inputs, as the strips either side collect signals from the unbonded strips.

The number of extra responses seems to be related to the physical distribution of the beam, with areas illuminated well by the beam giving more extra responses than weakly illuminated areas. This would appear to support the assertion that the spikes are a consequence of the beam.

One major implication of the 'extra hits' is that strips either side of dead strips give signals which could originate from the dead strip *or* the strip itself. It should certainly be considered (in addition to the list of dead strips below) that results from dead strips ± 1 should be discounted, and depending on the size of the clusters observed in the HERA tunnel, cluster centres of gravity may be affected significantly even as far away as the dead strip ± 2 strips.

In total, there were 87 faulty strips from a total of 768, which corresponds to around 11%. A list of the dead strips, which should not be used for analysis follows:

```
APV1:
2,6,16,34,36,48,54,60,62,72,78,96
APV2:
16,66,80,86,106,108,113
APV3:
114,128
APV4:
32,34,38,48,52,54,55,56,64,72,84,92,96,122,126
APV5:
4,12,14,16,20,26,28,30,36,38,40,42,44,48,52,54,56,68,70,72,
74,76,80,82,84,86,88,94,98,100,102,112,120
APV6:
12,30,34,36,38,42,44,54,58,60,68,70,74,78,88,92,102,126.
```

11 The Fiber Data Analysis and Results

11.1 Introduction

As mentioned in Section 5, the radiation dose at the silicon detector is estimated to be 1.9 Mrad/year [18]. This may disturb the linearity of the response of the silicon detector during its operation forseen until 2006 i.e. silicon detector radiation damage. In order to correct for it, a calibration detector with a scintillating fiber was installed as shown in fig. 2.

As described in the previous sections, the beam profile in the vertical direction can be reconstructed using the silicon detector information[4]. If the events, in which particles hit the fiber, are selected, you will obtain a sharp distribution (which reflects the diameter of the fiber, 1 mm) around the fiber position (y_{si}) on the profile. The vertical position of the fiber (y_{fib}) can be adjusted independently using the stepping motor with the order of 1 μm precision. Therefore, it is possible to correct the response of the silicon detector, by comparing the y_{si} to the y_{fib}: this is the idea of the linearity calibration using the fiber detector.

In order to estimate the accuracy of this calibration method, the data were taken with different fiber positions. The fiber scans were carried out with 10, 15 and 20 GeV electron beams and 10 GeV positron beams. When the measurements were done with electron beams, the fiber was moved within ± 20 mm with respect to the center position of the silicon detector and the typical step size was 1 mm. During the measurements with positron beams, finer scans were carried out: the typical step size was 100 μm within the range of ± 27.5 mm. This section summarizes the analysis results obtained from the fine scan with the 10 GeV of positron beams.

11.2 Reconstruction and Event Selection

The output signals from both PMTs were fed into an amplifier mounted in the TPOL detector light-tight box and amplified by the factor of 100 as described in section 3.4. The amplified signals were transported via coaxial cables to the control room and read out by a flash ADC. For each event, the pulse heights were sampled 16 times with the interval of 25 ns. The upper plots in fig. 62 show the typical event displays for PMT1 and PMT2 in case there is an energy deposit in the fiber. In this example, the signal is observed in the fifth sample, which is displayed as smaller values (inverted signal) compared with the

[4] In this section, we adopted the silicon reconstruction method and clustering algorithm, which were developed during the DESY test beam and summarized in [1].

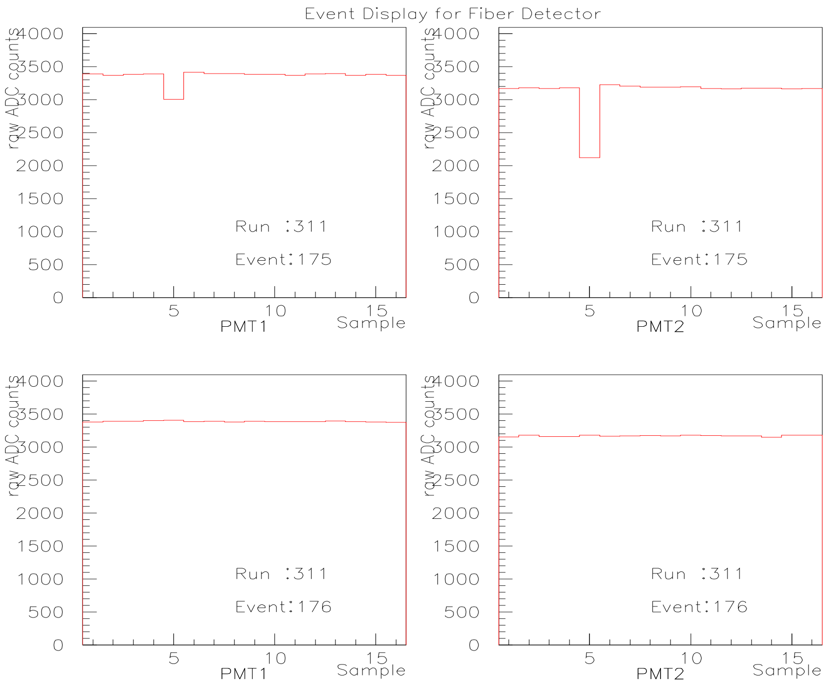

Figure 62: *Event displays of the fiber detector. The upper and lower figures show typical signals and pedestals, respectively.*

pedestals. One ADC count corresponds about 1 mV. As seen in this event, the signal is usually observed only in one sample because the typical signal width is about 10 ns. As a result of an eye scan, we found that signals were found only in the forth, fifth or sixth samples in all events. On the other hand, the lower plots in fig. 62 are the event displays for pedestal events taken by the **ARTIFICIAL TRIGGER**.

Selecting the events taken by the **ARTIFICIAL TRIGGER**, the distributions of ADC counts in all the sample numbers (1-16) were examined to determine the pedestal values. There was no correlations between the ADC counts in different sample numbers, and little fluctuation was observed through each run. The one pedestal value for each PMT was determined as the mean value of ADC counts in all 16 samples. The pedestal values were calculated in each run. Fig. 63 shows the typical pedestal distributions for both PMTs. The typical σ values were found to be about 10 ADC counts.

Fig. 64 shows some event displays after the pedestal subtraction. Here the inverted values are plotted as a function of the sample number. The upper plots are for a signal event and the lower ones are for a pedestal event. The horizontal lines around 40 counts correspond to 4σ of the pedestal distributions.

In the first plot of fig. 65, the events were accumulated in the bins of sample numbers if the ADC counts exceeded the 2σ of pedestal distributions. The histogram and dots are for PMT1 and PMT2, respectively. The second and third plots are the similar ones

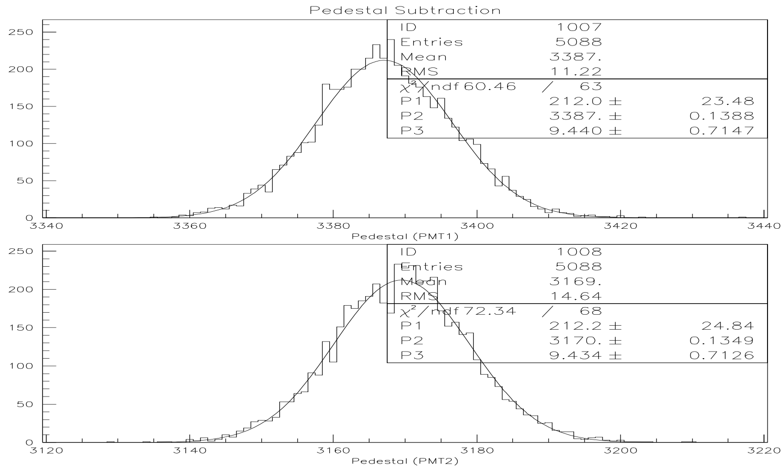

Figure 63: *Pedestal distributions for both PMTs.*

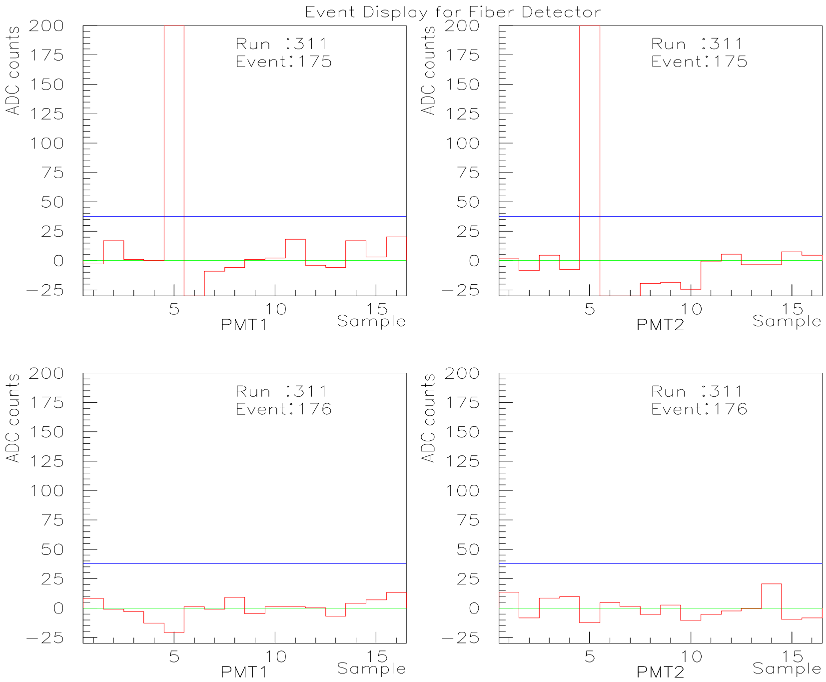

Figure 64: *Event displays after the pedestal subtraction.*

with the threshold values of 3σ and 4σ, respectively. From these figures, it is clearly seen that there remains less noise as the threshold value is increased. The last figure shows the event occupancy of forth, fifth and sixth sample as a function of the threshold value (unit is σ of the pedestal distributions). This figure indicates that an event contains real signal if the ADC count in one of the forth, fifth and sixth exceeds 4σ of the pedestal distribution.

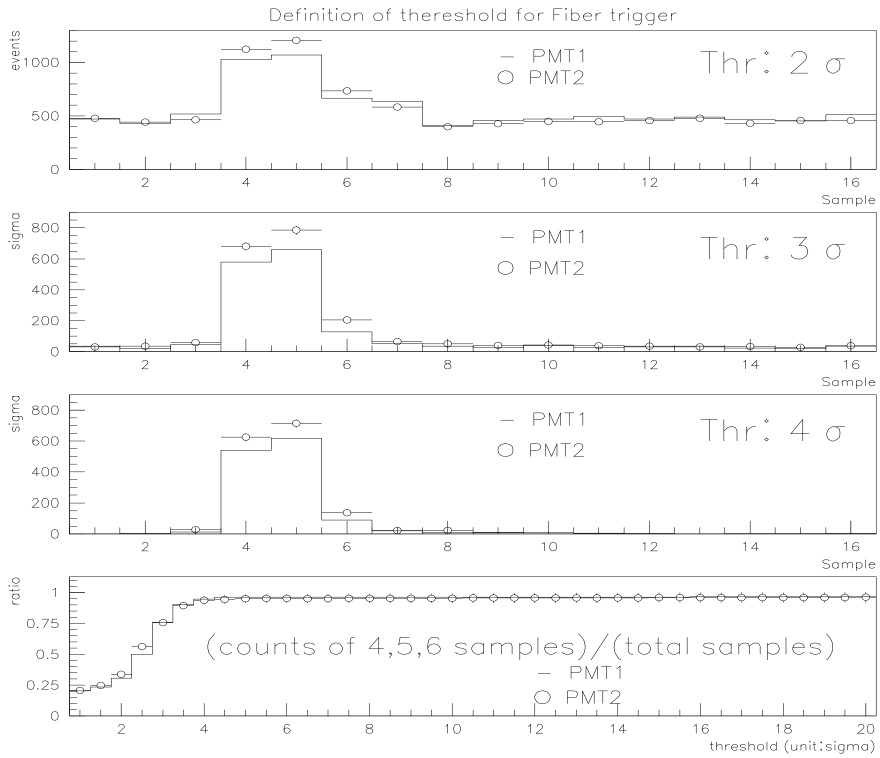

Figure 65: *The upper three figures show the number of accumulated events in the sample numbers after the thresholds of 2σ, 3σ and 4σ. The lower figure shows the event occupancy of forth, fifth and sixth samples as a function of the threshold value.*

If an event satisfied the conditions:

- at least one of the ADC counts in the forth, fifth and sixth exceeds the 4σ of pedestal value, and
- both PMT satisfied the above condition,

we regard that there was a hit in the fiber detector in that event. Hereafter, such event is called 'Fiber event'.

11.3 Comparison with Silicon Data

The upper histogram in fig. 66 shows the distribution of y_{si} reconstructed with the silicon detector [1]. The unit of the horizontal axis is the strip number in the silicon detector. The one unit corresponds to $80\,\mu$m. The events in which at least one cluster exists are filled in the open histogram. If more than one clusters were found, the y_{si} was calculated as the weighted mean position.

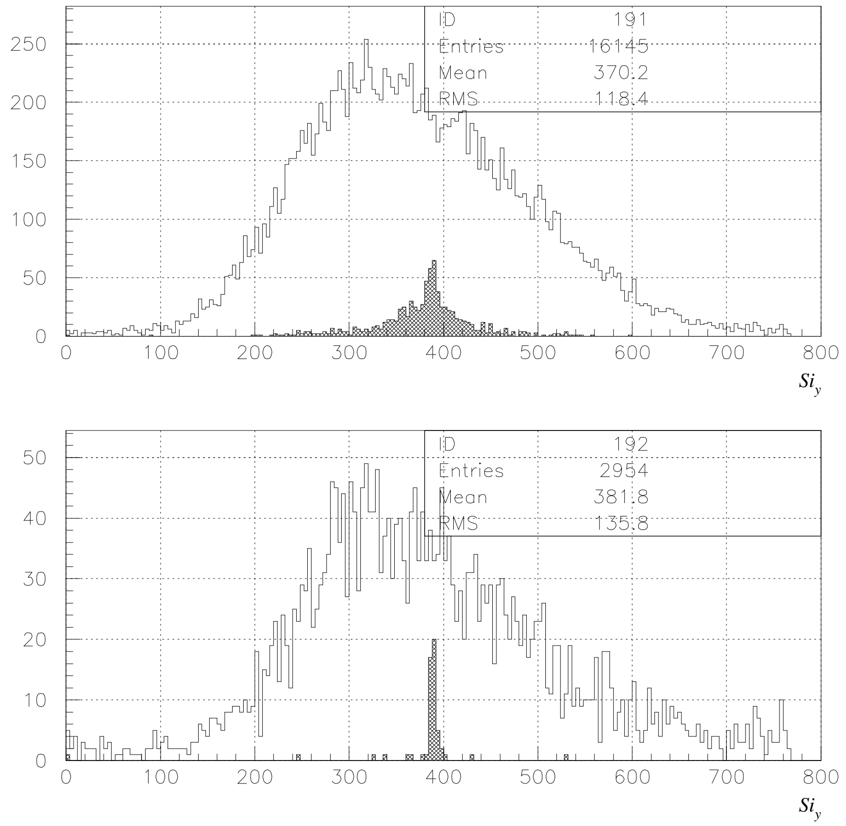

Figure 66: *The upper figure shows the distribution of y_{si} reconstructed with the silicon detector. The hatched histogram shows the Fiber events. The lower figure also shows the y_{si} distribution. In this figure, only the 1-cluster events are selected.*

The hatched one in the same figure shows the histogram for the Fiber events. When this run was taken, the fiber sat around y_{si}, which is clearly seen as a peak in the figure. However, in addition to the peak, the events were also selected far from the fiber position.

In order to understand these events distributed broadly compared with the diameter of the fiber, we selected the events in which only one cluster (refer to as '1-cluster events') was found with the silicon detector in the lower histograms in fig. 66. About 20 % of the events survived this criteria. As shown in the hatched histogram, the Fiber events in the tails disappeared after selecting the 1-cluster events. The width of the distribution is comparable to the diameter of the fiber, 1 mm. The efficiency is turned out to be about 50 % at the peak position.

One of the possible reasons for the broader distribution of the hatched histogram in the upper figure is the multi-particle emission in the pre-shower in front of the fiber detector. If only the part of the particles originating from the electromagnetic shower in the pre-shower hit the fiber, the weighted mean position y_{si} is not necessarily the same with the real fiber position y_{fib}.

In the next section, the 1-cluster events are used to estimate the precision of the accuracy of the linearity calibration using the fiber detector.

11.4 Linearity Calibration

After selecting the Fiber events, fig. 67 shows the mean values of y_{si} as a function of the vertical position of the fiber y_{fib}. The unit of y_{si} was translated into mm in this figure. The absolute value of y_{si} was determined from the $\eta - y$ correlation using the results in section **??** : $y_{si} = 0$ represents the center position of the calorimeter.

The line in the figure shows the result of a linear function fit. The slope is consistent with unity. The upper left histogram shows the distribution of the residual to the fitted line. The RMS is obtained to be about 50 μm. Therefore, we would conclude that the precision of the linearity calibration of the silicon detector response using the fiber detector turned out to be about 50 μm in the CERN test beam setup.

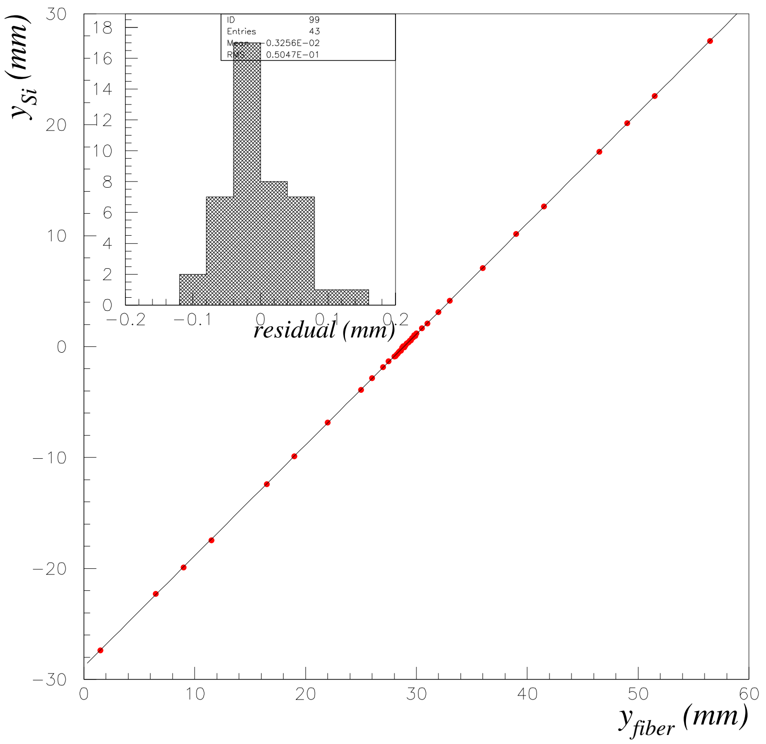

Figure 67: *The mean values of y_{si} for fiber events as a function of the y_{fib}. The line shows the result of a linear function fit. The upper left histogram shows the residual distribution.*

12 Conclusions

The TPOL group carried out an electron/positron test-beam measurement at CERN in summer 2001 (23/07/01-3/08/01). The aim of the CERN test beam was to study the TPOL polarimeter at higher energies (not possible at DESY) in its final setup, before its installation in the HERA tunnel. The CERN test-beam aims have been obtained and the results can be summarized as follows:

- Calorimeter: The calorimeter has a very good linearity and spatial uniformity of the calorimeter, energy resolution $\sigma_E = 25\%$, spatial resolution $\sigma_y = 0.3\ mm$ for 10 GeV positrons at $y = 0$.
- Silicon Detector: The silicon strips have a very stable pedestal, the strip noise is about 2 ADC counts, and the strip average signal is around 55 ADC counts. There are about 10% dead-faulty strips distributed over the whole silicon detector. These dead-faulty strips have a higher noise ($>$ 3.5 ADC counts) and a small average signal ($<$40 ADC counts), which allows to differentiate between live and dead strips. The strip Signal to Noise ratio is $\sim$30. When finding silicon clusters care must be taken to exclude the dead-faulty strip areas. The η-y transformation was measured with a relatively good precision.
- Fiber Detector: The stepping motor was installed in order to control remotely the vertical position of the scintillating fiber in the fiber detector. The fiber scan was carried out when the data with 20 GeV of electron beams were taken. The precision of the linearity calibration turned out to be better than 50 μm.

The upgraded TPOL was installed in the HERA tunnel near HERA-B (HERA WEST RIGHT), during the HERA 3 day access 19-21/11/2001. The dead strip problem is due to the defective Kapton pitch adaptor, which bonds the silicon strips to the APV25 readout chips. Two new silicon detectors, with a new pitch adaptor, (aluminium on glass pitch adaptor), are being prepared and tested at IC London. The new pitch adaptor would prevent the dead strip problem from happening again. One silicon detector will measure the vertical impact point y, the other silicon detector will measure the horizontal impact point x. These detectors will be installed in the HERA tunnel during the next long HERA shutdown (March 2003).

13 Appendix

In this appendix the silicon pitch adaptor connectivity studies and tests are reported. Theses studies have been carried out to investigate the silicon dead strip problem, in the newly constructed Y-silicon plane, which was tested in the CERN test beam. In section 10 the silicon dead strip data analysis is reported.

ZEUS POLARIMETER PITCH ADAPTOR REPORT

The following report is a synopsis of the tests carried out on samples of the Zeus Polarimeter Pitch Adaptors.

A number of tests were carried out to investigate whether a bonding failure had occurred and if so, why, and ways to overcome it, so that it could be prevented in the future.

The TPOL Experiment Pitch Adaptor (P/A) was constructed using a P.C.B. bottom (B) layer and a Kapton top (T) layer. The decision to use this particular combination was to ensure as close a match of levels as possible for bonding the APV's.

APV height = 300µm + 150µm Cu foil heat sink.

P/A height = 500µm P.C.B. (B) + 100µm kapton (T).

This method had been developed and used successfully on a previous experiment.

Given the required track quantity (384) and resolution (50µm on 88µm pitch), using 5µm Cu thickness on 100µm kapton substrate, proved to be difficult but we managed to produce some usable samples. The tracks on the [T] kapton layer were slightly over etched resulting in thinner tracks (38µm-40µm) than those on the [B] P.C.B. layer (50µm). At the time it was believed that this would not be a problem, providing the tracks could be bonded.

When the data from the TPOL experiment was analyzed we discovered that 66 of the 68 failures occurred on the kapton. The B layer had only 1bonding failure (+1 known cut track).

A number of Tests were set up concentrating on the following points to determine:

1. **Where** the fault occurred.
2. **Why** the fault occurred.
3. **How to prevent** the fault reoccurring.
4. **Repeat tests** to confirm the above.

In all the samples one end of each track was bonded to a common point and the connectivity tested between the other end of each track and the common point.

Test 1

Using 5µm Cu/ .5mm PCB Bonding wire 25µm.
Board # 8 / sample 2 Y/B
Samples were chosen because of the track width, ≈38-40µm as on the kapton (T) P/A.

The current standard bonding settings of 4 for F (force), 3 for T (time), 3.3 for P (ultrasonic energy), were used. [The values of F/T are usually kept the same. The value of P can be changed according to the requirements of the substrates].

384 Tracks were bonded and connectivity tested.
By visual inspection all bonds looked good but a small percentage failed the connectivity test.
The failed connections were then investigated further. Page 1

To assess if there was any damage to the track it was tested for connectivity all along its length. Still no connectivity was observed. The probe was then applied directly onto the 2nd bond. When the track was retested, after pressure had been applied to the bond, connectivity had been restored. (Fig. 1)

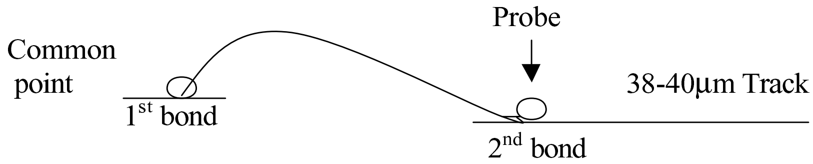

Fig. 1

This procedure was carried out on several failed bonds. Connectivity was always restored after pressure had been applied to the bond. This test indicated that the problem was on the 2nd bond and possibly caused by poor adhesion to the metal.

<u>Test 2</u>

Using 5µm Cu/ .5mm P.C.B. Bonding wire 25µm

Board # 6 / sample 3 Y/B

Maintaining the same bonding settings (F/T/P- 4/3/3.30 as for test 1) the P/A was bonded from the Detector side where the tracks are 80-100µm wide. Connectivity test was done. There were no failures.

As both the substrate type and metallization were the same for the tests, the result suggests that the width of the track was important and a possible factor in the bonding failure.

<u>Test 3</u>

Using 5µm Cu/ .5mm P.C.B. Bonding wire 25µm

Board #6/ sample 3 Y/T

Here are some causes that prevent bonding taking place:

1. Poor metallization on the substrate.
2. Dirt on the bonding wedge or sample.
3. Not enough P (ultrasonic energy) being applied to suit the material on the substrate.

The metallization is, usually, done by an outside firm. The wedge and sample should be clean. If the value of P is too low you increase the P setting to a value where bonding takes place. If the P value is too high the bond appears squashed. If the track is wide enough the P value isn't as crucial as when the track is too thin i.e. 38-40µm wide this is because there isn't enough area on the track to accommodate the bond footprint produced by the bonding process. Resulting in a bond that doesn't adhere properly onto the track (Fig. 2).

Fig. 2

To confirm this, on test 3 the P value was increased from 3.30 to 4.00 and decreased from 3.30 to 2.70. The same number of bonds was also done using P value 3.30.

Connectivity testing showed that when P was 4.00 the number of failures increased. For the P value 2.70 there were no failures.

<u>Test 4</u>

Using 5µm Cu/ .5mm P.C.B.   Bonding wire 25µm

Boards #8 sample 2
#6 sample 3
#8 sample 5
#9 sample 4

On this test an equal number of bonds were done varying only the value of P.

768 tracks 38-40µm wide, bonded P-value 3.30
768 tracks 38-40µm wide, bonded P-value 4.00
768 tracks 38-40µm wide, bonded P-value 2.70

They were all connectivity tested.

Also:

Extra 256 tracks 38-40µm wide, P-setting 2.70 were bonded and connectivity tested. No failures.

A number of 80-100µm wide tracks, on various other types of substrates, using P-setting 3.30-4.10 were bonded and tested for connectivity.
Total # =630. No failures were observed.

A number of bonds using P-setting 2.00-3.00, (to establish bonding window), on 38-40µm tracks were also done on a variety of substrates. They were connectivity tested.
Total # =1007. No failures occurred.

4197 Tracks in total were bonded and connectivity tested, in the course of these tests.

The results showed:

1. If value of P used was too high, on 38-40µm tracks, there was bonding failure on some tracks.
2. At a width greater than 80µm no failure occurred regardless of P value.
3. On tracks < 50µm the P value becomes crucial for bonding to be successful.

ZEUS POLARIMETER PITCH ADAPTORS
CONNECTIVITY TESTS RESULTS

DATE	Sample No	Substrate	Ref: No:	Track Width In µm	Test No	F / T / P Force/Time/Power Settings	No of Tracks Bonded	Test Total	No of Failures	Failure Rate	Comments
14-02-02	2	5µm Cu/.5mm PCB	8 YB pg-1	38/40	1& 4	4/3/ **3.30**	384		8	2%	
20-02-02	3	5µm Cu/.5mm PCB	6 YB pg-2	38/40	4	4/3/ **3.30**	64		6	9%	
25-02-02	3	5µm Cu/.5mm PCB	6 YT pg-3	38/40	4	4/3/ **3.30**	64		1	1.5%	
18-03-02	5	5µmCu/.5mmPCB	8 YT pg-8	38/40	4	4/3/ **3.30**	64		--	--	
26-03-02	5	5µm Cu/.5mm PCB	8 XB pg-10	38/40	4	4/3/ **3.30**	128		4	.7%	
05-04-02	5	5µm Cu/.5mm PCB	8 XT pg-11	38/40	4	4/3/ **3.30**	64		3	4.6%	
								768	**22**	**2.9%**	
21-02-02	3	5µm Cu/.5mm PCB	6 YT pg-3	38/40	3& 4	4/3/ **4.00**	128		42	32.8%	
05-04-02	3	5µm Cu/.5mm PCB	6 XB pg-12	38/40	4	4/3/ **4.00**	128		29	22.6%	
05-04-02	3	5µm Cu/.5mm PCB	6 XT pg-13	38/40	4	4/3/ **4.00**	64		8	12.5%	
05-04-02	5	5µm Cu/.5mm PCB	8 XT pg-11	38/40	4	4/3/ **4.00**	64		12	18.7%	
05-04-02	5	5µm Cu/.5mm PCB	**8 YT*pg-14**	38/40	4	4/3/ **4.00**	384		95	24.7%	*2nd Test on sample
								768	**186**	**24.2%**	
26-02-02	4	5µm Cu/.5mm PCB	9 YB pg-4	38/40	4	4/3/ **2.70**	384		--	--	
27-02-02	4	5µm Cu/.5mm PCB	9 YB pg-5	38/40	4	4/3/ **2.70**	384		--	--	
								768	--	--	
25-02-02	3	5µm Cu/.5mm PCB	6 YT pg -3	38/40	4	4/3/ **2.70**	128		--	--	
13-03-02	5	5µm Cu/.5mm PCB	**8 YT*pg-8**	38/40	4	4/3/ **2.70**	64		--	--	*1st Test on sample
01-03-02	**14**	5µmCu/**1.6mmPCB**	**14 YB pg-7**	38/40	4	4/3/ **2.70**	64		--	--	
								1024	**None**	**None**	
20-02-02	3	5µm Cu/.5mm PCB	**6 YB*pg-2**	100*	2	4/3/ **3.30**	**320***1st test	**320**	**None**	**None**	*Detector Side
01-03-02	3	5µm Cu/.5mm PCB	6 YB pg-6	38/40	-	4/3/ **2.00 ***	128		--	--	* P-Values used to
01-03-02	3	5µm Cu/.5mm PCB	6 YB pg-6	38/40	-	4/3/ **2.50 ***	128		--	--	Establish bonding
01-03-02	5	5µm Cu/.5mm PCB	8 YT pg-8	38/40	-	4/3/ **2.60 ***	128		--	--	window

ZEUS POLARIMETER PITCH ADAPTORS
CONNECTIVITY TESTS RESULTS

DATE	Sample No	Substrate	Ref: No:	Track Width In µm	Test No	F / T / P Force/Time/Power Settings	No of Tracks Bonded	Test Total	No of Failures	Failure Rate	Comments
01-03-02	5	5µm Cu/.5mm PCB	8 YT pg-8	38/40	-	4/3/ **3.00***	128		--	--	
21-03-02	5	5µm Cu/.5mm PCB	8 XT pg-9	38/40	-	4/3/ **3.00***	128		--	--	
01-03-02	14	5µmCu/1.6mmPCB	14 YB pg-7	38/40	-	4/3/ **2.50/2.60***	128+128		--	--	Also on 07-03-02
								896	**None**		
11-03-02	1	5µmCu/100µmkapt	YB/Apv1pg15	38/40	-	4/3/ **4.10**	32		9	28/%	
11-03-02	1	Kapton ‘’ ‘’	‘’ ‘’ ‘’	‘’	-	4/3/ **3.00**	32		**None**		
11-03-02	1	Kapton ‘’ ‘’	‘’ Apv2 ‘’	100*	-	4/3/ **4.10**	64		**None**		*Detector side
11-03-02	1	Kapton	‘’ Apv3 ‘’	38/40	-	4/3/ **3.00**	32		**None**		
11-03-02	1	Kapton ‘’ ‘’	‘’ Apv4 ‘’	38/40	-	4/3/ **3.00**	15		**None**		
→							Only	**175***		***Sample**	**Contaminated**
15-02-02		PCB(old sample)	MPXAlt(1991)	100	-	4/3/ **3.30**	50		--		
18-02-02		5µmCu/**1.6mm**PCB	Apv25s1May00	100	-	4/3/ **3.30**	29		--		
18-02-02		PCB Test samples	#’s4,5,6,7	100	-	4/3/ **3.30**	14x4=**56**		--		
19-02-02		18µmCu/.5mmPCB	Apv6Harris (1998)	100	-	4/3/ **3.30**	55		--		
19-02-02		2µm Al on glass	BRSMS P/A	50	-	4/3/ **2.40/1.80**	56		--		
								246	**None**		
→		**Grand total=**	768+768+1024	+320+	836	+175+246 =		**4197**			

RECORDS

Test 1+4 - 14/02/02 Board# 8 /sample 2 YB P-setting 3.30 (page 1) total = 384 bonds
Test 4 - 20/02/02 Board# 6 /sample 3 YB P-setting 3.30 (page 2) total = 64 ‘’
‘’ - 25/02/02 ‘’ ‘’ YT P-setting 3.30 (page 3) total = 64
‘’ - 18/03/02 Board# 8 /sample 5 YT P-setting 3.30 (page 8) total = 64
‘’ - 26/03/02 ‘’ ‘’ XB P-setting 3.30 (page 10) total = 128
‘’ - 5/04/02 ‘’ ‘’ XT P-setting 3.30 (page 11) total = 64

TOTAL No: 768

Test 3+4 - 21/02/02 Board# 6 /sample 3 YT P-setting 4.00 (page 3) total = 128
Test 4 - 5/04/02 ‘’ ‘’ XB ‘’ ‘’ (page 12) total = 128
‘’ ‘’ ‘’ ‘’ XT ‘’ ‘’ (page 13) total = 64
‘’ ‘’ Board# 8 /sample 5 XT ‘’ ‘’ (page 11) total = 64
‘’ - 5/04/02 ‘’ ‘’2nd test YT ‘’ ‘’ (page 14) total = 384 bonds on the 1st test removed, sample rebounded. Results confirmed by Vera
TOTAL No: 768

Test 4 – 26/02/02 Board# 9 /sample 4 YB P-setting 2.70 (page 4) total = 384 (results confirmed by Sarah).
Test 4 - 27/02/02 ‘’ ‘’ YT ‘’ ‘’ (page 5) total = 384 (samples kept for periodic testing over time)

TOTAL No: 768
Also P- setting 2.70 25/02/02 Board#6 /sample 3 (page 3) YT total =128
‘’ ‘’ 18/03/02 ‘’ #8 ‘’ 5 (page 8) YT (test 1) total = 64
‘’ ‘’ 1/03/02 ‘’ #14 (1.6mm) (page 7) YB total = 64
TOTAL# of bonds P-setting 2.70 =**1024**

20-02-02 Board #6 (1st Test) sample 3 YB P-setting 3.30 (pg.2) detector side total=**320**

Also (to establish bonding window):

1-03-02 Board #6 /sample 3 YB P-setting 2.00 (page 6) total =128
1-03-02 ‘’ ‘’ ‘’ ‘’ ‘’ 2.50 ‘’ total =128
1-03-02 ‘’ #8 /sample 5 YT ‘’ 2.60 (page 8) total =128
1-03-02 ‘’ ‘’ ‘’ 5 YT ‘’ 3.00 ‘’ total =128
21-03-02 ‘’ #8 ‘’ 5 XT ‘’ 3.00 (page 9) total =128

1-03-02/7-03-02 1.60mm/5μm Board 14 /YB P-setting 2.50 (page 7) total =128
‘’ ‘’ ‘’ ‘’ 2.60 ‘’ total =128
TOTAL# of bonds P-setting 2.00 = 128
TOTAL# of bonds P-setting 2.50 = 256
TOTAL# of bonds P-setting 2.60 = 256
TOTAL# of bonds P-setting 3.00 = 256
Total = 896

14 Acknowledgments

We thank several people at IC-London for the work done, advice and support given, in building the silicon microstrip detector and for the test beam preparation: B. Cameron, M. Raymond, A. K. Jamdagni, L. Toudup, S. Greenwood, M. Kasey, M. Khaleeq, G. Barber, P. Savage D. R. Price, I. Clark and D. Clark.

We would like to thank ATLAS Japan group who provided us with the silicon micro-strip chips.

We would like to thank G.Barber and P.Savage for the mechanical design and construction of the fiber detector. We also would like to thank S.Greenwood, M.Kasey and M.Khaleeq for the cable connections between the stepping motor and the drive. We are grateful to K.Tokushuku who privided us the scintillating fibers. We are also grateful for the financial support given by the Japanese Ministry of Education, Science and Culture.

We thank Peter Schuler and Norbert Meyners, for their collaboration in preparing and modifying the spare TPOL calorimeter that was used in the test-beam.

We thank S. Ketels for helping us organizing the van transport of the TPOL, and also a lot of other CERN matters related with the test beam. We also thank the U.K. liaisons at CERN.

We thank CERN for giving us the opportunity to use a high energy test beam, which was not possible at DESY.

References

[1] C. Collins-Tooth et al., *The Transverse Polarimeter (TPOL) Test Beam at DESY in January-February 2001* (unpublished), June 2001, available on `http://www-zeus.desy.de/ZEUS_ONLY/zeus_notes/notes01.html`. ZEUS-01-019.

[2] *Future Physics at HERA Volumes I and II*, ed. G. Ingelman, A. De Roeck, R. Klanner, 1996.

[3] F. Zetsche, *Proc. Workshop on Future Physics at HERA*, G. Ingelman, A. de Roeck and R. Klanner (eds.), Vol. 1, p. 222. Hamburg, Germany (1996).

[4] Polarization 2000 Group, *Polarization 2000* (unpublished). DESY-PRC 98-07, 1998.

[5] D.P. Barber et al., Nucl. Inst. Meth. **A 329**, 79 (1993).

[6] D.P. Barber et al., Nucl. Inst. Meth. **A 338**, 166 (1994).

[7] M. Ruh et al., *Construction and Beam Test of a Spare Calorimeter for the HERA Transverse Polarimeter* (unpublished). Hermes Internal Note, 1997.

[8] ZEUS Coll., U. Holm (ed.), *The ZEUS Detector*. Status Report (unpublished), DESY (1993), available on `http://www-zeus.desy.de/bluebook/bluebook.html`.

[9] M.Ruh et al., *Construction and Beam Test of a Spare Calorimeter for the HERA Transverse Polarimeter*. Internal Polarimeter Report 97-05 (1997).

[10] ATLAS Coll., *ATLAS 98-99 Silicon Microstrip Detector Layout* (unpublished), 1999, available on `http://www-ccint.kek.jp/managers/silicon/si_det.html`.

[11] L.L. Jones et al., *Fifth Workshop on Electronics for LHC Experiments*, p. 162. (1999), available on `http://www.te.rl.ac.uk/med`.

[12] CES, *RIO 2 8062*, available on `http://www.ces.ch`.

[13] CLRC Rutherford Appleton Laboratory, *CMS Front-End Driver PMC User Manual*, available on `http://www.te.rl.ac.uk/esdg/cms-fed/`.

[14] M. Morrissey, *SEQSI Manual*, 1996.

[15] E. Murer, *VI2C Manual*, 1997.

[16] ISEG, *VHQ 202M Precision High Voltage Supply VME Standard Operators Manual*, available on `http://www.iseg-hv.com/`.

[17] CAEN, *CAEN MOD. V513 16 Programmable I/O Register Technical Information Manual*, available on `http://www.caen.it`.

[18] R.Hamatsu, *Study of radiation dose in the silicon detector of the TPOL polarimeter using GEANT*, 2000, available on `http://heal1.phys.metro-u.ac.jp/~hamatsu/StudyOfTPOLDose.html`.